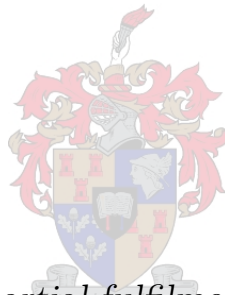


Towards a Paper-based Biosensor to Distinguish Between Bacterial and Viral Infections

by

Johannes Daniel Retief



*Thesis presented in partial fulfilment of the requirements
for the degree of Master of Engineering in Electronic
Engineering in the Faculty of Engineering at Stellenbosch
University*

Supervisor: Prof. W.J Perold

Co-supervisor: Prof. P.R Fourie

April 2019

Declaration

By submitting this thesis electronically, I declare that the entirety of the work contained therein is my own, original work, that I am the sole author thereof (save to the extent explicitly otherwise stated), that reproduction and publication thereof by Stellenbosch University will not infringe any third party rights and that I have not previously in its entirety or in part submitted it for obtaining any qualification.

Date: April 2019

Copyright © 2019 Stellenbosch University
All rights reserved.

Acknowledgements

I would like to dedicate this part of my thesis to thanking the long list of people who made it possible.

First of all, I would like to thank my two supervisors, Prof Perold and Prof Fourie, for their support and guidance. I would not have been able to finish this project without their humour and perspective, as well as wisdom in my times of anxiety, especially at the end.

The administrative staff of the department of Electrical and Electronic Engineering, specifically Mr Wessel Croukamp and Mrs Jenny Martin, made all of my fabrication and testing adventures possible. None of this would have happened as it did without their practical expertise and capabilities in procuring materials.

Most members of the SAND research group were indispensable to me in my work, and their willingness to discuss topics, refine ideas and troubleshoot problems not only added value to my project, but they became my close friends. To name a few, Alexander Lloyd, Stephan Schoeman, Dr. Frederic Isingiswe Nturambirwe, Whelan Mohali, Carel-Chris van Dyk, Dean Bradford and Thaakir Aricum made my time in the group easier. I would also like to offer thanks to Stephan for helping me create some of the illustrations in this document - his eye for design is far superior to my own.

Furthermore, the staff at Synexa Life Sciences were of immeasurable value to me in the biological side of this project, and they made it much easier for an engineer to understand a small part of immunology and practical laboratory work. Prof Patric Bouic, Dr Matti Kimberg and Dr Bertus Moolman all sacrificed some of their time to educate a group of engineers on the finer point of immunoassays and the practical implementation thereof.

For the part of this project that was concerned with viscosity measurements, Mrs Hanlie Botha was indispensable. She pointed me in the right direction for my ink dilutions and offered her help in doing the many measurements of the iterative process.

I would also like to thank my family, who made this possible; my parents for their encouragement, and my sister for her undying loyalty and support.

Last, but not least, I would like to mention Dr Anoop Menachery, from King Abdullah University of Science and Technology, and Keith Ryan, from Biocom Africa, for their assistance. Dr Menachery wisely kept me from letting the scope of my project creep even further, and Keith helped with the process of procuring the antibodies and proteins used during the course of my work.

Dedications

This thesis is dedicated to God, who gave me the capacity to complete the work in spite of my own inadequacies.

Abstract

Towards a Paper-based Biosensor to Distinguish Between Bacterial and Viral Infections

J.D Retief

*Department of Electrical and Electronic Engineering,
University of Stellenbosch,
Private Bag X1, Matieland 7602, South Africa.*

Thesis: MEng (Electronic)

April 2019

The increasing threat of antimicrobial resistance has become more prominent in recent years due to strains of common bacteria becoming resistant to the medication used to cure the infections they cause. One of the causes of this problem is the indiscriminate prescription of antibiotics to patients with ambiguous symptoms, breeding antimicrobial resistance. The current management strategy for this problem is to develop more effective means of distinguishing between bacterial and viral infections, and specifically to develop biosensors for this purpose.

This project aimed to develop a low-cost paper-based electrochemical transistor sensor to measure and detect the concentration of C-reactive protein in solution, with the goal of the transducers being used to distinguish between bacterial and viral infections in patients with ambiguous symptoms. C-reactive protein is known to be one of a group of proteins with promise in aiding diagnosis of different types of infections, and was chosen for its relatively low cost when compared to the alternatives. An inkjet printing system was developed to aid in the manufacturing process. After extensive modification, a regular desktop inkjet printer was converted to a flatbed configuration and could print structures with a minimum size of 70 μm . Layers of printed material could be aligned with a repeatability of 25 μm . Following successful implementation of the printer, a method was developed to manufacture organic electrochemical transistors onto paper substrates using printed silver electrodes. The transistors were subsequently functionalised and antibodies specific to C-reactive protein were immobilised onto the transducer surface. The transducers were tested and found to respond to CRP concentrations between 2.5 $\mu\text{g}\cdot\text{ml}^{-1}$ and 19.5 $\text{ng}\cdot\text{ml}^{-1}$, and the transducers were capable of quantifying protein concentrations over most of the clinically relevant range of concentrations for CRP. This means that the project was successful in developing a low-cost paper-based transducer to potentially aid in the differentiation between viral and bacterial infections.

Uittreksel

Bydrae tot 'n papier-gebaseerde biosensor om tussen bakterieële en virale infeksies te onderskei

(“Towards a Paper-based Biosensor to Distinguish Between Bacterial and Viral Infections”)

J.D Retief

*Departement Elektries en Elektroniese Ingenieurswese,
Universiteit van Stellenbosch,
Privaatsak X1, Matieland 7602, Suid Afrika.*

Tesis: MIng (Elektronies)

April 2019

Die hedendaagse probleem van antibakterieële weerstandigheid het onlangs begin om meer aandag te geniet weens die ontluiking van alledaagse bakterieë wat weerstandigheid ontwikkel het teen die middels wat voorheen gebruik is om hul te bestry. Een van die oorsake van hierdie probleem is die onverskillige voorskrif van antibiotika aan pasiënte met dubbelsinnige simptome, wat antimikrobiële weerstand vererger. Die huidige bestuurstrategieë vir hierdie probleem is om nuwe metodes te ontwikkel waardeur onderskei kan word tussen die oorsake van verskillende soorte infeksies, en spesifiek om nuwe biosensors vir hierdie toepassing te ontwikkel.

Die doel van hierdie projek was om 'n laekoste papier-gebaseerde elektrochemiese transistor sensor te ontwikkel om die konsentrasie van C-reaktiewe proteïene in oplossing te meet, met die doel dat die sensors gebruik kan word om tussen bakteriële- en virusinfeksies te onderskei vir pasiënte met dubbelsinnige simptome. Dié keuse van proteïene is gemaak omdat C-reaktiewe proteïene deel vorm van groep proteïene met potensiaal om gebruik te word om tussen verskillende infeksiesoorte te onderskei. Van die groep is C-reaktiewe proteïene ook die goedkoopste. 'n Inkspruitdrukker is as deel van die projek ontwikkel om sodoende die vervaardigingsproses van die sensors te vergemaklik deur silver elektrodes op papier te druk. Na voltooiing van die drukker kon strukture tot 'n resolusie van 70 µm gedruk word, en opeenvolgende lae kon tot binne 25 µm van mekaar belynd word. Volgende is 'n vervaardigingsproses ontwikkel waardeur organiese elektrochemiese transistors op papier vervaardig kon word deur van die drukker gebruik te maak. Die vervaardigde transistors is later met teenliggampies bewapen, en getoets. Die transistors was suksesvol darin om konsentrasies van CRP tussen 2.5 µg·ml⁻¹ en 19.5 ng·ml⁻¹ te meet, wat oor die meeste van die bereik van kliniese belang vir CRP strek. Dit beteken dat die projek darin geslaag het om 'n sensor te ontwikkel waarmee daar gepoog kan word om verskillende soorte infeksies van mekaar te onderskei.

Contents

Declaration	i
Acknowledgements	ii
Dedications	iii
Abstract	iv
Uittreksel	v
Contents	vi
List of Figures	viii
List of Tables	x
Nomenclature	xi
1 Introduction	1
1.1 Background and Motivation for Study	1
1.2 Objectives and Goals	2
1.3 Thesis Overview	2
2 Literature Review	4
2.1 Introduction	4
2.2 Biomarkers	6
2.3 Biosensor Definition	14
2.4 Biorecognition Elements	16
2.5 Transducer Mechanisms	19
2.6 OECT-Based Biosensors	23
2.7 Inkjet Printing for Sensor Development	30
2.8 Proposed Transducer Design	35
3 Methodology	38
3.1 Introduction	38
3.2 Printer Modification	38
3.3 Transistor Manufacture	39
3.4 Transducer Functionalisation and Antibody Immobilisation	40
3.5 Measurement Methodology	43
3.6 Conclusion	45

4	Printer Development	46
4.1	Introduction	46
4.2	Methodology	46
4.3	Choice of Printer and Disassembly	47
4.4	Design of Printer Modifications	51
4.5	Implementation of Printer Modifications	53
4.6	Assessment of Modifications	56
4.7	Discussion	74
4.8	Conclusion	75
5	Transducer Development	77
5.1	Introduction	77
5.2	Tranducer Layout	77
5.3	Methods and Materials	78
5.4	Transducer Manufacture	84
5.5	Transducer Functionalisation	91
5.6	Conclusion	96
6	Biosensor Tests	97
6.1	Introduction	97
6.2	Biorecognition Element Immobilisation	97
6.3	Test Procedure	99
6.4	Results	102
6.5	Discussion	107
6.6	Conclusion	110
7	Discussion	111
7.1	Printer Development	111
7.2	Transducer Development	112
7.3	Protein Measurements	113
7.4	Limitations of Study	114
7.5	Conclusion	114
8	Conclusion	116
8.1	Review of Aims and Objectives	116
8.2	Findings	117
8.3	Recommendations and Future Work	118
	Appendices	120
	A Datasheets and Technical Information	121
	B Technical Drawings	126
	Bibliography	128

List of Figures

2.1	Schematic representation of ELISA processes	8
2.2	Illustration of SPR Principle	9
2.3	FebriDx product information	11
2.4	Standard lateral flow assay illustration	11
2.5	AbioScope product	12
2.6	MeMed Key platform	13
2.7	Schematic diagram of biosensor function	15
2.8	Antibody types and distribution	16
2.9	ssDNA Biosensor schematic	17
2.10	Schematic of hairpin probe function	18
2.11	Simplified OECT cross-section	23
2.12	Current and voltage conventions	25
2.13	Typical OECT sensor output current characteristics	29
2.14	Typical OECT sensor transconductance characteristics	29
2.15	Diagram of basic ink-jet mechanism	32
2.16	Biofunctionalisation strategy	36
2.17	Proposed transducer cross-section	37
3.1	Unaltered PEDOT:PSS	40
3.2	APTES addition	40
3.3	BS ³ structure	41
3.4	Sulfo-NHS reaction with primary amines	41
3.5	BS ³ addition	42
3.6	Capture antibody addition	42
3.7	BSA blocking step	43
3.8	C-reactive protein addition	43
4.1	HP DeskJet Ink Advantage 4535 printer	47
4.2	HP 652 Cartridges	48
4.3	Cartridge nozzle spacings	48
4.4	Open printer	49
4.5	Detached carriage assembly	50
4.6	Exposed Feed Mechanism	51
4.7	Illustration of flatbed printer layout	52
4.8	Modified printer design	53
4.9	Rearranged carriage and feed assembly	54
4.10	Completed printer	54
4.11	Cut cartridges	55
4.12	Cleaned colour cartridge	56

4.13	Test patterns for printer evaluation	58
4.14	Inconsistencies in printed structures from vector format designs	58
4.15	SVG-defined electrodes	59
4.16	Initial GIMP-defined electrode dimensions	60
4.17	Comparison of printer performance in x- and y- directions	61
4.18	Printer resolution performance with improved configuration	62
4.19	Layer alignments tests	63
4.20	Surface properties of Mitsubishi and Semigloss papers	65
4.21	Surface properties of Ultragloss and JoJo Waterproof papers	65
4.22	Comparison of printed silver on different paper types	67
4.23	Surface characteristics of silver printed onto Mitsubishi and Semigloss paper	68
4.24	Surface characteristics of silver printed onto Ultragloss and Waterproof paper	69
4.25	Viscosity calibration tests	71
4.26	Viscosity tests of PEDOT:PSS dilutions	72
4.27	Printed PEDOT:PSS blocks on paper	73
4.28	Thickness of PEDOT:PSS printed on paper	74
5.1	Proposed transducer layout	78
5.2	Configuration of measurement circuit	81
5.4	Verification of measurement electronics function	83
5.5	Silver/Silver chloride gate electrodes	84
5.6	Electrolyte wells	84
5.8	Water contact angle comparison of before and after photoresist coating	86
5.9	Comparison of water resistance with and without photoresist treatment	86
5.10	Manufactured transistors	88
5.11	Currents through Transistor for drain voltage sweeps over time	89
5.12	(a) Output curve and (b) Reverse transfer curve for manufactured transistor	90
5.13	(a) Current vs. gate voltage sweep (b) and Transconductance vs. gate voltage	91
5.14	Fluorescent microscopy image of APTES functionalised PEDOT:PSS, labeled with FITC	92
5.15	(a) Current vs. gate voltage sweep (b) and Transconductance vs. gate voltage of transistors manufactured with high-PVA content before APTES treatment	93
5.16	Transfer curves for transistors with high PVA content after APTES treatment	94
5.17	Transfer curves for transistors with high PVA content after FITC addition	95
5.18	Verification of sensor principle by addition of FITC to functionalised transistors	95
6.1	Final transistor configuration with electrolyte well attached	99
6.2	Effect of PBS addition and removal on transistor function	100
6.3	Larger electrolyte wells for final experiment	100
6.4	Series resistance before APTES functionalisation	101
6.5	Negative control tests results, current over time	102
6.6	Raw measurement data for test 4 - concentration = $10 \mu\text{g}\cdot\text{ml}^{-1}$	104
6.7	Raw measurement data for test 25 - concentration = $0.31 \mu\text{g}\cdot\text{ml}^{-1}$	104
6.8	Raw measurement data for test 56 - concentration = $0.078 \mu\text{g}\cdot\text{ml}^{-1}$	105
6.9	Comparison of absolute current change over time	105
6.10	Normalised change in current over time	106
6.11	Plot of average response time over concentration	107
8.1	Proposed bridge configuration circuit	119

List of Tables

2.1	Comparison of commercial biosensor platforms	13
2.2	Selected examples of semiconducting polymers	24
3.1	Dilution series	44
4.1	Summary of resolution test results	62
4.2	Summary of parameters for printing	63
4.3	Paper types chosen for comparison	64
4.4	Calculated surface roughness for paper samples	66
4.5	Calculated surface roughness for silver on paper samples	69
4.6	Initial polymer ink dilutions	72
4.7	Refined Polymer Ink Dilutions	73
5.1	Average series resistance of printed transistors	87
6.1	Number of functional transistors per concentration test	103
6.2	Average response time per concentration	107
6.3	Cost estimation for sensors	109

Nomenclature

Variables

V_{dd}	Drain supply voltage	[V]
V_{gg}	Gate supply voltage	[V]
V_{sd}	Source-drain voltage	[V]
V_{sg}	Source-gate voltage	[V]
gm	Transconductance	[S]

Abbreviations

AMR	Antimicrobial Resistance
WHO	World Health Organisation
OECT	Organic Electrochemical Transistor
CRP	C-reactive Protein
PCT	Procalcitonin
MxA	Human Myxovirus Resistance Protein-A
ELISA	Enzyme-linked Immunosorbent Assay
SPR	Surface Plasmon Resonance
MRSA	Methicillin Resistant Staphylococcus Aureus
TRIAL	TNF-related apoptosis-inducing ligand
IL-8	Interleukin-8
HRP	Horseradish Peroxidase
TMB	3,3',5,5'-Tetramethylbenzidine
HbA1c	Hemoglobin A1c
HDL	High-density Lipoproteins
TSH	Thyroid Stimulating Hormone
IP-10	Interferon gamma-induced protein 10
DNA	Deoxyribonucleic acid
RNA	Ribonucleic acid
IgA	Immunoglobulin A
IgM	Immunoglobulin M
IgD	Immunoglobulin D
IgE	Immunoglobulin E
QCM	Quartz Crystal Micro-balance
E.coli	<i>Escherichia coli</i>

PVA	Polyvinyl Alcohol (Polyethylene Glycol)
GOPTS	3-Glycidyloxypropyl) trimethoxysilane
APTES	(3-Aminopropyl) triethoxysilane
CIJ	Continuous Inkjet
DOD	Drop-on-demand
HP	Hewlett-Packard
CD	Compact Disc
RFID	Radio-frequency Identification
BS ³	Bis(sulfosuccinimidyl) suberate
NHS	N-Hydroxysuccinimide
PEDOT	Poly(3,4-ethylenedioxythiophene)
PSS	Poly(styrene sulfonate)
PEDOT:PSS	Poly(3,4-ethylenedioxythiophene): Poly(styrene sulfonate)
BSA	Bovine Serum Albumin
DC	Direct Current
AC	Alternating Current
DAQ	Data Acquisition System
NI	National Instruments
PBS	Phosphate-buffered Saline
PMMA	Poly(methyl methacrylate)
GIMP	GNU Image Manipulation Program
AFM	Atomic Force Microscopy
DMSO	Dimethyl Sulfoxide
EtOH	Ethanol
PGMEA	Propylene Glycol Monomethyl Ether Acetate
FITC	Fluorecein Isothiocyanate
FDA	Food and Drug Administration
MSD	Mesoscale Discovery
P3HT	Poly(3-hexylthiophene)
PDDT	poly(4,4'-didecylbithiophene-co-2,5-thieno[2,3-b]thiophene)
Poly-dpot	poly-(3,3"-dipentoxy-2,2:5,2"-terthiophene)
Poly-dt	poly-(3,3"-didodecyl2,2:5,2-terthiophene)
PTAA	Poly[bis(4-phenyl)(2,4,6-trimethylphenyl)amin
PEDOT:TOS	poly (3,4-ethylenedioxythiophene):toslate
TIPS-pentacene	6,13-triisopropylsilylethynyl-pentacene
PBDT(T)TPD	benzo[1,2-b:4,5-b]dithiophene (BDT) copolymerized with thieno[3,4-c]pyrrole-4,6-dione (TPD)
P(NDI2HD-T)	poly[[N,N-bis(2-hexyldecyl)-naphthalene-1,4,5,8-bis(dicarboximide)-2,6-diyl]-alt-5,5-thiophene]
PTCDI-C8	N,N-dioctyl- 3,4,9,10-perylene tetracarboxylic diimide

P(NDI2OD-T2)
poly([N,N0-bis(2-octyldodecyl)- naphthalene-1,4,5,8-bis(dicarboximide)-
2,6-diyl]-alt-5,50-(2,20- bithiophene))

Chapter 1

Introduction

The aim of this document is to provide an account of a project that set out to develop a biosensor transducer capable of aiding primary healthcare professionals in distinguishing between bacterial and viral infections. The aim of this project was to develop a transducer that could detect the presence, and measure the concentration of a protein that has been determined to be relevant to distinguishing between bacterial and viral infections, towards the growing problem of antimicrobial resistance.

1.1 Background and Motivation for Study

As defined by the World Health Organisation, antimicrobial resistance (AMR) is the development of resistance by a microorganism to the antimicrobial drugs that were once used to treat infections by that organism.

Antimicrobials and their use as treatments for various illnesses have become ubiquitous in the current era of healthcare, but this wide use might also be the cause of them eventually losing their place as mankind's first line of defence against microbial infections. It has long been documented that overuse of antimicrobials will inevitably lead to resistance against these treatments [1]–[3], but we have nonetheless been surprised to find that many species of bacteria have already become immune to recently developed substances [4]. Many strategies to address the issue have been suggested, but very few have been implemented, although countries worldwide are beginning to organise themselves to take action against the problem [5], [6]. It falls to organisations such as the World Health Organisation (WHO) to set guidelines and policies to direct future use of antimicrobials [7] and act as stewards of the world's antimicrobial arsenal by coordinating worldwide efforts in this cause.

Evolution is the main mechanism by which microbes obtain resistance, and is aided by their rapid rate of reproduction. This is worsened by indiscriminate use of antimicrobial substances, effectively breeding bacteria to become resistant to these substances. It is unfortunately impossible to stop the process completely, but it can be slowed. Two of the most promising current methods of addressing this problem are to intelligently manage the use of antibiotics and apply them only where absolutely necessary, and to preferentially use highly specific antibiotics and avoid use of broad-spectrum treatments when at all possible [7], [8]. These two methods alone will necessitate the development of new

technologies and techniques with which to determine the cause of an illness, as the current battery of tests required to do so is still inaccessible to many due to the high price and limited availability of such tests.

Recent developments in the field of biosensors and electronics, such as the emergence of novel transistor-based sensors [9], [10] have shown that it is possible to create specific and sensitive sensors from relatively simple and inexpensive materials. Further development and optimization of these types of sensors could conceivably be used to complement the ongoing research into clinical biomarkers for early detection and identification of infection, to eventually reduce unnecessary use of antimicrobial drugs.

The investigation done during this project was aimed towards developing a low-cost implementation of a paper-based organic electrochemical transistor biosensor with which the concentration of certain blood-borne proteins could be quantified, to aid in the differentiation between bacterial and viral infections and in so doing contribute towards reducing unnecessary use of antimicrobials.

1.2 Objectives and Goals

The overarching goal of this project was to develop a low-cost, paper-based transducer for biosensor applications that can eventually serve to aid in the differentiation between bacterial and viral infections. This would then contribute towards antimicrobial stewardship and potentially reduce the rate at which antimicrobial resistance increases locally.

Objectives for the project were set according to the three stages of transducer development: First, a method was developed to manufacture the basic transducer and validate its function. Second, the transducer was functionalised and the functionalisation process was validated. Lastly, the transducers were tested and evaluated for their intended function.

1.3 Thesis Overview

This thesis consists of three primary sections, regarding the manufacture, functionalisation and evaluation of the transducer.

Chapter 2: This chapter contains an overview of the literature studied during the completion of this project. It starts with a study of biomarkers that have been identified as relevant to distinguishing between bacterial and viral infections, eventually choosing one to act as target for the transducer. Next, an in-depth study is done on the definition, function, applications and functional principles of biosensors. Further study is then done on the functional principles of Organic Electrochemical Transistor (OECT) - based transducers, and different manufacturing techniques for such sensors are studied. Finally, a study is done on functionalisation techniques for biosensors, and a proposed sensor design for the project is put forth.

Chapter 3 encompasses a roadmap for the project, and provides in-depth information of the methods used to complete the different steps of printer development, transducer

development and transducer evaluation.

Chapter 4 documents the process followed in development of an ink-jet printer with capabilities that would aid in the development of OECT-based transducers.

Chapter 5 contains a detailed account of the process followed to develop OECTs, and documents the process by which the transistors are functionalised with biorecognition elements.

Chapter 6 is an account of the final experiments and tests done to verify the transducers' functionality and also shows the results for protein detection.

Chapter 7 provides a discussion of the results obtained in the preceding chapters, and assesses the applicability of the developed transducers for their intended purpose. Finally, chapter 8 provides a summary of the whole project and delivers final remarks on the work done. A perspective on future work is also given and possible solutions are suggested to improve future projects in this field.

Chapter 2

Literature Review

The purpose of this chapter is to provide a review of the literature relevant to this project. First, a study was done to identify the biomarkers that have been shown to have promise in distinguishing between bacterial and viral infections. Three biomarkers were found: human myxovirus resistance protein-A (MxA), Procalcitonin (PCT) and C-reactive protein (CRP). CRP was chosen as the target for this project. Following biomarker identification, a study was done on the fundamental concepts of biosensors. An initial study was done on biosensor mechanisms to determine which mechanism would be most appropriate to the paper-based application of this project. After having chosen an electrochemical sensing mechanism, the subsequent choice was made to develop an organic electrochemical transistor-based biosensor. Therefore a study was done on OECT-based biosensors and their manufacturing methods. Next, the choice was made to manufacture the transducer by inkjet printing, and a study was done on inkjet printed electronics and sensors. Finally, based on the literature already reviewed, it was decided that a covalent method of antibody immobilisation would be used in this project, and an initial transducer design was proposed.

2.1 Introduction

The problem of antimicrobial resistance (AMR) has in recent years become more prominent due to the increased rate at which microbes develop resistance to the substances used to treat the infections they cause.

The history of antimicrobial resistance is almost as long as that of formal antimicrobials and instances of resistance have been documented almost immediately after discovery of the first widely accepted antimicrobial substances [3], [11]. The mechanism by which AMR is achieved is twofold [11], [12]: firstly due to increased selective evolutionary pressure, where bacterial strains that are naturally resistant to certain types of antibiotics have a tendency to survive such treatments and reproduce, and secondly by transference of resistance traits between different strains of bacteria through exchange of genetic material - in the form of plasmids¹ or by activity of bacteriophages².

¹Free-floating circular units of DNA that provide bacteria with genes that often only have benefits in specific situations.

²Viruses that only infect bacterial cells.

Penicillin was discovered in 1929 by Alexander Fleming [13] and was the first commonly accepted antibiotic substance known to man, but it had already been noted before this that bacteria could become resistant to environmental toxins through long-term exposure [11]. This however went largely unnoticed in the general excitement over the new wonder-drug that was the start of modern medicine. Antibiotics and other antimicrobials were consequently used in every field where it was thought to be advantageous, but most prominently in agriculture and human healthcare. It was later observed by Neu [1] and Witte [2] that this wide and uncontrolled use of antimicrobials had led to bacteria developing resistance to the antibiotics previously very effective in their treatment.

The strains that had developed resistance by ± 1990 included species from *mycobacteria* (Tuberculosis), *pneumococci*, *staphylococci* and *enterococci*, which are still common causes of infection today due to the resistance traits they developed in the past and continue to develop against new types of antibiotics.

2.1.1 Current State of AMR

The current state of antimicrobial resistance is deteriorating. Many of the most common species of bacteria have been found to have developed resistance to multiple types of antibiotics, such as the cases of *mycobacterium tuberculosis* and methicillin-resistant *staphylococcus aureus* (MRSA) that have become resistant to almost all current types of antibiotics [5].

At least 43 countries around the world currently have monitoring programs to keep track of the state of AMR [14], [15]. A recent study by Tadesse *et al.* [16] found that there was widespread resistance to most current antibiotics in many African countries. Wi *et al.* [17] and Wang *et al.* [18] also report that high degrees of resistance to antibiotics was found in *Neisseria gonorrhoeae* and *Salmonella enterica*, respectively, which were until very recently treated with relative ease.

The rapid overall increase in antibacterial resistance has been noted by the WHO, who have begun to develop guidelines and policies to help manage the use of current antibiotics [7], guide the development of new antibiotics [19] and direct development of new methods to decrease the rate at which resistance is developed against new antibiotics [7].

The currently suggested management strategy for AMR is antimicrobial stewardship, which entails the development of novel, highly targeted, antimicrobial substances, alongside development of novel detection and quantification methods to identify infection sources before treatment commences [7], [19]. Part of this strategy is therefore the development of novel biosensing applications aimed at identifying and distinguishing between different sources of infection, particularly bacterial and viral infections due to their making up the bulk of human infections [8]. However, it is currently unknown whether there is a biomarker, or pair of biomarkers, that can be used to identify the source of an infection, apart from directly detecting the cause of an infection, which would require an almost infinite number of sensors to be developed.

Therefore it must first be determined which biomarkers are relevant to the task of distinguishing between viral and bacterial infections, by studying the existing literature published on these subjects, before a sensor can be developed to do so.

2.2 Biomarkers

According to the WHO, a biomarker is defined as “any substance, structure, or process that can be measured in the body or its products and influence or predict the incidence of outcome or disease”[20]. This means that biomarkers are objective measurements of a persons health, and may not necessarily reflect their experience thereof [21]. Many possible biomarkers exist, most of which are irrelevant to the determination being made, for example whether a patient has a bacterial or viral infection. These biomarkers may include proteins, cells, enzymes, metabolites or ions concentrations, to name but a few. Recent studies have focussed on using blood-borne proteins [8], [22] as possible markers for the differentiation between sources of infection due to their close interaction with the human immune system, and specific attention has been given to biomarkers that are known to fulfil a role in the human immune response. The human immune system is able to recognise a pathogen and react accordingly - the aim of biomarker research is to learn to interpret these reactions and determine what the immune system is reacting to when faced with symptoms that may be caused by any number of pathogens.

2.2.1 Current Biomarker Research

Many studies have attempted to determine which biomarkers are relevant to distinguishing between bacterial and viral infections, as shown by Kapasi *et al.* [22], listing as many as 112 different proteins and other substances have been used in attempts to find combinations that provide the necessary specificity and sensitivity to allow effective differentiation between different types of infection. This is an area of ongoing research and it is not the focus of this project to determine the specific difference between types of infections, but to rather identify biomarkers that may have practical value based on published findings.

According to Kapasi *et al.* [22], the published literature can be divided into several distinct groupings of biomarkers: Blood cells and haematologic markers, inflammation markers, cytokines, cell surface markers, metabolic activity markers and other host biomarkers, mostly blood borne proteins not contained in the other groups. Of all the publications reviewed by Kapasi *et al.* [22], only nine biomarkers achieved a specificity and sensitivity of $\geq 85\%$ for the identification of bacterial infections. The list of potential biomarkers from Kapasi *et al.* [22] is: Heparin binding protein, CRP, IP-10, TRIAL, Lactate, procalcitonin, gene classifiers, MxA, IL-4, CD35, CD32, CD8 and MHC1. However, most of the studies done regarded a single biomarker in isolation. The most prominent of the studies reviewed by Kapasi *et al.* [22] was a series of studies that combined sets of host biomarkers to gain a better understanding of the interaction between different components of the immune system. This result is expected, and it seems intuitive that multiple biomarkers would be necessary to accurately describe the complex function of the human immune system. Of particular interest in the review by Kapasi *et al.* [22] is that a commercially available point-of-care assay was found to be very effective in distinguishing between bacterial and viral infections. The FebriDx test developed by Rapid Pathogen Screening Inc, which uses a combination of CRP and MxA in a lateral flow assay format to provide qualitative information on CRP and MxA threshold levels [23].

Further study of the literature suggests that combinations of several well-known and novel biomarkers may be of clinical value to diagnosing bacterial or viral infections. The protein known as MxA, or human myxovirus resistance protein-A, has been shown by

Chieux *et al.* [24] to be an indicator of viral infections in children presenting with ambiguous symptoms. Likewise, MxA has been shown by Sambursky and Shapiro [25] to be very effective in discriminating between bacterial and viral infections when combined with a semi-quantitative CRP measurement, although CRP was not found to be effective when considered on its own.

Another marker that has shown promise is PCT, or procalcitonin, and it has been shown to be highly specific to bacterial infection on its own [26], and has been used for many years to effectively diagnose bacterial infections [8], including in combination with IL-8 and CRP [27].

The results from the literature seem to indicate that CRP, PCT and MxA are well-suited to be used in combination with one another to distinguish between bacterial and viral infections. Other biomarkers or combinations of biomarkers do exist that would fulfil the same role, such as the combination of TRIAL, CRP and IL-8 [27], but some of these have already been implemented in proprietary systems, as will be discussed later..

2.2.2 Current Methodologies of Biomarker Detection

The following is an overview of some of the more prominent methodologies for the detection and quantification of biological species, and are specifically used to distinguish between bacterial and viral infections by measuring the proteins or biomarkers that have been identified as promising in this regard. Following this investigation, a review is done to compare three current commercial biosensor platforms, aimed towards distinguishing between viral and bacterial infection.

2.2.2.1 ELISA

The enzyme-linked immunosorbent assay, or ELISA, is an assay that makes use of antibodies to recognise the presence of biological substances [28], and is currently one of the golden standard tests available for pathological tests. The ELISA test is usually done in one of four variants on the structure, but all incorporate the characteristic colorimetric amplification strategy that gives it its name. This is done by attaching an oxidising molecule, usually horseradish peroxidase (HRP) to an antibody that binds to the molecule that is of interest. A substrate, such as 3,3',5,5'-Tetramethylbenzidine (TMB) for a blue colour, is then added to the dish, and the HRP causes a colour change directly proportional to the concentration of HRP present on the surface of the assay plate, which is in turn determined by the original concentration of the analyte by affecting the number of conjugated antibodies present on the plate.

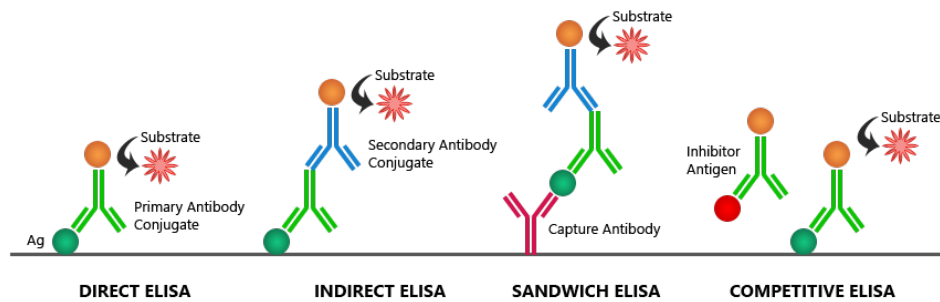


Figure 2.1: Schematic representation of ELISA processes [from [29]]

The direct ELISA is the simplest of the four, and directly adsorbs the analyte to an assay dish, usually agarose or something similar, and then uses a detection antibody conjugated with HRP to activate the colour changing substrate. This approach, however, has a distinct disadvantage in that it is not guaranteed that the molecule of interest will be adsorbed to the assay dish, and the measured concentration may not be truly reflected in the result of the test.

The indirect ELISA is similar to the direct ELISA, with a single difference - the detection antibody is not conjugated with HRP, but left unchanged. A secondary antibody is rather used to bind with the detection antibody, and this secondary antibody is conjugated with HRP. The indirect ELISA has higher sensitivity than direct ELISA due to more than one secondary antibody being able to bind to a primary detection antibody, thereby amplifying the signal from the binding event. Conversely the disadvantage of using indirect ELISA is also due to the secondary antibody - it may bind directly to the adsorbed antigen and in so doing add background noise to the measurement [30].

The third, and most commonly used, type of ELISA is the sandwich-type ELISA. This assay uses two antibodies, one for capture and the other for detection, to bind to either side of the target analyte. The capture antibody is bound to the assay dish, often by adsorption, and used to capture the target molecules when they are added to the dish. The detection antibody, either unconjugated or with HRP attached, is then added to bind to the opposite end of the target molecule than the capture antibody. This combination of antibodies makes the sandwich ELISA highly specific and sensitive, as the likelihood of nonspecific bindings taking place is drastically reduced, while the background noise is also lowered [29]. The disadvantage of the sandwich ELISA is that it is often labour intensive to optimise the combination of antibodies necessary to perform the assay, as many iterations must be done with different combinations of antibody clones to determine the binding affinity and epitope of each antibody and antibody pair.

The competitive-format ELISA is the most complex of the four, and is used to identify the presence of unknown antigens. This is done by allowing a competitive reaction to take place between the one analyte and another pre-bound to an antibody. First, the first analyte is incubated with its antibody, which is left unconjugated. The other analyte is then adsorbed on an assay dish, and washed. The first antigen-antibody pair is then added to the second dish to adsorb onto the surface in a competitive reaction, after which a second antibody is added, to which HRP is conjugated, to bind to the unlabelled analyte.

The ELISA format tests are incredibly versatile and have been adapted to use colorimetric, fluorescent and chemiluminescent detection methods, and are used in the detection of proteins [31], cells [32], viruses [33], antibodies [34] and other mostly biological materials [35], [36].

Companies such as Synexa Life Sciences [37] and PathCare [38] extensively use ELSIA-style assays in a variety of applications, and the principle often forms the basis of much of their business.

2.2.2.2 Surface Plasmon Resonance

Of the commercially used detection technologies, surface plasmon resonance (SPR) is another widely used methodology [39]. The working principle of SPR is concerned with optical reflectance and transmittance, as illustrated in Figure 2.2. The SPR sensor consists of three main regions. The first region consists of a dielectric region, through which a light source is directed at the sample region. Between the sample region and the dielectric region lies a thin layer of metal, through which the surface plasmon interaction is generated. Past the metal layer is the sample layer, where biorecognition elements such as antibodies or DNA probes are immobilised for detection [40].

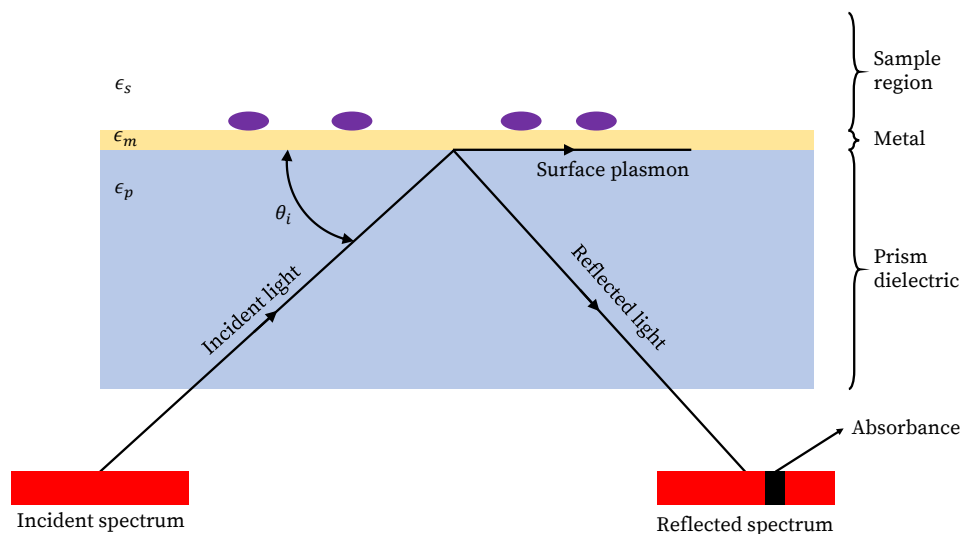


Figure 2.2: Illustration of SPR Principle [based on [39], [41]]

SPR functions on the principle of a TM-polarised electromagnetic surface wave, the surface plasmon polariton, that travels parallel to the surface interface at a change in material dielectric constant [39]. The magnetic field-vector (not shown) of the surface plasmon is perpendicular to the interface between metal and dielectric.

For the configuration above, the incident light passes through the prism dielectric, changing its amplitude and phase velocity. The wave vector for the light incident on the metal interface is given by

$$k_{in} = \frac{2\pi}{\lambda} \sin(\theta_i) \sqrt{\epsilon_p} \quad (2.1)$$

where θ_i is the incident angle, ϵ_p is the relative dielectric constant of the prism material and λ is the wavelength of the incident light [39]. The surface plasmon is then created as an evanescent wave that decays exponentially beyond the metal interface [42], and the wave vector of the surface plasmon is given by

$$k_{sp} = \frac{\omega}{c} \sqrt{\frac{\epsilon_m n_s^2}{\epsilon_m + n_s^2}} \quad (2.2)$$

where ϵ_m is the relative dielectric constant of the metal film, n_s is the optical index of the sample region, ω is the angular frequency of the incident wave and c the speed of light in vacuum [43].

Resonance between the incident wave and the surface plasmon is then achieved when the wave vectors of the incident wave and the surface plasmon are equal [43], and the result is an absorbance line in the reflected spectrum. For such resonance, a specific k_{sp} exists for each combination of materials and light frequencies, and the resonant point can be found by adjusting the angle of the incident wave, θ_i .

The absorbance line in the reflected spectrum is then directly dependent on the specific dielectric properties of the material in the sample region immediately adjacent to the metal interface. This sensitivity is such that small variations, for example proteins adsorbing to the surface, can change the wavelength at which the absorbance line occurs. This phenomenon is then exploited to create highly sensitive sensors.

SPR systems are commercially produced by companies such as BioNavis [44], FortéBio [45] and Biosensing Instruments [46], to name a few. These companies produce equipment capable of quantifying analytes varying from DNA-based assays to whole cells and biofilms.

2.2.2.3 Commercial Biosensing Platforms

Three commercial products have been recently developed to either distinguish between bacterial and viral infections at the point of care, or to perform analysis of some of the associated biomarkers as a desk-top device. The companies of Rapid Pathogen Screening Inc., MeMed Diagnostics Limited, and Abionic SA were investigated to determine whether their methodologies could serve as a point of reference for this project.

The first test reviewed is the FebriDx, which consists of a pair of lateral flow assays to detect whether MxA and CRP are above certain thresholds, shown in Figure 2.3. Lateral flow assays are methods of applying a sandwich-type assay, similar to an ELISA, in a manner that happens without the need for human interaction between processing steps.

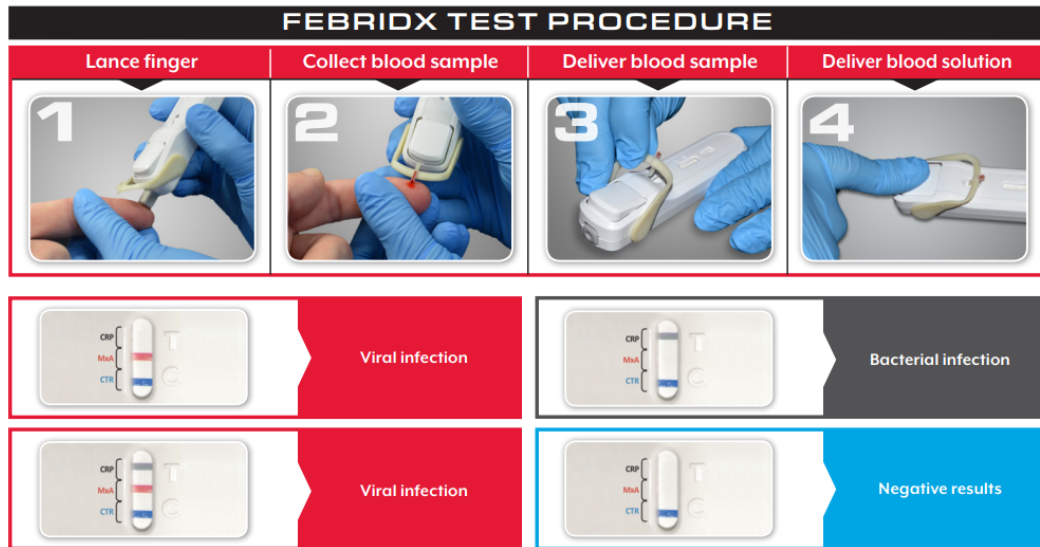


Figure 2.3: FebrIDx product information [from [47]]

The test uses a fingerprick blood sample, which is then drawn into the lateral flow assay, illustrated in Figure 2.4.

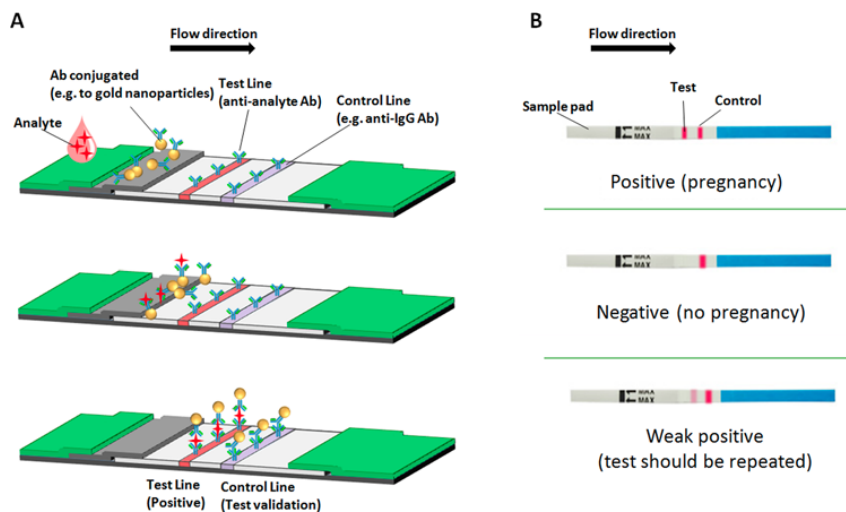


Figure 2.4: Standard lateral flow assay illustration [from [48]]

The blood sample is drawn into the assay strip, across a region impregnated with detection antibodies for MxA and CRP that are conjugated with some dye - in this case red and blue, respectively. The sample is then drawn past a region where capture antibodies targeted to the detection antibodies are immobilised - to verify if the test was successful and that the results are valid. Finally, the sample, now with MxA and CRP labelled with conjugated antibodies, are drawn past two more regions with capture antibodies for either protein, where the proteins are bound on a different epitope than the detection antibody. If the proteins are present in sufficient concentrations, the assay strips will change colour according to the marker molecule attached to the detection antibody. The illustration used here is for the ubiquitous pregnancy test strip, which works in the same manner, apart from only testing for a single biomarker, human chorionic gonadotropin (hCG). The

results from FebriDx are purely qualitative and cannot give an estimation of how serious the infection is, although it is fast (10 minutes) and has independently been reported to have a high degree of accuracy [25]. In a clinical study, the test was found to classify negative subjects correctly with 90% accuracy, subjects with bacterial infections with an accuracy of 80% and subjects with viral infections with an accuracy of 70% [25].

Following the FebriDx test is the AbioScope platform, shown in Figure 2.5, which is aimed towards healthcare professionals to perform diagnostic tests at the point of interview, or care. The platform is currently capable of determining concentrations of glycosylated hemoglobin AC1 (HbAC1), high-density lipoproteins (HDL), triglycerides, thyroid stimulating hormone (TSH), and CRP, with a dynamic range of 1 - 700 ng·ml⁻¹.



Figure 2.5: AbioScope product [from [49]]

Rather than determining the difference between viral and bacterial infection, the AbioScope attempts to gauge the severity or progression of infection and whether sepsis has occurred. The platform is reported to use a patented nanofluidics test, and tests consist of a capsule into which a sample is loaded. It is not reported whether the assay is done using a colorimetric, SPR, or other detection method. The capsule is then inserted into a CD-like reader, after which results are displayed on the built-in screen after 5 minutes. The results from AbioScope are given in a quantitative manner, and the results can be interpreted in any number of ways.

The third, and final, commercial platform reviewed is the MeMed Key, which is based on the MeMed ImmunoXpert test, and is shown in Figure 2.6. The platform utilises a chemiluminescent ELISA test to determine concentrations of TNF-related apoptosis inducing ligand (TRIAL), interferon-gamma induced protein-10 (IP-10) and CRP. This test, however, does not use the typical threshold-value method of determining the state of a patient, but rather uses an algorithm to assign a score to the combination of marker levels, from which a determination is then made. The results of this test is both qualitative and quantitative, in that each biomarker value is available, along with the algorithmic score and determination of infection cause. The results of the tests are reported to be available within minutes, although a specific number is not given. The test has been reported to have a sensitivity (positives measured as positive) of 86.7% and a specificity of 91.1% (negatives measured as negative) [50], which is comparable to the results from FebriDx, although the numbers are reported in a slightly different format.



Figure 2.6: MeMed Key platform [from [51]]

Of the three tests reviewed, only two were validated in published clinical trials, and only one of these was done using a double blind, multicentre validation study - MeMed ImmunoXpert/Key[50]. The common factors of the three products are shown in Table 2.1.

Table 2.1: Comparison of commercial biosensor platforms

Name	Markers Measured	Time To Results	Sample Volume	Assay Technology	Readout Type
FebriDx	MxA, CRP	10 min	Fingerprick	Lateral flow assay	Qualitative
Abioscope	HbA1c, HDL (cholesterol), triglycerides, TSH, CRP	5 min	Fingerprick (50 μ l)	Nanofluidic	Quantitative
MeMed Key	TRIAL, IP-10, CRP	15 min	Fingerprick	ELISA (Chemiluminescence)	Quantitative

Other commercial tests of note are ImmunoXpert, the precursor to MeMed Key, and SeptiCyte [52]. SeptiCyte is unique in that it utilises a proprietary combination of RNA parameters to distinguish between a wide variety of infections. Not only can it distinguish between viral and bacterial infections, but it can also identify herpes, protozoa, onset of sepsis and other specific bacterial infections [52]. SeptiCyte was not reviewed in detail due to the unavailability of information regarding the specific biomarkers targeted.

Of the systems reviewed, CRP was the common denominator, present in all but SeptiCyte, which uses a proprietary set of RNA markers. The device with the most thorough documentation and validation procedures was MeMed's ImmunoXpert, and MeMed Key,

with multiple published trials and validations studies. Of the others, only FebriDx was documented properly, and that in only a single published study.

2.2.3 Choice of Biomarker

Due to the nature of this project being a proof-of concept development, a single biomarker was chosen as target for the transducer. The choice was between CRP, PCT and MxA, which were identified as being of potential value, and have been a common theme in a large body of research done into the problem of distinguishing between bacterial and viral infections. The three markers have also been shown to have potential for use on their own, and therefore a test that can quantify or detect any one of them would already of value.

The choice was made to target the transducer to CRP for two reasons. The first is that CRP is a standard test that can be done for a price of R202.7 [38] at certain pathology laboratories (PathCare, Western Cape, South Africa), and it is already widely used as indicator of patient health [8]. As shown previously, CRP is also the common denominator between several tests that have been successful in distinguishing between viral and bacterial infections. This provides a benchmark for the performance and price of the transducer, and potentially allows comparison with industry standards once the transducer has been refined past a proof-of-concept.

Therefore this project developed a transducer aimed at detecting and quantifying concentrations of CRP, as a representative for the other promising biomarkers.

The clinically relevant range of concentrations for CRP, when being used as a means for distinguishing between bacterial and viral infections is in the range of $1 \mu\text{g}\cdot\text{ml}^{-1}$. It is widely held that nominal CRP concentrations for healthy individuals is in the region of $2 \mu\text{g}\cdot\text{ml}^{-1}$. Values of CRP higher than this value would then be indicative of some form of infection being present, and studies have used threshold values of $10 \mu\text{g}\cdot\text{ml}^{-1}$ and $125 \mu\text{g}\cdot\text{ml}^{-1}$ to guide diagnostic decisions [22], with the lower threshold used to classify bacterial infections and the higher to determine the onset of sepsis. It would therefore be necessary for a sensor developed for this purpose to be sensitive to the presence of the target protein in this general range of concentrations, or for significantly lower concentrations to allow for sample dilution and preprocessing.

2.3 Biosensor Definition

As defined by the Collins dictionary, a biosensor is “a sensor device for detecting and measuring very small quantities or changes in a biochemical or chemical substance, in which a microelectronic component registers reactions related to the substance and translates them into data”[53]. This definition immediately implies that a biosensor consists of two parts: a transducer that translates biological or biochemical reactions to electrical signals, and a signal processing component that translates electrical signals to data or information. This definition can be expanded further, as the transducer and signal processing components are themselves composed of multiple units [54]. The transducer usually consists of a combination of a biorecognition element and an electronic transducer. The signal processing part also consists of multiple components, namely an amplification stage fol-

lowed by quantization and interpretation. Figure 2.7 shows a schematic representation of a biosensor.

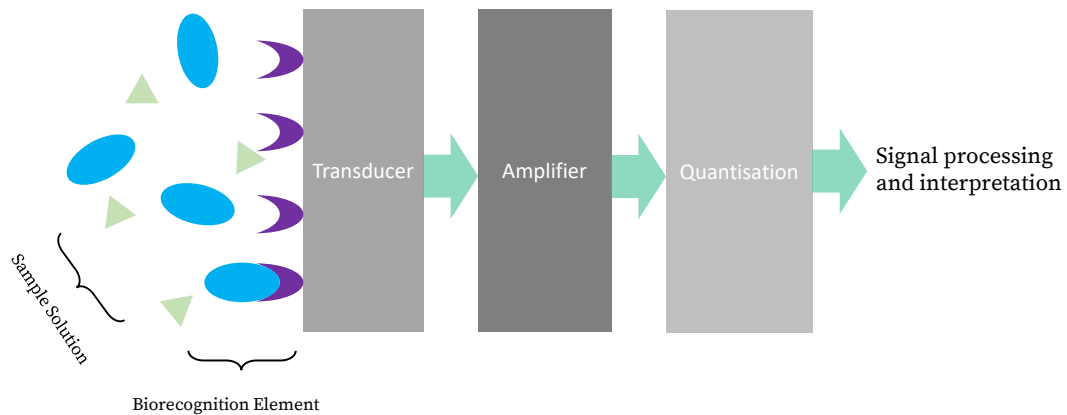


Figure 2.7: Schematic diagram of biosensor function

Such a sensor operates on the principle that a binding event between the biorecognition element and target analyte will cause a detectable change in the output signal from the transducer, which will then be amplified, quantified and used to measure the concentration or presence of the target analyte in solution after signal processing.

Biorecognition elements are typically immobilised onto the transducer, or attached to its surface in some manner, to allow effective transmission of a binding event. Many different types of biorecognition elements exist, such as antibodies, DNA, RNA, aptamers and peptide complexes, to name but a few. These molecules are designed or manufactured to react only with a highly specific target substance.

The transducers in biosensors can be designed to measure changes in light, electrical charge, mass, temperature, the presence of specific ions, or physical size, amongst others. This means that the potential applications for biosensors are practically limitless, as each combination of transducer, biorecognition element and signal processing method would have different advantages in specific scenarios.

When considering the basic layout of a biosensor, one can classify each in terms of two parameters: the type of biorecognition element, and the transducer type. Three types of biorecognition elements were found to be relevant to distinguishing between bacterial and viral infections: Antibodies, DNA and RNA probes, and aptamers. It was also found that there exists four main types of transducer mechanisms: optical, piezoelectric, impedimetric and electrochemical, although each of these can be divided into further subtypes. Studies were done to determine which choice of biorecognition element and transducer would be most suited to distinguishing between viral and bacterial infections by measuring concentrations of CRP.

2.4 Biorecognition Elements

The first component that should be chosen when developing a biosensor is the biorecognition element, as it will determine the transducer mechanism that can be utilised to convert a recognition event to an electrical signal. A short study was done on the different types of biorecognition elements, which can be divided into antibody-based sensors, DNA-based sensors, RNA-based sensors and aptamer-based sensors.

2.4.1 Antibodies

Antibody-based sensors are one of the most common types of sensors, and are in wide use. Antibodies, or immunoglobulins, form part of an organism's self-defence mechanism, and are both recognition elements that notify the rest of the immune system of foreign materials, and an active part of the immune system that kills or neutralises certain substances. This means that antibodies have a high affinity for the substances they bind to, and this property is what biosensors exploit when using antibodies as biorecognition elements. Several types of antibodies exist, shown in Figure 2.8, such as the isotypes of IgG, IgM, IgA, IgD and IgE [55]. All of these molecules fulfil a function in the body's immune response, but one specific isoform is of particular interest to the field of biosensors: IgG.

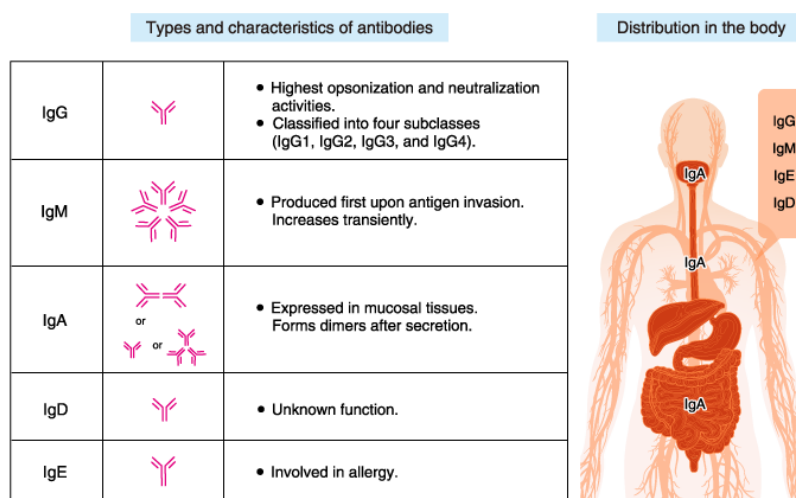


Figure 2.8: Antibody types and distribution [from [55]]

IgG isoforms of antibodies are divided into four groups, with specific functions, but all of these are of use to biosensors due to the high affinity that IgG molecules have for their target antigens.

IgG antibodies can also be easily immobilised onto sensor surfaces to act as biorecognition elements due to their convenient structure - the two ends of the “Y” structure, or Fab region, bind to antigens, while the stem, or Fc region, can be used to attach the molecule to the sensor surface [56].

Antibody based sensors have been used to detect almost any antigen imaginable, but predominantly focus on detection of bacterial cells [56], such as *E. coli*, or proteins [56], [57] due to the nature of the animal immune system more easily binding to epitopes on

biological substances.

The advantages of antibody-based sensors are their relative simplicity and versatility, due to the passive nature of antibody-antigen interactions and it being possible to tailor-make highly specific and sensitive antibodies to target almost any substance. Conversely, the main disadvantage of antibody-based sensors is that their sensitivity and selectivity makes them susceptible to small changes in target epitope expression, and changes in environmental factors that affect the target organism or material can render them obsolete [56]. Antibodies also have the disadvantage that they do not readily react with substances that do not cause an immune reaction, making it difficult or even impossible to create antibodies for such antigens [58].

2.4.2 DNA and RNA Probes

DNA-based biosensors utilise strands of DNA immobilised onto the sensor surface to detect complementary strands of DNA. This is, however, misleading, as the specific type of DNA that can be immobilised must take one of two forms to act as biorecognition element. The first group of sensors that use DNA make use of single-stranded DNA, or ssDNA, to identify the presence of complementary strands of oligonucleotides in a sample [59]–[61] by signalling a change in surface properties upon a binding event taking place, such as the example shown in Figure 2.9 [62].

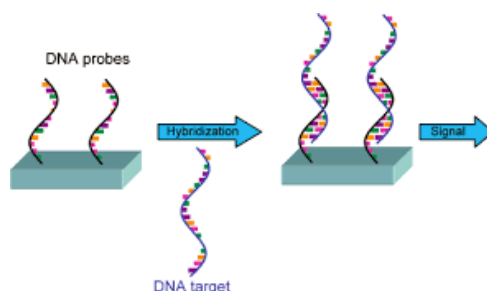


Figure 2.9: ssDNA Biosensor schematic [62]

The second group of DNA-based sensors utilise DNA hairpin probes, which are DNA strands containing self-complementary regions that are folded back onto themselves to form a structure strikingly similar to a hairpin. The hairpin structure is usually used to conceal a signalling molecule, for example a fluorescent marker or redox probe, while the probe remains unbound. The signalling molecule then serves as an amplifier when a binding event takes place, greatly improving the sensitivity of such sensors [63], [64]. An example of such a reaction is shown in Figure 2.10 [65]. Both ssDNA and hairpin-probe sensors have been used to detect the presence of bacterial DNA [63], tuberculosis [66] and HIV DNA [67].

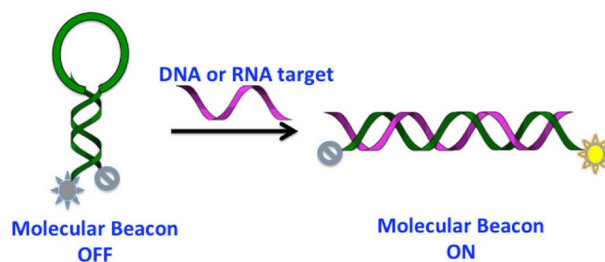


Figure 2.10: Schematic of hairpin probe function [from [65]]

The main disadvantage of DNA-based biosensors is that the reaction between DNA strands is temperature mediated, and a very specific temperature cycle is necessary for hybridisation to take place. This added layer of processing increases the complexity of the sensor and introduces room for errors to take place. These DNA-based sensors are however highly effective due to the high sensitivity and specificity of the biorecognition element. DNA-based sensors can often also quantify base pair mismatches, where a strand of complimentary DNA, with a few nucleotides not matching the probe exactly, has bound to the probe. This means that DNA as a biorecognition element is very versatile, and may potentially be used to track mutations in target DNA sequences [68] - for example in HIV.

RNA-based sensors work on the same principle as DNA-based sensors, in that either a single strand of RNA or a hairpin probe can be immobilised onto the sensor surface to bind to a targeted complementary strand under the right conditions, in a similar manner to Figures 2.9 and 2.10 [69], [70].

2.4.3 Aptamers

Aptamers are oligonucleotide-based biorecognition elements, similar to RNA and DNA, and consist of chains of oligonucleotides that have been folded into a shape that recognises and binds to a specific target molecule. They are sometimes referred to as synthetic antibodies. Aptamers can also be divided into RNA and DNA aptamers, based on the specific oligonucleotides involved [71].

These chains of oligonucleotides have been identified to bind to proteins, peptides, amino acids, drugs, metal ions and cells, and can be targeted to almost anything. Aptamers have the advantages over natural receptors, such as DNA and antibodies, that they can be selected for very high selectivity and specificity and can be reproduced at large scale once the refinement process has been selected [71]. They are also largely free of the difficulties faced in DNA or antibody production - reliance on animals, variation between batches and temperature sensitivity [58].

Aptamers have been widely used as biorecognition elements in biosensors, including for the detection of endotoxin [72], prostate specific antigen(PSA) [73] and arsenic [74], to name but a few.

2.4.4 Choice of Biorecognition Element

Following the study of the applications of the different classes of biorecognition elements, and comparison of their manufacturing and immobilisation methods, it was decided to

utilise antibodies for the transducer developed in this project. DNA/RNA probes were excluded due to their not being compatible with binding to proteins, such as CRP. Aptamers, while very versatile, sensitive and easy to use, require specialist knowledge of biochemistry to produce, and they were deemed to be outside the scope of this project.

2.5 Transducer Mechanisms

The mechanisms by which biosensor transducers detect changes can be divided into three main categories: optical biosensors, electrochemical biosensors and piezoelectric biosensors. A short study was done to determine the working principle and applications of each, so as to effectively compare the relative advantages and disadvantages of each. Following this study, it was decided to develop an organic electrochemical transistor (OECT)-based transducer, and further study was done on the method of operation and fabrication of OECTs.

2.5.1 Optical Biosensors

Optical biosensors are concerned with light - either intensity, colour (wavelength) or phase, generated or changed in a number of ways.

Optical biosensors can be roughly divided into two groups: enzymatic and immunosensors. The enzymatic family of sensors are concerned with detecting changes in colour, optical permittivity or fluorescence due to a chemical reaction mediated by an enzyme, which then stimulates any of the previous mechanisms, or combinations thereof. The family of immunosensors utilise antibodies to bind targeted material to the surface of a substrate, and in so doing causes a change in reflectance, transmittance or some other parameter of the substrate [75]. SPR-based sensors would be a good example of such an optical sensor, where the intensity of reflected light and the wavelength of the change in intensity is dependent on the number of molecules binding to the biorecognition element.

Optical sensors can be both label-free or utilise labels in their detection strategy. The label-free group are most often enzymatic in nature, where a chemical reaction causes a change in colour or reflectivity that can be measured by the sensor. Variants that utilise a label use antibodies or some form of biorecognition element to label the molecule of interest, and in doing so cause a measurable change in sensor characteristics.

An example of a successful optical immunosensor is given by Aray *et al.* [76]. In this work, the authors construct an SPR-based immunosensor by immobilising anti-CRP antibodies with NHS-EDC chemistry onto the surface of an optical fibre after coating the fibre with a thin layer of gold. The absorbance spectrum for the sensor is then calculated using laboratory light sources and spectrometers, and comparison is made between the spectra before and after protein addition. The limit of detection is given to be $0.009 \mu\text{g}\cdot\text{ml}^{-1}$, with a working range of $0.006 - 70 \mu\text{g}\cdot\text{ml}^{-1}$, which covers the full clinically relevant range for CRP.

The main disadvantage of such optical sensors is that they often require complex and expensive measurement equipment to quantify the very small changes caused by the binding-events. The sensors are also not disposable, nor bio-degradable due to the requirements

for the materials involved. Optical sensors offer high sensitivity and dynamic range while keeping the price per sensor low [42], at the cost of often expensive external components.

2.5.2 Piezoelectric Biosensors

Piezoelectric sensors operate on the principle of converting a force to an electrical signal - piezoelectricity means to convert physical pressure to electrical voltages.

Multiple applications exist for piezoelectric sensors, and the two most common modes of operation are direct-voltage measurement, and measurement of resonant frequency in oscillatory devices [77], [78].

The most often used methodology for piezoelectric sensors by far is the measurement of a shift in resonant frequency due to addition of mass to the transducer [77] - either by use of a quartz crystal microbalance (QCM), or a microcantilever. Antibodies or other biorecognition elements would be immobilised to the sensor surface, changing the sensor resonant frequency, whereafter another change in frequency would be measured upon a binding event taking place with the target molecule. The change in resonant frequency would usually be given by the well-known Sauerbrey equation for QCM sensors [79],

$$\Delta f = -\frac{f^2 \Delta m}{NA\rho_q} \quad (2.3)$$

where f is the fundamental frequency of the quartz crystal, N the frequency constant for the cut crystal and A the area of the crystal. This relation shows that a decrease in resonant frequency will be observed when analyte target molecules are bound to the surface [79]. The change in frequency can be measured in two manners: either the crystal can be integrated into a resonator design, where the output frequency of the resonator is determined by the crystal, or the crystal impedance can be actively measured to determine the resonant point of the equivalent impedance [77]. It has also been documented that QCM sensors have been integrated into signal-mixing circuits, to automatically subtract the baseline frequency from the output frequency of the functionalised transducer, thereby simplifying the measurement process [79].

This type of sensor has been found to be highly versatile and sensitive [80], capable of detecting very low concentrations of analytes both in solution and in atmosphere [77].

Piezoelectric sensors utilising direct voltage measurement utilise the piezoelectric substrate itself as a voltage generator to report small deformations in the material height due to molecules binding to the sensor surface. This can be done by immobilising biorecognition elements to piezoelectric nanowires, often Zinc Oxide (ZnO), where the diameter of the nanowires are small enough to allow the structure to deform from the miniscule weight of molecules binding to the surface [78]. This type of sensor can also be integrated into QCM form sensors to further enhance the sensitivity of their measurements [77].

Applications of these types of sensors include detection of Tuberculosis [81] (microcantilever), detection of immunoglobulins [78] (nanowires) and neutrophils [80] (QCM), to give an example of each type.

These types of sensors, while versatile, low-cost and easy to use, can be challenging to manufacture effectively. The silicon and high-frequency electronics industries have optimised the manufacturing processes for QCM crystals, but the consistent growth of nanowires [78] and microcantilevers [80] remains challenging. The main disadvantage of piezoelectric sensors is the equipment necessary to perform accurate and precise measurements of the transducer parameters - typical operating frequencies are in the 10's of MHz, which is well outside of what can be measured with simple electronics.

2.5.3 Electrochemical Biosensors

Electrochemical biosensors measure a change in sensor due to an electrochemical reaction taking place, which is controlled or initiated by an applied voltage or current through the sensor. These types of sensors typically fall into one of four subsets, depending on the specific reaction taking place and the effect of the reaction on the sensor. These sensors usually consist of three electrodes: the reference, working and counter electrodes [82], and the electrodes are enveloped in an electrolyte solution in which the electrochemical reaction takes place. In a typical electrochemical cell, the voltage is applied to the working electrode, while the counter electrode provides a closed loop for current from the working electrode to flow through. The reference electrode can be used to either provide a reference voltage for the analyte solution, or to measure the potential of the solution.

The specific reaction that takes place in/on the sensor is dependent on the configuration and design of the sensor, but generally the reaction takes the form of electron exchange, electron accumulation, or ion exchange. These three mechanisms correspond to four measurement methodologies typically employed in this field: amperometry, potentiometry, conductometry and field-effect surface-charge measurement [82], [83].

Amperometry is the measure of a change in current due to an electrochemical reaction mediated by an applied voltage. The voltage is used to cause a redox reaction in the electroactive contents of the electrolyte. The voltage applied in this manner is usually kept constant with respect to the reference electrode [83]. If the voltage is not kept constant, but rather varied over time, the measurement of the corresponding current is called voltammetry. In this measurement scheme, the peak current measured for a given potential is directly proportional to the concentration of the analyte in solution, although a redox mediator, such as ferricyanide or ferrocene, may be necessary to allow such a reaction if the analyte is not inherently capable of being electrically reduced/oxidised in the reaction [82]. Amperometry is also known to have greater sensitivity than potentiometry, due to the active nature of the measurement [84]. An example of this would be the ubiquitous blood-glucose sensor used by individuals with diabetes worldwide to measure their blood glucose concentrations. These sensors work by immobilising the enzyme glucose oxidase (GOx) onto the working electrode, which allows the glucose present in a blood sample to be oxidised. This reaction converts the glucose to gluconalactone, and in the presence of a redox mediator the reduced GOx is oxidised while the mediator is reduced. The reduced mediator is then regenerated, releasing an extra electron and increasing the current flowing between the electrodes [85]. This method of detection has been extensively used in many industries, including healthcare [85] and water quality monitoring [86].

Potentiometry is the measure of potential, or a voltage between two electrodes. This method uses ion-selective membranes or electrodes to separate ions and cause a difference

in voltage between the working and reference electrode, and provides information regarding the ion-content of a system [83]. The most common form of this type of sensor is the humble pH meter, which separates hydrogen ions between the electrodes to measure the potential caused by accumulation of the ions. This relative voltage is then directly related to the ion concentrations, and thereby the pH. To illustrate this with another glucose oxidase example: when glucose is in the presence of GOx along with dissolved oxygen gas, it is converted to gluconalactone and hydrogen peroxide. The gluconalactone, together with water, is then converted to gluconate and a free hydrogen ion (H^+). This hydrogen ion then has the effect of raising the pH of the solution, which will be directly related to the concentration of glucose that was present before the reaction started [75]. This type of sensor utilises electrodes with high impedances to prevent the applied voltage from having an effect on the chemical reaction being monitored, and the current flowing through the sensor is kept to a minimum [83]. Glass-electrodes are often used as ion-selective membrane, due to their becoming ion-permeable upon inclusion of certain metal oxides, such as Na, Al, B and Ca. Newer ion-selective membranes include Polyaniline [87] or Nafion [88], and their uses range from water-quality analysis to heavy-metal detection [89].

Conductometry is the measure of conductivity, or the capacity for a material to conduct current. These types of sensors have been strongly associated with measuring enzyme activity, such as GOx, and their nature to release ions. A higher ionic concentration would correspond with an increase in conductivity [82], [83]. It would appear the conductometric sensors are of limited use, as the ionic concentration of clinical samples vary wildly between samples, making it difficult to establish a baseline for comparison [82]. This is however not strictly the case, as other methodologies for conductometric measurements through a substrate have emerged recently. Mayberry [90] and Viviers [91] have shown that conductivity, or resistance, measurements of conductive substrates during antibody-protein binding to the surface of the substrate shows a marked change in substrate conductivity, without changing the ionic content of the electrolyte in which the interaction occurs. The method of conductometry, however, when combined with ion-selective transistors, lends itself to the measurement of ionic concentrations in a manner very similar to potentiometry, but with the measured parameter being current instead of voltage [92].

The field-effect surface-charge measurement is a method by which ion-sensitive field-effect transistors (ISFET) can be used as sensors by constructing them in such a manner to allow their characteristics to be influenced by ionic concentrations [83]. The mechanism by which these transistors then function is that the channel conductivity is determined by the surface charge of the gate electrode due to selective ion permittivity. The transistor can be configured to allow selective ion sensitivity, and so become an ionic sensor similar to a potentiometric sensor [93], [94]. Another use for this type of transistor is to functionalise it in such a manner so as to introduce charge to the surface of the channel region or gate electrode, and so change the drain/channel current due to analyte binding events. Many methods exist to construct such an ISFET. The earliest versions reported were simple FETs with ion-selective membranes attached to the insulated gate electrodes, where the drain current was directly determined by the ionic concentration permitted through the ion-selective membrane. Further work saw ISFETs combined with enzymatic reactions to actively create certain ionic species in the presence of the gate electrode, and in so doing influence the current characteristics of the transistor [92]. The

advent of conducting polymers, and specifically semiconducting polymers, introduced another field-effect measurement - that of organic field effect transistors, or OFETs [95]. OFET devices, and specifically organic electrochemical transistors (OECTs), allow the direct manipulation of transistor characteristics based on ionic concentrations and interactions, modulated by applied voltages to the three terminals of the devices [10], [95].

The advantages of electrochemical sensors are that they are simple to manufacture and their measurement methodologies often do not require complex electronics to provide meaningful information [82], due to the measurement of voltage. The sensors can be easily miniaturised, along with the measurement electronics, to provide portable and versatile sensing platforms. Conversely, the disadvantages of electrochemical sensors can also be the complexity of the electronics necessary to perform the measurements. The complexity of the measurement electronics is highly dependent on the measurement being made, be it amperometry, voltammetry, conductometry, electrochemical impedance spectroscopy or field-effect surface-charge related.

It was decided to investigate the characteristics and working principles of field-effect based sensors further, and it was found that organic electrochemical transistors (OECTs) have very promising characteristics for biosensor development, and specifically paper-based sensing. Further investigation was done on the working principles of OECTs and their applicability as biosensors for protein detection.

2.6 OECT-Based Biosensors

OECT-based sensors, and biosensors, operate on the principle that the electrolyte and analyte contained therein becomes a functional component of the device. These transistor devices do not consist of doped silicon or germanium semiconducting regions, but are most often rather composed of intrinsically conducting organic polymers.

The OECT is a composite device that consists of three main components: electrodes, an electrolyte region and an organic semiconducting material. The basic structure of an OECT is shown in Figure 2.11.

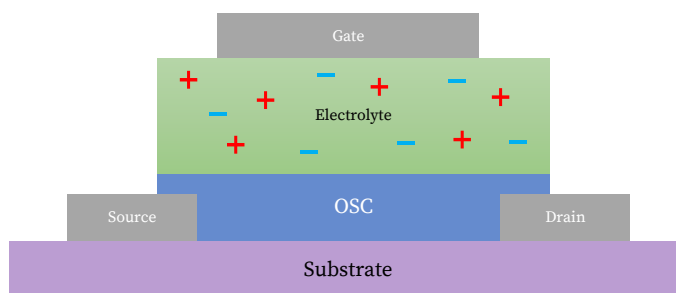


Figure 2.11: Simplified OECT cross-section

OECT devices are in reality a subset of EGOFETs - electrolytically-gated organic field-effect transistors. The difference between the two types of devices is that the polymer used in an OECT is ion-permeable, whereas the polymer used in an EGOFET is not [96]. The polymeric semiconductor used in the OECT can be either p-type, to conduct holes,

or n-type, to conduct electrons, although p-type devices are far more common than n-type due to difficulties in processing and stabilising n-type materials, as well as reduced mobilities in n-type polymers [96], [97].

Shown in Table 2.2 is a selected range of polymers that have been shown to be used in either OFET, EGOFET or OECT devices³. Of these polymers, poly(3,4-ethylenedioxythiophene) (PEDOT), poly(3,4-ethylenedioxythiophene):poly(styrenesulfonate) (PEDOT:PSS) and various other derivatives of PEDOT are by far the most commonly used, due to the chemical stability, easy processability and relatively high conductivity of the PEDOT family of polymers [84].

Table 2.2: Selected examples of semiconducting polymers

p-Type	n-Type
P3HT [98]	Polycarbazole [99], [100]
PDTT [95]	PBDT(T)TPD [101]
Poly-DPOT [102]	P(NDI2HD-T) [103]
Poly-DT [102]	PTCDI-C8 [104]
PEDOT:PSS [105]	P(NDI2OD-T2) [106]
PTAA [107], [108]	
Pentacene [109]	
PEDOT:TOS [110]	
TIPS-Pentacene [108], [111]	

The structure of an OECT device allows two forms of conduction to take place, ionic and electronic, which is what gives these devices their unique characteristics. The OECT functions as a transistor by manipulating the density of charge-carriers in its semiconducting region, as do all transistors, but in an OECT this is not done by an electric field alone. The electric field from the gate electrode is used to move ions from the electrolyte into the semiconducting region to change the doping concentration of the polymer. For a p-type device, which is the most common, movement of cations from the electrolyte into the polymer layer would have the effect of decreasing the conductivity, and vice versa [112]. In this type of device, the main charge carriers are holes in the p-type semiconductor. The cations in the electrolyte solution are used to control the number of holes being conducted, and effectively change the electrical conductivity of the channel material [112].

In spite of the difference in the physical mechanism by which the drain current of an OECT is modulated, the electrical model for such a device remains strikingly similar to the classical model for a MOSFET device [112].

³The expanded names of these polymers are left in the nomenclature, as most are incomprehensibly long and would make the table unreadable.

For the case of a p-type OEET, the model is given by

$$I_d = \begin{cases} \mu C^* \frac{Wd}{L} \left(1 - \frac{V_G - \frac{1}{2}V_D}{V_T} \right) V_D & \text{for } V_D > V_G - V_T \quad (\text{non-saturation}) \\ -\mu C^* \frac{Wd}{2LV_T} (V_G - V_T)^2 & \text{for } V_D < V_G - V_T \quad (\text{saturation}) \end{cases} \quad (2.4)$$

where I_d is the drain current through the transistor, C^* is the volumetric capacitance of the semiconductor/electrolyte interface, μ is the carrier mobility, V_G is the gate-voltage, V_D is the drain voltage, W is the channel width, V_T is the threshold voltage, L is the channel length and d is the channel thickness (semiconductor layer thickness), with conventions as indicated in Figure 2.12. Volumetric capacitance is a parameter of the organic semiconductor, where the capacitance is directly proportional to the volume of the semiconductor [113].

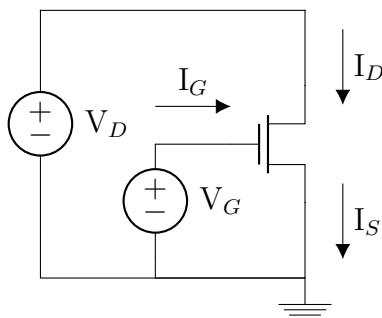


Figure 2.12: Current and voltage conventions

OEETs have no inherent polarity to their current directions, hence the absence of an arrow on the transistor symbol. The direction of current flow is determined by the voltage applied across the width of the channel, and the gate voltage is chosen accordingly. Therefore the drain and source terminals could be reversed, depending on the current direction chosen.

It can be seen from the model, Equation 2.4, that the current is dependent on the thickness of the channel material, due to the ions from the electrolyte permeating the channel material instead of remaining on the surface as in the case of an EGOFET.

Functionalisation of OEET sensors is done by immobilising biorecognition elements onto the channel surface, although it is not always necessary as the right choice of polymer can allow the channel material itself to act as recognition element [114].

The model also shows that the devices will be sensitive to changes in the volumetric capacitance of the transistor/electrolyte interface, which is where biorecognition elements such as antibodies or DNA probes would be immobilised. This change in volumetric capacitance is the main mechanism by which biosensors utilising immobilised biorecognition elements would function, due to the nature of the volumetric capacitance itself being determined by the surface chemistry of the device [113]. The volumetric capacitance for a specific

device has been determined to be a function of the number of sites available for ions to be injected into the semiconductor region [113], and binding of molecules to the device surface would necessarily have an effect on the number of these sites available. The most significant advantage of this sensor type is its active nature - voltages are applied to two of the three electrodes and the transistor architecture provides inherent amplification of any change to the device parameters [84]. Changes in ionic composition, distribution or type all have an impact on the gate/volumetric capacitance, and lead to a change in the measured transistor characteristics. Similarly, accumulation of charge at the channel surface, as is the case when charged molecules bind to biorecognition elements, causes a shift in the effective gate voltage and modifies the device characteristics to either increase or decrease the drain current.

OECT-based sensors can be divided into three broad categories: ionic sensors, enzymatic sensors and immunosensors. The following Section is a study of the functional mechanisms of such sensors, and some of the difficulties in their manufacture/implementation.

2.6.1 Review of OECT-Based Biosensors

The first type of OECT-based sensors developed were enzymatic in nature, and as with the first electrochemical sensors, the first attempts at this type of sensor were done with glucose oxidase [84]. The first GOx-based sensors made use of the reaction between dissolved glucose and GOx where glucose is converted to gluconalactone and hydrogen peroxide (H_2O_2). The H_2O_2 is then oxidised by a platinum electrode to form water and hydrogen, and provide a free electron, which increases the conductivity of the OECT. GOx was typically immobilised onto the channel surface, or left in suspension in the electrolyte, although immobilisation was the more sensitive and reliable approach [84]. Initially these types of sensors encountered the challenge of making the reaction specific enough to not detect acids such as uric- or ascorbic acid in biological samples [115]. However, addition of Nafion membranes to the gate electrodes successfully prevented the oxidation of other species than H_2O_2 , making the GOx-based sensor much more selective to glucose [115]. Later work by Liao *et al.* [116], in 2013, utilised graphene modified gate electrodes to further increase the sensitivity of GOx OECT sensors. In this work, the gate electrodes were modified with a combination of GOx and graphene-oxide, and the polymer mix of PEDOT:PSS was used as channel material. This combination of materials, with a Nafion membrane added to the gate electrode, showed a working concentration range from 10 nM to 1 μM , which was an improvement of two orders of magnitude from the design without graphene oxide. In 2015, Welch *et al.* [117] used a polymer-brush method to polymerise reactive groups onto the surface of a PEDOT:PSS channel for a GOx sensor, and used platinum nanoparticles to improve the sensitivity of the sensor - the platinum nanoparticles provided a greater surface area than typical electrodes and increased the efficiency of the GOx-glucose- H_2O_2 reaction to allow detection of glucose between concentrations of 10 μM to 100 nM, covering the full range of concentrations for glucose in human blood, which is similar to the results from Kergoat *et al.* [118] from the previous year. Later work by Currano *et al.* [119] used a combination of spincoating and screen-printing techniques to fabricate an OECT sensor functionalised with lactate oxidase onto Kapton film, a flexible substrate, for the monitoring of lactate concentrations in sweat. This system utilised lactate oxidase immobilised onto a gold/platinum gate electrode to allow the same type of reaction as is typical with GOx, and achieved a working range of concentrations from 11 nM to 1 nM. It is of note that the polymer PEDOT:PSS is used

very extensively in this type of sensor for its mechanical and chemical stability - all of the more recent publications reviewed made use of PEDOT:PSS. This type of sensor has been highly successful in detecting the presence of reactive species, such as H_2O_2 , created during the interaction between -oxidase molecules and their target molecules. The next type of sensor evaluated is the OECT-based ionic sensor.

Ionic OECT-based sensors utilise the inherent sensitivity of OECT devices to the ionic content of the electrolyte to manipulate the sensor characteristics, and in doing so amplify the signal generated from a recognition event. The more frequently recognised materials in this case are charged molecules that can have an effect on the conductivity of the polymer film, such as neurotransmitters and certain drugs. In 2012 Karuwan *et al.* [120] utilised an inkjet printer to fabricate a graphene-modified PEDOT:PSS biosensor for the detection of salbutamol, which is a prohibited performance enhancing substance in competitive sport. This sensor operated on the principle that the PEDOT:PSS polymer might act as a redox mediator on its own, and thereby enhance the oxidation of salbutamol in solution for cyclic voltammetry sweeps of the channel electrodes. The work was successful in sensing salbutamol for concentrations between $50 \mu\text{M}$ to $100 \mu\text{M}$. Tria *et al.* [121] used an OECT-based sensing platform to measure the metabolic activity of cells immobilised onto the sensor surface. The working principle for this sensor was that the metabolic waste from such cells would influence the ionic content of the surrounding liquid and in so doing change the transistor characteristics. The work showed that this approach to cell monitoring had the same, if not better, sensitivity than the methods typically used in practice. Of particular interest in this type of sensor is that PEDOT:PSS is well-known for the difficulty it presents in immobilising biorecognition elements directly onto its surface - the chemical structure of the polymers does not allow easy binding to the polymer chain without disrupting the conducting bonds between the constituent monomers [122]. In 2015, it was suggested by Strakosas [110] to include a third polymer into the transistor channel material to rather provide the functional groups for biorecognition element immobilisation. Crosslinking chemistry could then be used to link between the included polymer and any biorecognition elements instead of binding to the PEDOT:PSS directly. In this case the polymer known as polyvinyl alcohol (PVA), or polyethylene glycol (PEG), was used to provide surface oxygen groups to which GOx was bound using the organosilane (3-Glycidyloxypropyl)trimethoxysilane (GOPTS) in a crosslinking reaction. This scheme was shown to be successful in both binding the GOx to the sensor surface, and in preventing the PEDOT:PSS layer from being damaged by the immobilisation reaction.

Apart from measurement of ionic concentrations or redox reactions, the next most popular use of OECT sensors is in the measurement of neurotransmitter and metabolite concentrations. Tybrandt *et al.* [123] used fast-scan voltammetry in combination with a PEDOT:PSS OECT to measure dopamine concentrations of as low as $10 \mu\text{M}$ without the use of a Faraday cage, which was previously necessary to protect the sensitive measurement equipment used for such measurements. Later work by Gualandi *et al.* [124] showed that OECTs could be used to selectively sense adrenaline, dopamine and ascorbic acid. This was done by using a textile-based screen-printed OECT utilising PEDOT:PSS as channel material. In this case the measurements were done using differential-pulse voltammetry to identify the redox-peaks from the three molecules, which were found to be detectable in concentrations between $10 \mu\text{M}$ to $160 \mu\text{M}$. Further work by Gualandi *et al.* [125] showed the selective detection of dopamine in the presence of other molecules, such as ascorbic acid and uric acid, which as in the case for enzymatic sensors are a source of considerable

difficulty for OECT sensors. This was done by using an atypical measurement method of varying the gate voltage periodically to obtain cyclic voltammetry-like redox peaks for the transconductance of the transistor, and to calibrate these peaks for each of the three substances. Following the work by Gualandi *et al.* [125], a similar approach to dopamine detection was used by Wang *et al.* [126] to detect dopamine in solution by periodically varying the gate voltage of an OECT and measuring the transconductance. This approach seems inferior to that of Gualandi *et al.* [125], where a characteristic signal waveform was found for each analyte, but the results from Wang *et al.* [126] showed a superior limit of detection to Gualandi *et al.* [125] of 1 nM compared to 63 nM, respectively. This difference may be due to the different approaches in manufacturing methods, or the measurement equipment used.

The last family of OECT-based sensor to be reviewed is that of the immunosensors, or sensors that utilised biorecognition elements such as DNA, antibodies or aptamers to bind to a target molecule. The working principle for this type of sensor is founded on the principle that biological molecules in solution possess surface charge, and that the binding of such a molecule to the surface of an OECT would introduce that charge to the surface of the sensor. This would then in turn alter the ionic concentration in the channel region by either attracting or repelling ions to change the doping conditions of the transistor [127]. In 2010 Kim *et al.* [128] used such a scheme to detect prostate specific antigen (PSA) using a PEDOT:PSS based OECT. This publication achieved remarkable sensitivity due to their addition of a second antibody, similar to an ELISA test, but with a gold nanoparticle attached. This nanoparticle then acted as molecular amplifier to the change due to the PSA binding, as gold nanoparticles are known to have a negative surface charge when in solution [84]. Kim *et al.* [128] achieved a working range for their sensor of $1 \text{ pg}\cdot\text{ml}^{-1}$ to $100 \text{ ng}\cdot\text{ml}^{-1}$. Further work by Faddoul *et al.* [129] showed that inkjet printed transistors, of PEDOT:PSS, could be used to detect the deposition of antibodies onto the transistor surface, showing that the transistors can be manufactured using very simple methods. Lin *et al.* [130] also showed that OECTs with ssDNA immobilised onto the surface of the channel could be used as biorecognition element. The effective recognition of *E. coli* by an OECT-based sensor has also been shown by He *et al.* [127], where concentrations of the bacterium could be measured down to 10^3 cfu/mL .

Examples of typical output characteristics of OECT-based sensors are shown in Figures 2.13 and 2.14.

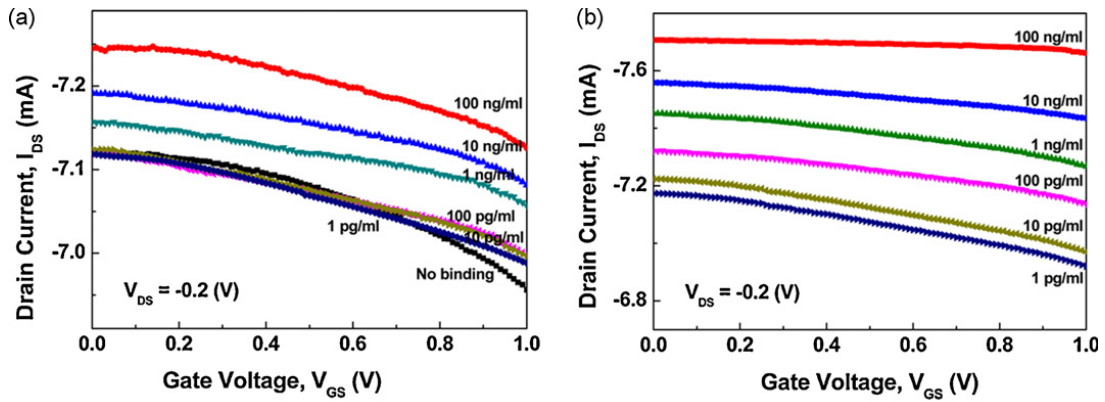


Figure 2.13: Typical OECT sensor output current characteristics [from [128]]

Figure 2.13 shows the output current characteristics achieved by Kim *et al.* [128] for two versions of the PSA sensor. This figure clearly shows that the sensors' output current, and the decrease therein, was dependent on the concentration of analyte present in the sample. Shown in Figure 2.14 is the output characteristics achieved by Wang *et al.* [126], where a clear correlation between the transconductance of the sensor and the concentration of the analyte can be seen.

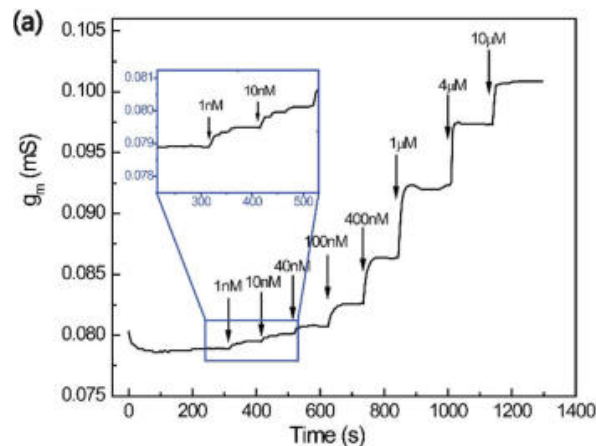


Figure 2.14: Typical OECT sensor transconductance characteristics [from [126]]

OECT sensors have been shown to be highly sensitive to a wide variety of analytes including ions, metabolites, cells, bacteria, acids and proteins. Therefore it was decided to utilise an OECT-based approach for the transducer developed in this project.

2.6.2 Choice of Conducting Polymer and Manufacturing Method

A clear trend was observed in the literature regarding the manufacturing methods of OECTs, and OFETs in general, towards using low-cost and additive methodologies such as screen-printing and inkjet printing to manufacture newer generations of sensors. This manufacturing method seemed attractive for two reasons: additive manufacturing is less wasteful than other methods, and inkjet printing is a well-known mechanism that can now

be used in innovative ways to simplify the manufacturing processes of various devices [131].

Furthermore, the conducting polymer mixture of PEDOT:PSS is well known as being compatible with inkjet printing, and is a widely-used polymer in general manufacturing of OECT devices. The polymer has many beneficial characteristics for biosensor development, including biocompatibility and mechanical and chemical stability [132], [133].

It was therefore decided to evaluate inkjet printing of PEDOT:PSS for the manufacturing method of the transducer in this project, and to use two other manufacturing methods to compare their applicability to the technology of paper-based sensors.

However, the SAND research group had no access to an inkjet printer capable of depositing the necessary materials for such a transducer. Therefore a further literature study was done to determine the process by which one could modify a commercial desktop inkjet printer to perform the necessary functions for material deposition.

2.7 Inkjet Printing for Sensor Development

The use of paper in this project as the sensor substrate immediately calls to mind the ubiquitous desktop printer - what else does one use to form patterns onto paper? From the successes of the inkjet printed sensors in the previous section it was decided to develop an inkjet printer system to use as part of the sensor fabrication process. The following is a study of some of the literature concerning inkjet printing, inkjet manufacturing and the modifications necessary to adapt a desktop inkjet printer to become a material deposition device.

2.7.1 Inkjet Definitions

The definition of an ink-jet printer, as given by the Oxford English Dictionary[134] is:

A printer in which the characters are formed by minute jets of ink.

This definition, however, is slightly misleading, as the result of the printing process is rather that markings are formed on a substrate by the droplets ejected from the print-head - the word "jets" can be taken to mean a continuous stream of liquid.

The method of ink-jet printing was first developed during the 1950's and has since become an almost universal method of physical document production. Four manufacturers of ink-jet and other printers make up most of the commercial market, namely, HP, Epson, Brother and Canon. Other manufacturers focus on more specialised products, such as Xaar who manufacture printheads and other components for large-volume industrial applications, or Fujifilm who produce material deposition systems for scientific and experimental use (such as Dimatix).

Although different uses of the ink-jet technique each call for slightly different applications of the principle, these can all be divided into two categories: Continuous Stream ink-jet (CIJ) and Drop On Demand ink-jet (DOD). The difference between these two types is that CIJ produces a constant stream of droplets from a single orifice that are individually aimed towards a target site, and DOD systems typically have arrays of orifices

that produce droplets on demand to form a desired pattern. CIJ systems are more often used in commercial marking systems, such as those on production lines where products receive serial numbers on manufacturing dates - DOD systems are more widely used and can be found in commercial, scientific and household environments.

The mechanisms used by ink-jet systems to propel droplets of ink can mostly be divided into three groups (although other methods do exist):

- Thermal ink-jet
- Piezoelectric (piezo) ink-jet
- Ultrasonic ink-jet

Of these techniques, thermal DOD and piezo DOD are the most common, with HP and Canon mainly using thermal mechanisms and Epson and Brother keeping to piezoelectric mechanisms - although HP has occasionally produced piezoelectric printing systems in the past.

2.7.2 Overview of the Inkjet Mechanism

A basic diagram of a typical ink-jet configuration is shown in figure 2.15. Such a system can typically be divided into two main segments: the ink reservoir that contains the ink mixture, and the printhead from which ink is projected onto the substrate and that contains the electronic components that make its operation possible. These segments can be either housed in one device, such as the disposable cartridges manufactured by HP and Canon for many of their home-use printers, or separate with only the reservoir being disposable as in many professional or industrial printer systems. Epson has however followed the approach taken by Brother and begun to solely manufacture printers for home or office use with large ink-tanks connected to the printhead through pipes, although their industrial products have remained modular.

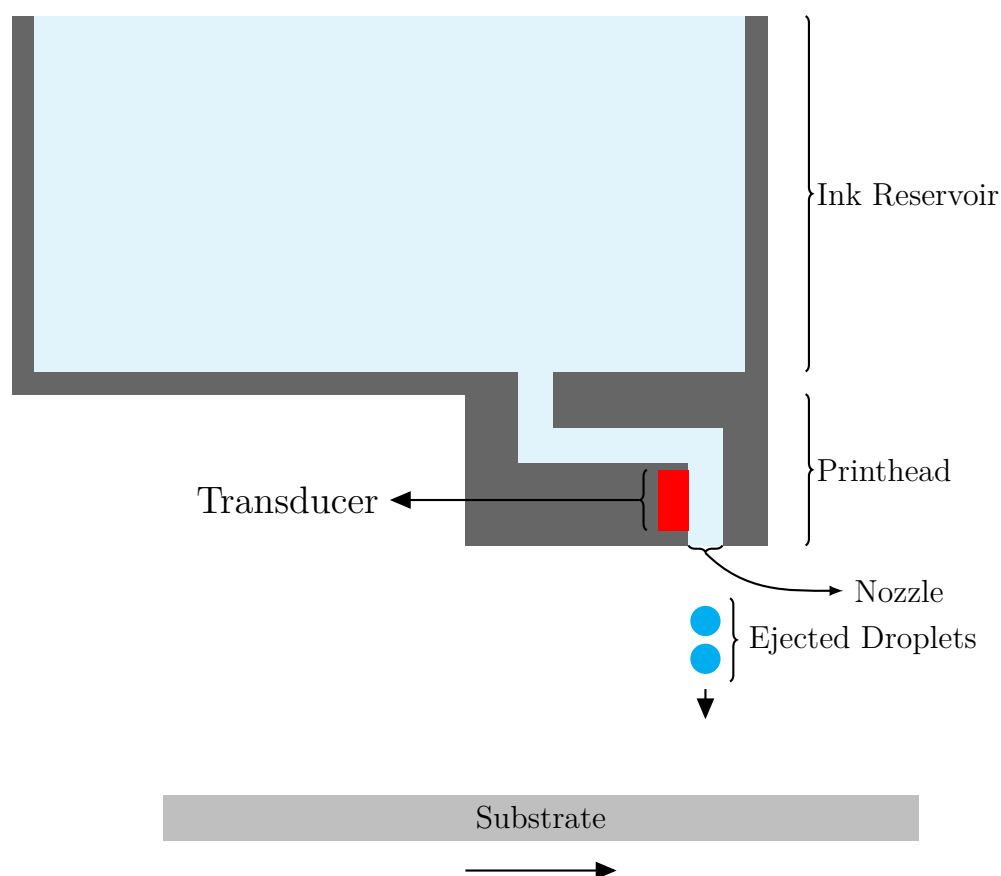


Figure 2.15: Diagram of basic ink-jet mechanism⁴

The main functional component of the deposition system is the transducer, which usually operates based on one of the mechanisms mentioned previously. The transducers force droplets of ink with a set volume from the nozzle of the printhead onto the substrate. Different methods of ejecting droplets are employed by each of these mechanisms: the piezo and ultrasonic mechanisms respectively use physical deformation or vibration in the transducer to physically propel a drop from the nozzle, while a thermal mechanism heats a small resistor to temperatures upwards of 300 °C [135] to almost instantaneously vaporise a small volume of ink. The expanding bubble of vapour then forces the liquid between the transducer and nozzle opening through the nozzle. Capillary forces then replenish the liquid that was ejected, priming the nozzle to fire again. Although these systems use differing mechanisms to achieve their goals, the result is the same: That a small volume of ink is propelled from the nozzle of the printhead due to imparted energy.

The difference in operation between these mechanisms has immediate implications for the type of ink used for each type of printer, as piezo and ultrasonic mechanisms do not have a significant opportunity to affect the properties of the fluid being deposited, but thermal mechanisms do due to the high temperatures involved. This means that piezo- and ultrasonic-based ink-jet printers should be better suited for use as scientific material deposition systems than those using thermal mechanisms.

⁴This diagram was compiled based on explanatory diagrams provided by Epson, Xaar and HP.

2.7.3 Study of Previous Projects

Some of the earliest attempts at using ink-jet or other printing techniques for material deposition can be traced to Bernard *et al.*[136] or Hayes *et al.*[137] in 1998. Bernard *et al.* succeeded in patterning protein monolayers for use in biological assays on selected substrates using microcontact printing, and Hayes *et al.* successfully used an ink-jet/microjet printing process to manufacture electronic components such as resistors and solder pads directly onto substrates. Both of these projects appear to have constructed their own printing systems and provide a point of reference for what could be possible with ink-jet printing systems.

Following the initial projects, several researchers started experimenting with ink-jet printing in research fields such as material engineering[138], [139], printed electronics[140]–[142] and tissue engineering[135], [143]–[145]. Two main methodologies were identified in these projects, namely:

1. Use of custom-built printing systems [137], [138], [141], [145], and
2. Use of modified desktop/commercial printing systems[135], [139], [142]–[144].

Many of the identified printing systems made use of thermal printing mechanisms, often of HP manufacture, to achieve their results, which seems to show that the high temperatures involved do not affect the material in the ejected droplets adversely, possibly due to the very short duration of the elevated temperature and the possible insulating effect of the expanding bubble of gas, which might prevent the droplets from reaching temperatures high enough to damage their contents. No information either supporting or disproving this hypothesis could be found, however, and it seems that many researchers later switched to piezoelectric-based systems, possibly because of the uncertainty that the thermal mechanism introduced unknown or unwanted variables into their experiments. However, Cui *et al.*[146] has shown that the thermal ink-jet mechanism does not necessarily damage living cells to a greater extent than general handling procedures.

Later experiments, such as those by Mabrook *et al.*[147] or Boland *et al.*[148] in 2007 made use of modified desktop printing systems. In the case of Mabrook *et al.* no modifications other than opening and purging the contents of cartridges were made in order to fill them with a conducting polymer mixture containing polyaniline nanoparticles, but Boland *et al.* extensively modified their HP printing system to facilitate vertical movement of the substrate and allow printing of 3D structures in addition to filling their cartridges with a combination of collagen and cell-based inks to print biological structures.

In 2009 Eom *et al.*[149] used a commercial scientific ink-jet deposition system from Unijet, Korea to fabricate organic polymer solar cells based on PEDOT:PSS. In the same year Pepper *et al.*[150] designed and built a 2D bioprinter based on a commercial HP printer cartridge and modified driver electronics, which entailed a completely custom-designed printer system with complete control of the printing platform in two directions, allowing patterning of biological materials such as cells and proteins. Srichan *et al.*[151] also used a desktop Canon printer to print PEDOT:PSS and successfully produced structures with a minimum feature size of 150 μm - the printer was reported to be completely unmodified.

The experimentation done by D'haeseleer [152], in 2013, was of particular interest due to

it dissecting the basic function of an inkjet printer for use as a material deposition device. It was shown that many modern commercial inkjet cartridges have nozzles sizes that are too small to print living cells, and that the nozzles have internal filters that could prevent printing with coarser materials. They went on to construct a bioprinter using multiple disassembled CD drives and an older generation printer cartridge that had larger nozzle sizes than what is the current norm, and showed that the printer could be used to deposit living *E.coli* cells.

Yoshihiro *et al.* [153] and Matsuda *et al.* [154] used the commercial Brother DCP-J540N inkjet printer along with silver nanoparticle ink from Mitsubishi Paper Mills, NBSIJ-MU01, to print functional electronic prototypes, such as RFID antennas and paper-based heaters for microfluidics applications.

The work done on inkjet printers, specifically to use commercial printers for alternative purposes, showed that it was very possible to use modified inkjet printers to do work comparable to that of commercial scientific material deposition systems.

2.7.4 Considerations in Printer Design

It became clear from the literature that certain properties of an ink-jet system are more important than others when it is to be used as material deposition device. The following is a list of these properties, assessed from the perspective of modifying an existing ink-jet printer.

Printing Mechanism: It appears that there is little difference in the results obtained from thermal- and piezoelectric ink-jet systems, although piezoelectric systems seem to be preferred for research purposes. A possible reason for this preference may be that thermal printing systems introduce unknown variables to an experiment in the form of possible modification or degradation of the material being deposited, whereas the piezoelectric mechanism does not suffer this drawback for most materials. It is, however, known that cells may be damaged by the high-frequency vibrations, as noted by [135]. Therefore it is desirable to use a piezoelectric system, but not absolutely necessary.

Nozzle Diameter: It is clear from the literature that the nozzle diameter of the print-head plays a role in the type of material that can be printed: smaller nozzles tend to cause damage to biological materials such as cells [150]. Therefore larger diameter nozzles are desirable, around 50 μm , but only if printing of biological materials is a critical part of the experiment. Nozzle diameter also has an impact on the range of possible inks that can be used with a specific system. This is because the nozzle diameter determines the amount of energy that has to be expended to eject a droplet from the nozzle, which is determined by the ink viscosity, and increases for decreasing nozzle diameter. Therefore larger nozzles are desirable for inks with higher viscosities, but smaller nozzles are preferred for higher resolution.

Nozzle Spacing: The resolution of structures that can be realised by a printer system is determined by a combination of the nozzle spacing and nozzle diameter of the printhead: smaller nozzles packed closely together will be able to realise smaller feature sizes than larger nozzles or nozzles spaced further apart. This is due to smaller nozzles ejecting smaller droplets onto the substrate, which make smaller dots and therefore

smaller structures, while nozzles packed tightly together can realise finer patterns than nozzles further apart. Therefore closely-spaced, small nozzles are desirable if small feature sizes are necessary, but the trade-off with biological printing capability and ink variety must be taken into account if nozzles smaller than $50\ \mu\text{m}$ are used [150].

Ink Compatibility: The chemical composition of inks that are to carry materials to the substrate should be compatible with the material from which the cartridges are constructed. Solvents that damage or interact with the cartridge materials will compromise the validity of any experiments performed with such a system and may cause damage to the cartridge or its internal electronic components. Ink viscosity, surface tension and particle size must also be controlled to allow deposition with a specific printhead/printing system. Typical viscosity ranges for inks in commercial ink-jet printers are 1-10 cPs, with surface tensions around $30\ \text{mN}\cdot\text{m}^{-1}$. Particles with a diameter of more than $1\ \mu\text{m}$ cannot be printed due to the diameter of the internal channels and filters of most ink-jet systems [152].

Feed System: The main concern with the feed system of typical printers is that the substrate is usually bent in some way along the path to the printhead. The substrate should remain as flat as possible for reliable production of any type of sensor or conducting device, as bending of the substrate may introduce faults in the printed layers. The substrate also comes into direct contact with various rollers and unknown surfaces, potentially introducing contaminants to a sensor and compromising subsequent experiments. Typical printer feed systems also only make allowance for substrates of a very specific thickness, impeding experimentation with substrate materials. Therefore flat feed systems are preferred for material experimentation.

Formulation of the aforementioned points into high-level specifications lead to the following:

1. The printer should preferably utilise a piezoelectric printhead,
2. The printhead should make use of small nozzles ($<50\ \mu\text{m}$) packed tightly together,
3. The printer should use disposable cartridges, for easy replacement of cartridges due to clogged nozzles,
4. The printer feed should be as flat as possible, and easy to modify, and
5. The cost of the printer should be as low as possible.

The first specification limits the choice of printer to those of Epson and Brother manufacture, but the ink-tank system employed by both manufacturers disqualifies them as per the second specification. It was decided to rather consider a printer of Canon or HP origin, due to the fact that a thermal printhead should have little to no effect on the printed materials. Both Canon and HP manufacture low-cost ink-jet printers with disposable cartridges.

2.8 Proposed Transducer Design

Following the study on potential biorecognition elements for biosensor functionalisation, it was decided to utilise an antibody-based approach for this project. This was chosen

for two reasons: it is well-known that antibodies have been developed to target CRP, and antibody immobilisation strategies are well-established and relatively simple to achieve effectively.

Furthermore, it was found from the literature that organic electrochemical transistor (OECT)-based sensors have a unique inherent capacity for amplification of analyte binding events taking place on the transducer surface, due to the gate-voltage dependent nature of the device. Following this it was decided to utilise a PEDOT:PSS-based OECT design for the transducer in this project. However, it is also well-known that PEDOT:PSS is not the easiest of polymers to functionalise for biorecognition element immobilisation [122].

The biological integration methods developed by Strakosas [110], pictured in Figure 2.16, have many attractive features, foremost of which is the inherent solution processability of all materials required - PEDOT:PSS, PVA and GOPS can all remain in solution for the processing steps. This specific combination of materials is however not necessarily ideal for the immobilisation of antibodies onto sensor surfaces. Specifically, the binding of GOPTS to proteins may cause deformation of the protein structure, and in doing so, cause inactivation of the protein. Therefore an adaptation to this methodology is suggested for this project: that a similar mixture of PEDOT:PSS and PVA be used for transistor manufacture, but that an alternative organosilane be used to express functional groups on the transistor surface. These functional groups can then be used to link to antibodies using a known antibody crosslinker that has a lower probability of inactivating the antibody function.

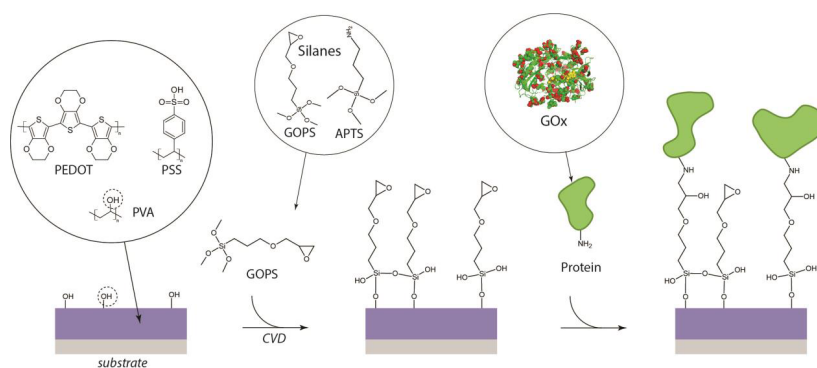


Figure 2.16: Biofunctionalisation strategy [from Strakosas [110]]

The silane chosen for this approach is (3-Aminopropyl)triethoxysilane, or APTES, which is widely used to express primary amine groups on sensor surfaces, shown in Figure 2.16, along with the immobilisation method from Strakosas [110]. This silane, along with GOPTS and (3-Aminopropyl)trimethoxysilane (APTMS) can be used to provide a wide variety of functional groups on the surface of a transducer. In this case it was chosen to use APTES for the amine ($-NH_2$) groups that would be formed, for which many crosslinking strategies exist. The crosslinker known as BS³ (bis[sulfosuccinimidyl] suberate) was chosen to fulfil this role for its homobifunctional structure, which reduces the necessary number of processing steps for antibody immobilisation [155].

A schematic of the proposed transducer design is shown in Figure 2.17. The basis for the transistors will consist of a paper substrate, onto which silver electrodes will be printed.

The PEDOT:PSS layer will be deposited on top of the electrodes, containing PVA to facilitate crosslinking.

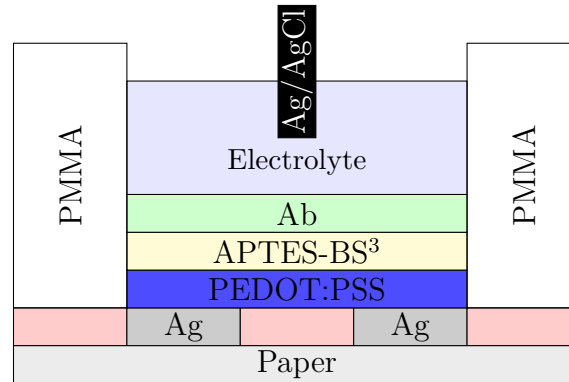


Figure 2.17: Proposed transducer cross-section

On top of the PEDOT:PSS layer will be deposited a monolayer of APTES for surface functionalisation, after which antibodies will be immobilised to the transducer surface using BS³. The whole device will be contained in a set of poly(methyl methacrylate) (PMMA) electrolyte wells to provide the device with the necessary depth to house the electrolyte solution. The gate electrode of the transistors will be made of Silver/Silver chloride for chemical stability. The light red layer indicated in the layout represents a layer of material that may be added to improve the water resistance properties of the paper substrate, to prevent water from a sample from penetrating into the paper and causing a short circuit between the electrodes.

Chapter 3

Methodology

The goal of this chapter is to serve as a roadmap for the development process followed during the course of the project. The project can be divided into three distinct parts: printer development, transducer development and transducer validation. The first phase was dedicated to developing and characterising an inkjet printing system capable of depositing the inks necessary for biosensors development. The second phase consisted of manufacturing paper-based transistors and verification of their function. The final phase of the project was taken up by testing the developed transducers with protein solution.

3.1 Introduction

Development was done of an organic electrochemical transistor based biosensor transducer for the detection and measurements of CRP. The development process was divided into three stages, corresponding to the development of one of the manufacturing methods, manufacturing of the transistors, and testing of the functionalised transducers.

3.2 Printer Modification

The manufacturing method for the paper-based transistors had to be developed before the transistors could be manufactured. To achieve this, it was decided to construct an inkjet printer to act as a material deposition device, to deposit as many of the materials required to produce the transistors as possible. The process of printer modification was started by doing a literature study of projects that attempted similar work in the past. From this study, a list of requirements were composed for a printer that would be suited to such modification and capable of performing the function of a robust material deposition system. The requirements are given in Chapter 2.7. A list of possible printers were then compiled and their characteristics were compared. Finally, a printer was chosen and acquired.

The printer, an HP DeskJet 4535, was disassembled and extensively modified to function as a flatbed printer, with capabilities added to align printed layers to one another. The printer cartridges were also modified to allow printing of silver nanoparticle ink and PEDOT:PSS ink.

Comparison was also done of silver ink printed onto different paper types to determine

whether a better combination of ink and paper was possible than that suggested by the ink manufacturer.

3.3 Transistor Manufacture

It was decided to attempt transistor manufacture using three manufacturing methods, for comparison of their resulting devices. The methods of inkjet printing, spincoating and manual droplet deposition were chosen for comparison.

The first iteration of transistors were chosen to not contain any PVA, for the reason that PVA is known to introduce hysteresis in thin-film transistors [156]. This was done to offer a point of comparison for the sensors containing PVA, and to verify that the manufactured transistors worked correctly before functionalisation.

The transistors were functionalised with an APTES monolayer, and the transistor characteristics were compared between processing steps to gain insight into the effect of the immobilisation process on the transistors. A full documentation of the process can be seen in Chapter 5, where the complete method of transducer manufacture is developed.

Inkjet printing: In short, the process of inkjet printing transistors was done by printing successive layers of ink onto paper, building the transistor structure up vertically. The first layer consisted of silver electrodes printed onto the paper substrate. After printing silver, the water resistance of the paper was improved by spincoating a solution of diluted photoresist onto the printed electrodes without having the photoresist cover the electrodes themselves, but merely absorb into the paper. Afterwards, successive layers of PEDOT:PSS ink was printed onto the electrodes and aligned by using the alignment system built into the redesigned printer. After the necessary number of layers of PEDOT:PSS ink had been printed, the piece of paper was removed from the printer and baked for 90 min at 120 °C in a laboratory oven to dry the ink mixture before testing.

Spincoating: A simplified protocol was followed to spincoat transistors, due to the absorbent properties of paper. Immersion in photoresist developer for photolithographic processes would have rendered the paper unusable. As an alternative, pieces of adhesive tape were used to mask off the areas where PEDOT:PSS ink was not desired before it was spincoated onto the paper substrate with pre-printed electrodes. After spincoating, the spincoated devices were baked in a laboratory oven to dry all of the deposited materials.

Manual drop deposition: The manual drop deposition method was the simplest of all. The first step was to print silver electrodes onto a piece of paper, whereafter the paper was spincoated with diluted photoresist to improve water resistance. After spincoating, 5 µl droplets of PEDOT:PSS ink were deposited onto the electrodes, and baked in a laboratory oven to dry out the inks.

3.4 Transducer Functionalisation and Antibody Immobilisation

As mentioned in Section 2.8, an adapted version of the biofunctionalisation strategy developed by Strakosas [110] was used to immobilise antibodies onto the transducer surface. The crosslinker known as BS^3 was chosen to anchor the antibodies to the transducer surface for its simplicity in use combined with NHS-ester chemistry, which is well known to be an effective antibody immobilisation strategy for biosensors [122].

3.4.1 Surface Modification

The first step in manufacturing a functioning transducer was to functionalise the surface with primary amine groups by growing an APTES monolayer onto the -OH groups provided by the PVA in the polymer mixture, shown in Figure 3.1.

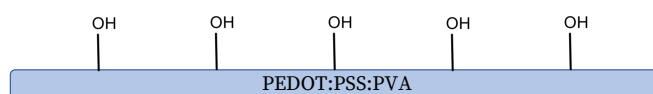


Figure 3.1: Unaltered PEDOT:PSS

After manufacturing the transistors by using the previously mentioned methods, a 10% w/w mixture of APTES in anhydrous toluene was deposited onto the transducers and incubated overnight at room temperature to grow a silane monolayer onto the surface of the polymer. Shown in Figure 3.2 is a graphical representation of the result of the silanisation reaction on the transducer surface.

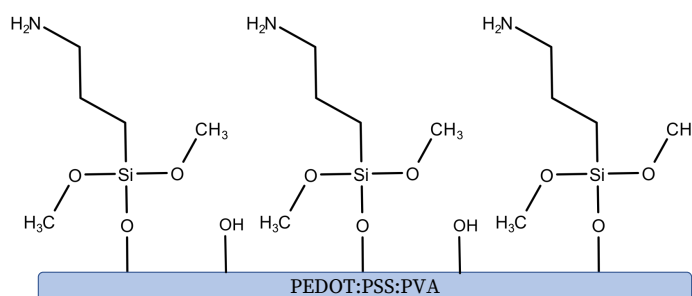


Figure 3.2: APTES addition

Antibodies can now be bound to the surface of the transducer by using a crosslinking method, and BS^3 will be used to do so.

3.4.2 Antibody Immobilisation

Immobilisation of antibodies by binding to amine groups at various locations, primarily at the Fc region. The crosslinker known as BS^3 was used to bind to the antibodies using sulfo-NHS chemistry to selectively bind to the amine groups present on the antibody

structure - primarily located at the Fc region. A schematic of the structure of BS³ is shown in Figure 3.3, and the sulfo-NHS groups at the ends are clearly visible.

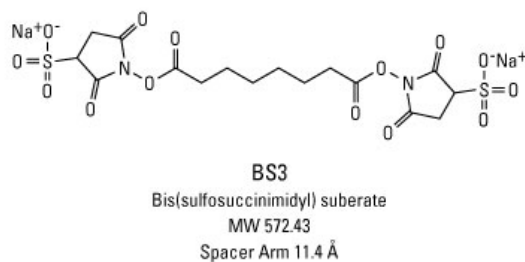
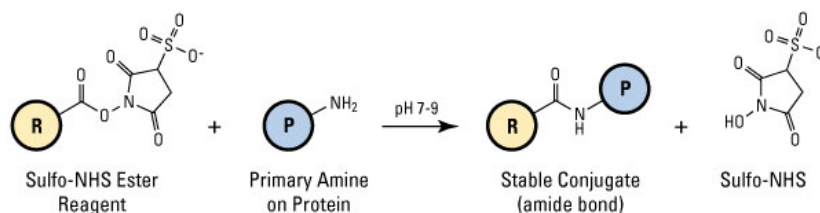


Figure 3.3: BS³ structure [from [157]]

The chemical reaction of sulfo-NHS groups binding to primary amines is depicted in Figure 3.4, where the generalised molecule with either of the reactive groups is shown. The reaction occurs at a pH of between 7 and 9, where the sulfo-NHS esters are activated and hydrolysed. Upon hydrolysis of the NHS-ester a competitive reaction is started with the primary amine groups, and a covalent bond is formed between the two molecules with the result of a sulfo-NHS molecule being released.



Therefore, the next step towards antibody immobilisation onto the transistors after APTES functionalisation was to react the primary amine groups of the APTES with BS³, which was done by pipetting a solution of BS³ with a concentration of 0.6 mg·ml⁻¹ onto the APTES coated transistors. The solution was incubated on the transistors for 2.5 h at room temperature to allow as many of the primary amines present on the transducer as possible to be reacted by BS³ molecules. The result of this step is shown in Figure 3.5. The BS³ molecule now protrudes above the transducer surface and presents another sulfo-NHS-ester group to link to the primary amine groups present of the antibody structure.

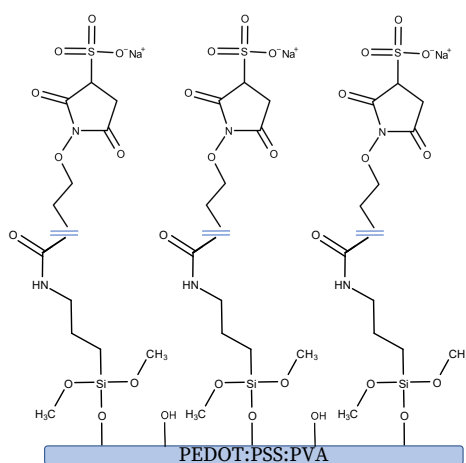


Figure 3.5: BS^3 addition

After BS^3 coating, a solution of the capture antibodies with a concentration of $4\ \mu\text{g}\cdot\text{ml}^{-1}$ was added to the transistors and incubated at room temperature for another 2.5 h to, once again, allow as many of the binding positions to be taken up as possible. Shown in Figure 3.6 is a simplified representation of the transducer at this point, with the antibodies at the top of the diagram, ready to bind with C-reactive protein.

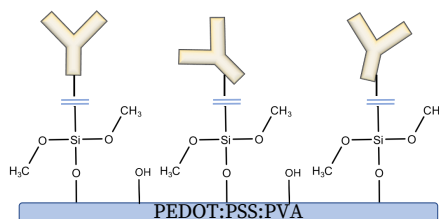


Figure 3.6: Capture antibody addition

However, before the protein could be introduced, a blocking step was done to block any areas on the transducer surface that was not occupied by either APTES, BS^3 or an immobilised antibody. This was done to prevent any interaction between the transducer surface and introduced particles other than that by binding with the antibodies. The blocking step was done by adding a 3% w/w solution of bovine serum albumin (BSA) to the transducers after the antibodies had been added, and incubating the transducers at room temperature for 1.5 h to adsorb BSA onto any unoccupied transducer surface. The result of this step can be seen in Figure 3.7

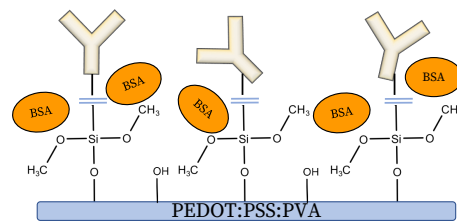


Figure 3.7: BSA blocking step

After BSA blocking, the transducers were ready to be used. A total of 8.5 hours were necessary to perform all of the steps involved to immobilise antibodies onto the transducer surface. Following protein addition, the target proteins will bind to the Fab region of the antibodies, and thereby cause a change in the transducer characteristics. The result of such a reaction is shown in Figure 3.8.

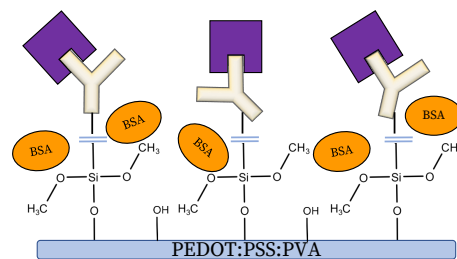


Figure 3.8: C-reactive protein addition

3.5 Measurement Methodology

The transducers were tested with dilutions made of recombinant CRP protein, As mentioned previously in Section 2.8, this project attempted to combine two signal generation methods to compare their performance in reflecting the change in transistor characteristics due to a protein binding event.

The two measurement methods in question are the standard method of measuring the DC current through the drain of a transistor, and measurement of the small-signal transconductance of the transistors.

The measurement configuration for this technique is shown and discussed in Section 5.3.7. It consisted of a National Instruments Data Acquisition system, the cDAQ-9174, connected to a simple reference circuit to allow the calculation of the current through both the transistor gate and drain by measuring the voltages across two resistors. It was thought that the binding of antibodies and proteins to the transducer surface may have a similar effect on the apparent carrier mobility, due to impeding ion transfer across the semiconductor-electrolyte interface. Therefore a combination of AC and DC measurements were done, with a small AC signal superimposed on the DC biasing voltages for

the transistors to evaluate the potential change in transconductance for the transistor upon protein bindings taking place.

3.5.1 Protein Dilutions

The clinically relevant range of concentrations for CRP is below $10 \mu\text{g}\cdot\text{ml}^{-1}$ [158], [159] for young individuals. Therefore, the dilution series for the final experiment should start at the upper limit of the clinically relevant range and proceed to decrease at a power-law for each dilution in the series. It was decided to half the concentration for each dilution and to do a series of 10 dilutions to better gain insight into the transducers' performance across a large dynamic range. The concentrations of protein made for the final experiment are shown in Table 3.1.

Table 3.1: Dilution series

Dilution Number	Dilution Concentration
1	10
2	5
3	2.5
4	1.25
5	0.625
6	0.3125
7	0.15625
8	0.078125
9	0.0390
10	0.01953

The dilutions were prepared in the following manner:

- Step 1: 240 μl of PBS is added to 9 1 ml sample holders,
- Step 2: 4.8 μl of stock protein solution is added to 475.2 μl of PBS in a 10th sample holder and gently pipetted up and down to mix,
- Step 3: Half of the volume in the first sample holder, 280 μl is removed and added to the next sample holder,
- Step 4: The dilution is gently pipetted up and down to mix,
- Step 5: Repeat Steps 3 and 4 until all 10 of the dilutions have been made, with the final sample holder containing 480 μl of liquid.

These prepared samples were then used during the procedure of testing the transducers.

3.6 Conclusion

This chapter shortly provided a roadmap for the development process of a biosensor transducer targeted towards CRP, to potentially distinguish between viral and bacterial infections.

The development process was divided into three stages: printer development, transducer development and transducer validation. For the first stage, a commercial desktop printer was converted to a flatbed configuration and modified to print with silver nanoparticle ink and PEDOT:PSS polymer inks. For the second stage, three methods of manufacturing OECTs were investigated, and the most appropriate method for this project was chosen. Finally, the transistors were functionalised with antibodies and tested with samples of CRP protein.

The following chapter documents the process of printer modification.

Chapter 4

Printer Development

This chapter documents the process of modifying a desktop ink-jet printer into a material deposition system, with which an attempt will be made to print organic electrochemical field-effect transistors (OECTs). The HP DeskJet InkAdvantage 4535 was chosen to be modified as a material deposition system. Next, the process of mechanical modification is discussed, during which the printer is converted to a flatbed configuration to allow printing onto substrates of varying thicknesses, as well as alignment of subsequent printed layers. After completion of the mechanical modifications, the process of cartridge preparation is discussed. Following cartridge preparation, performance of the printer is assessed by three tests: minimum achievable resolution, layer alignment and printing with the conductive polymer PEDOT:PSS. Printing performance is also compared for different paper types. Finally, the suitability of the printer to this project is assessed. A summary of a very early version of this chapter was presented at the 3rd South African Biomedical Engineering Conference, 2018, [160]

4.1 Introduction

Ink-jet printers have become a popular tool for researchers working in the fields of flexible and organic electronics, as well as tissue engineering, and have been successfully used to manufacture various electronic devices and other constructs over the last ten years or more. This popularity is because of the speed at which new prototypes can be manufactured due to the simplicity of the process, combined with the versatility of ink-jet technology in the sheer number of materials that can be used as ink, such as biomaterials, polymer solutions and metal nanoparticle suspensions. Ink-jet printing works on the premise of depositing ink droplets in a pattern, defined by the user, to form the desired end product - usually an image, text document or combinations thereof. The goal of this chapter is to attempt to exploit this functionality of ink-jet printers to print structures with different materials, such as metal nanoparticle inks or conducting polymer solutions, towards the goal of manufacturing OECT-based biosensors.

4.2 Methodology

For this chapter an initial literature study was done, discussed in Chapter 2.7, and it was determined that the printer modified for this project would need to fulfil certain criteria:

1. The printer should preferably utilise a piezoelectric printhead,
2. The printhead should make use of small nozzles ($<50\ \mu\text{m}$) packed tightly together,
3. The printer should use disposable cartridges, for easy replacement of cartridges due to clogged nozzles,
4. The printer feed should be as flat as possible, and easy to modify, and
5. The cost of the printer should be as low as possible.

These criteria were then used to choose a printer to modify, but as mentioned in Chapter 2.7, the recent changes in Epson and Brother products make them unsuitable to use for this purpose, due to their recent move to use ink tanks and fixed printheads. It was then decided to rather use a printer from HP.

The chosen printer was then disassembled, evaluated and reconfigured into a flatbed configuration. Following the modification process, the printer was evaluated by performing three types of tests, namely printing resolution, layer alignment and printing onto different paper types for comparison. Lastly, the printer was modified to print with PEDOT:PSS inks, by modification of the ink viscosity.

4.3 Choice of Printer and Disassembly

After much consideration the choice was made to use the HP DeskJet Ink Advantage 4535 ink-jet printer for the project, shown in Figure 4.1. This printer was primarily chosen for two reasons. First and foremost, the printer utilises simple and relatively inexpensive cartridges that can be replaced easily in the event that one stops functioning due to clogged nozzles. Secondly, the resolution reported by the manufacturer is within the specifications for development of printed electronics.



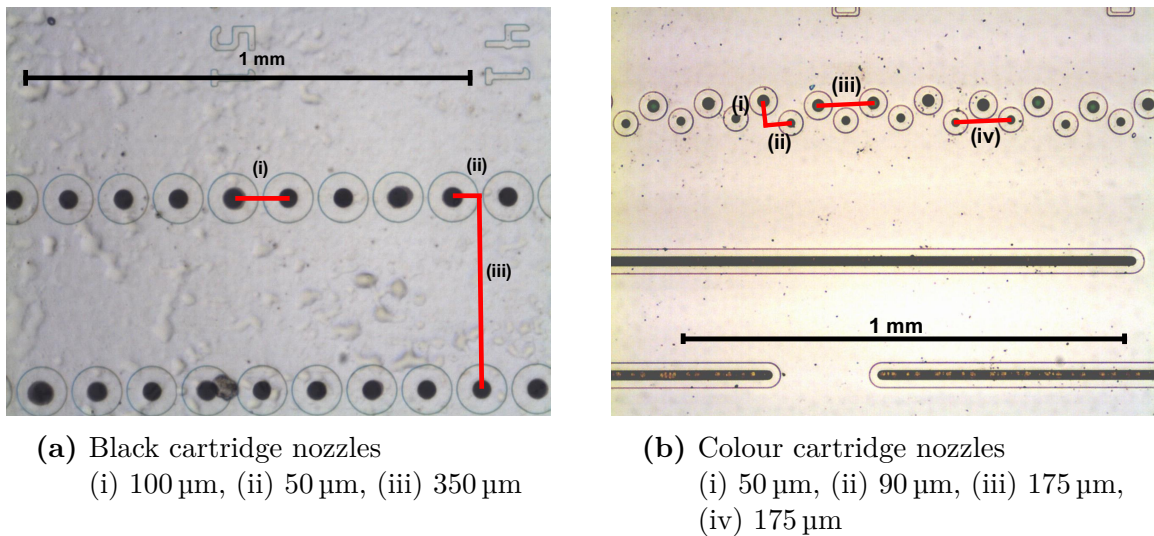
Figure 4.1: HP DeskJet Ink Advantage 4535 printer [from] [161]]

The HP DeskJet 4535 printer has multiple functions as scanner, fax and printer, but only the printer functionality is relevant to this project. It must, however, be determined whether the other functions, particularly scanning, will impede the normal function of the printer once disassembled.

The HP Deskjet 4535 uses a thermal ink-jet mechanism, with two disposable cartridges - one for black ink (HP 652 Black) and another for the colours of cyan, magenta and yellow (HP 652 Tricolor), shown in Figure 4.2. The two cartridges have different nozzle sizes and spacings, shown in Figure 4.3. The black cartridge, in Figure 4.3(a), utilizes nozzles with a diameter of $35\ \mu\text{m}$, spaced at intervals of $50\ \mu\text{m}$ in two rows, $350\ \mu\text{m}$ apart. The reported resolution of the black cartridge is 1200×600 dpi in the vertical and horizontal directions, respectively. This means that it should be able to place 22 pl drops at intervals of about $21\ \mu\text{m}$ vertically, and $22\ \mu\text{m}$ horizontally.



Figure 4.2: HP 652 cartridges [from [162]]



(a) Black cartridge nozzles
(i) $100\ \mu\text{m}$, (ii) $50\ \mu\text{m}$, (iii) $350\ \mu\text{m}$

(b) Colour cartridge nozzles
(i) $50\ \mu\text{m}$, (ii) $90\ \mu\text{m}$, (iii) $175\ \mu\text{m}$,
(iv) $175\ \mu\text{m}$

Figure 4.3: Cartridge nozzle spacings

The colour cartridge has two sizes of nozzles, shown in Figure 4.3(b), one with a diameter of $40\ \mu\text{m}$ and the other $30\ \mu\text{m}$. The nozzles for the colour cartridge are arranged in an alternating pattern of the two sizes, with $175\ \mu\text{m}$ separating nozzles of the same size and $90\ \mu\text{m}$ separating adjacent nozzles. The two rows of nozzles are spaced $50\ \mu\text{m}$ apart. The reported resolution of 4800×1200 dpi in the vertical and horizontal directions, respectively,

should correspond to droplet spacings of $5\ \mu\text{m}$ and $22\ \mu\text{m}$ in the two directions. It would appear that the reported droplet resolutions for the two cartridges are very different from what the nozzle measurements seem to indicate. Further investigation will be done to ascertain the minimum resolution attainable by the printer.

Opening the printer lid to inspect its mechanical components reveals that the cartridges are mounted on a linear rail, with a microswitch mechanism to sense the lid position. A piece of adhesive tape was used to permanently close the switch and allow operation with the lid open. Figure 4.4 shows the internal space of the printer.

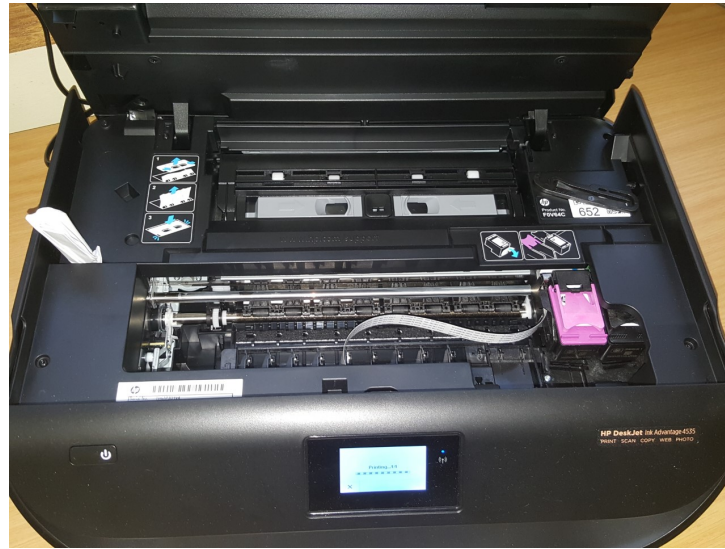


Figure 4.4: Open printer

Disassembling the printer further revealed that the scanner is connected to the motherboard by a single ribbon cable, and that disconnecting this cable does not prevent the printer from printing normally. Unplugging the scanner causes an error message to appear, reporting that there is a problem with the scanner that needs attention.

Further investigation into the function of this printer revealed that the paper positioning system is either based on time elapsed between steps, or more probably, on measurement of the absolute positions of the respective components. The reason for this hypothesis is the presence of rotary encoders on each of the rotating parts of the feed system, as well as a linear encoders on the carriage assembly. Interestingly, a single switch is used to indicate whether a page has been retrieved from the paper tray, located on the back of the original chassis in the path through which paper is drawn from the paper tray. Upon initiation of the printing process, a page is retrieved and brought to a microswitch that is triggered to signal the position of the page. The motor of the feed mechanism is continuously activated during this process. If arrival of the page is delayed, the feed mechanism pauses for approximately 500 ms, after which the feed motor is activated once again for a few seconds. If the microswitch is not triggered after this, an error message is displayed on the screen of the printer indicating an empty paper tray, and the printer returns to standby mode. However, upon experimentation with the timing of the microswitch trigger, it was found that it could be triggered during the brief pause of the feed system to allow normal operation, with the precise location of the page now known.

This functionality could be exploited to print multiple layers of black ink on top of one another, by positioning a page at the same position before initiating a print cycle. This is due to the pause in the feed process occurring at the same position relative to the paper starting position for each print cycle.

Following this, it was found that the printing mechanism consists of two primary components, that could be removed and reconfigured. First is the cartridge carriage assembly, which contains the two cartridges, mounted onto a linear rail and moved about by an electric motor, shown in Figure 4.5.

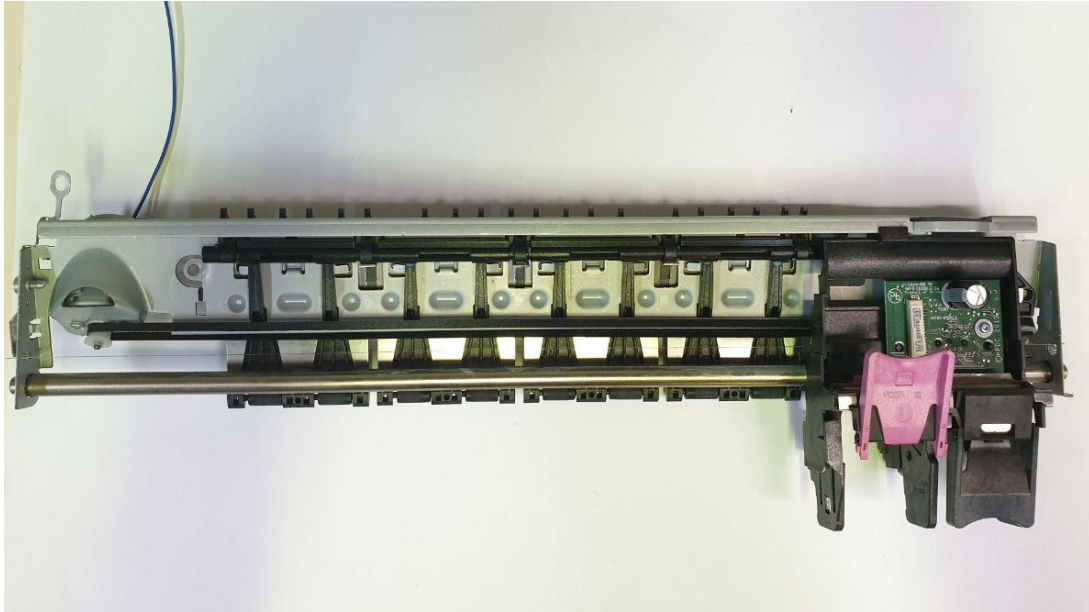


Figure 4.5: Detached carriage assembly

The second part of the printer system consists of the motor and mounting assembly for a trio of rotating steel rods, responsible for moving pages around the feed mechanism. The first roller, at the top of Figure 4.6, is fitted with four large plastic wheels and is responsible for transporting new pages from the paper tray below and aligning them for printing. The second roller, in the middle of Figure 4.6, is coated with a mildly abrasive coating to firmly grip onto pages and steadily feed them through the area where ink is deposited. The third and final roller, fitted with thin rings of rubber for grip, is responsible for guiding pages from the printing area and into the tray of pages that have completed the printing process.

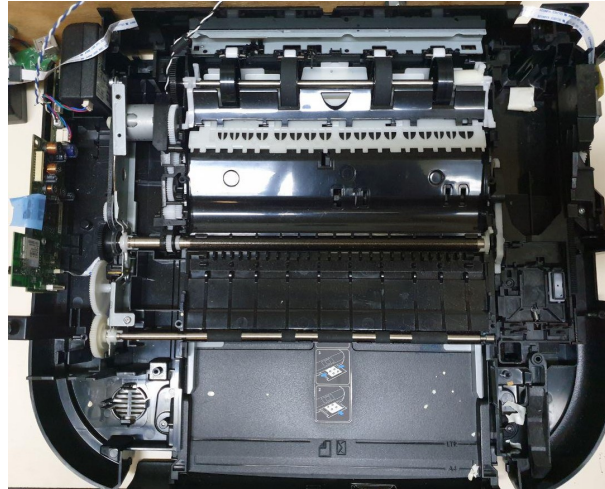


Figure 4.6: Exposed Feed Mechanism

These two main components of the printer, carriage- and feed mechanism, seem to be built in such a manner that would allow their rearrangement so as to facilitate simple material deposition and manufacturing of electronic components.

Comparison of the two available mechanisms, carriage and feed, to the positioning systems of commercial inkjet and 3D printing systems makes it clear that the printer can easily be modified to transport a rigid platform on rails past the carriage, and allow ink to be deposited onto the substrate. It was therefore decided to convert the printer into a flatbed configuration, similar to many typical 3D-printer configurations, but without a vertical positioning system.

4.4 Design of Printer Modifications

Following the disassembly of the DeskJet 4535 printer, it was decided to use its paper feed- and carriage mechanisms to build a flatbed printer, as illustrated in Figure 4.7. The flatbed configuration was chosen for three main reasons. First is that it allows adjustment of the height of the printheads relative to the substrate, to accommodate substrates of various thicknesses. Furthermore, the flatbed configuration seems to directly fulfil the requirement for the printer to be capable of multilayer alignment. It also does not require the substrate to be bent in any manner, preventing any mechanical damage to layered devices, and prevents contamination of the printed devices by limiting contact with the rollers to the bottom of the substrate platform.

Two of the rollers from the feed mechanism (the third is detachable) will be mounted directly under the carriage to transport the platform which supports the substrate. The platform itself will rest on two sets of metal guides to lower friction and allow alignment of printed layers, by making it possible to place the platform in the same starting position for each print when the guides are combined with endstop blocks. The function of these blocks is to allow the printing platform to be reset to the same position after each subsequent layer of printing, allowing alignment of multiple layers and the manufacture of multilayer devices.

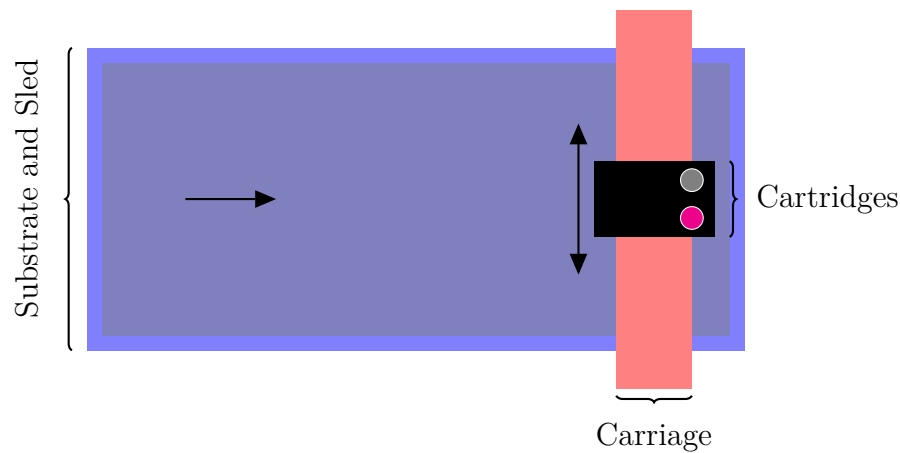


Figure 4.7: Illustration of flatbed printer layout

The modified printer would operate in the following manner:

- Step 1: The user positions the substrate platform to the predefined starting position, as per the endstop blocks,
- Step 2: The user then places the substrate of their choice on the platform, at a predefined position to allow alignment of layers,
- Step 3: The user initiates the printing process from a connected computer and waits until completion, and
- Step 4: The process is repeated if multiple layers are desired, with cartridges being exchanged before printing if multiple materials are used.

The length of the new printer chassis was determined before complete disassembly of the original printer, and was done by connecting several A4 pages end-to-end. The long piece of paper was then positioned with its leading edge against the first of the feed rollers, beneath the carriage. The printer was then set to print a full A4 page with horizontal lines placed at the top and bottom edges of the page. The chassis length was then determined by measuring the distance between the leading edge of the long page and the line at the bottom of the printed page. This length was found to be 405 mm. It was therefore decided to construct a chassis with a length of 810 mm, and to place the carriage in the middle of the new chassis. The metal guides would be mounted 2 mm below the tops of the rollers to allow easy movement of the platform. The platform was fabricated of 3 mm thick PMMA, or Perspex. The width of the chassis, and platform, was determined by the distance between the existing mounting screws available on the carriage, and was found to be 19 cm. This is slightly narrower than the width of an A4 sized page, but the intent is not to print very large structures and the smaller working area will be more than sufficient for the purpose of this project. A 3D rendering of the chassis design can be seen in Figure 4.8, showing the guides and positioning of the feed rollers. A technical drawing of the design can be found in Appendix B.

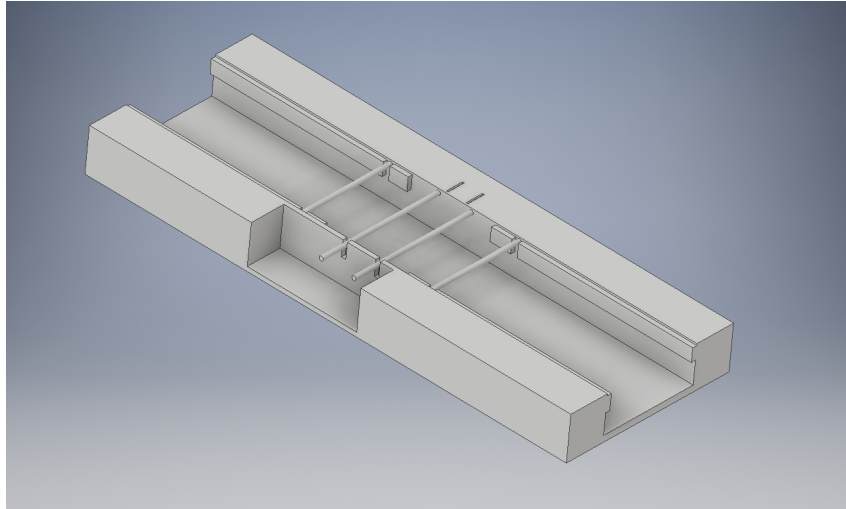


Figure 4.8: Modified printer design

The final addition to the printer design is that of endstop blocks. The endstops were designed and manufactured by 3D-printing after construction of the rest of the printer, due to their design being highly dependent on the materials used.

4.5 Implementation of Printer Modifications

The final printer was constructed using a combination of wood, aluminium, steel and PMMA, or Perspex. The two halves of the chassis were constructed of wooden planks, kept in place with 5 mm diameter threaded rods to allow adjustment of the chassis width. The mounting points for the feed mechanism to the chassis were constructed of 2 mm thick steel sheets, with holes drilled to accommodate the rollers and mounting points for the carriage assembly. The carriage assembly was mounted onto adjustable steel pillars, to allow the positioning of the printheads to be adjusted as necessary for substrates of varying thicknesses. Shown in Figure 4.9 is the mounted carriage assembly, with the aluminium angle-bars used as guides and the front roller of the feed mechanism visible.

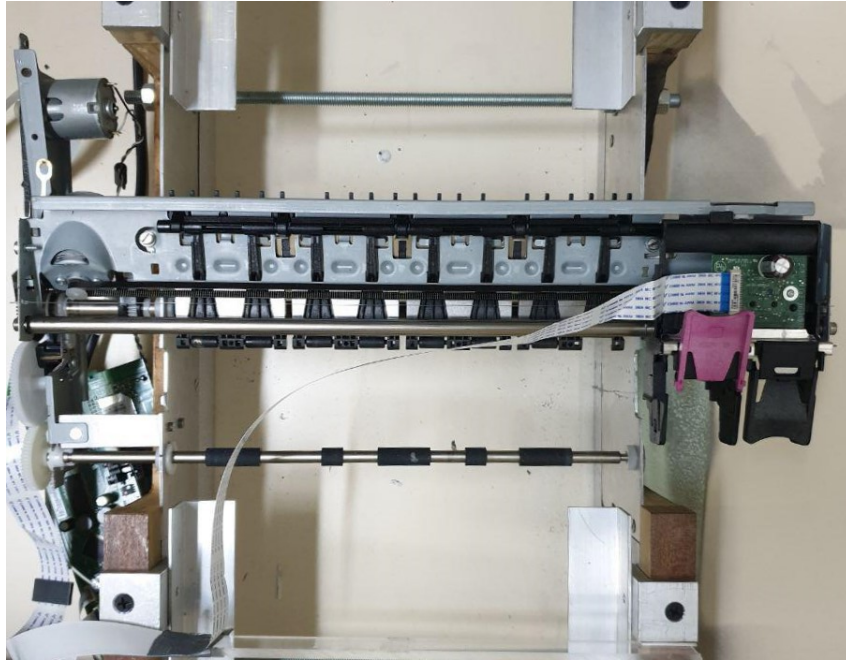


Figure 4.9: Rearranged carriage and feed assembly

The completed printer is shown in Figure 4.10, with the old chassis serving as a mounting point for the motherboard and the microswitch responsible for paper positioning, along with the PMMA platform positioned below the carriage assembly. Also visible in this image are the 3D-printed endstop blocks, attached to the left of the chassis.

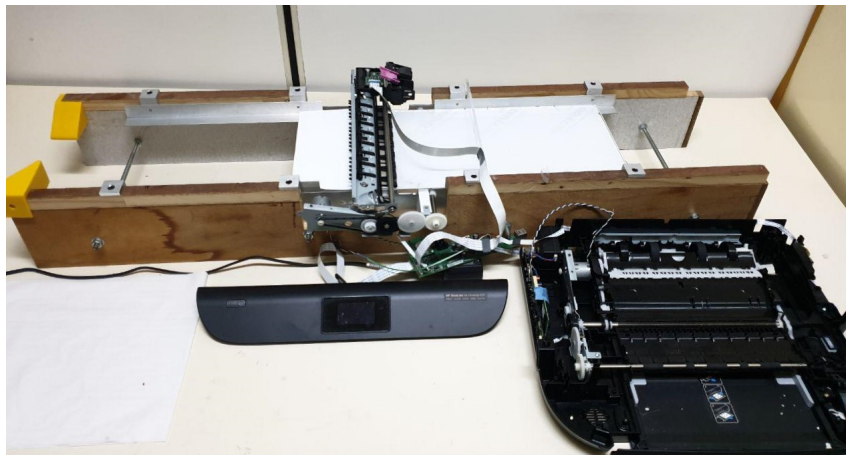


Figure 4.10: Completed printer

4.5.1 Cartridge Modification

A small part of the modification process of the printer included modifying the cartridges to be filled with inks other than those intended by the manufacturer. This meant that the ink already in the cartridges had to be removed, and the cartridges then cleaned before alternative inks could be introduced.

The procedure used to clean a cartridge started with using a saw to make incisions into the top covering of the cartridge, shown in Figure 4.11. The incisions are made at specific

positions, 3 mm below the label and at the top edge of the “652” to allow easy access to the sponges within without impeding reinsertion of the cartridges into the carriage. Next, a screwdriver or other flat implement was inserted into the cut and used to pry the covering off of the cartridge.



Figure 4.11: Cut cartridges

After having opened the cartridge, it was revealed that sponges are used to control the rate at which ink flows towards the nozzles. This is probably done to maintain a constant pressure behind the nozzles for consistent printing performance. The sponges were then removed and rinsed thoroughly in deionised water (16 M Ω) until long after any ink could be seen in the waste from rinsing. After rinsing the sponges, the inside of each cartridge was rinsed in deionised water until no ink could be seen in the waste. Next, the printhead of each cartridge was pressed against a paper towel to indicate whether any ink remained in the nozzles. If there was any indication of ink being present, the cartridge was rinsed again, until no ink could be observed after being pressed against a paper towel. After being rinsed, each cartridge was placed in an ultrasonic bath filled with deionised water and cleaned for 15 minutes at a temperature of 30 °C to remove any remaining ink. After sonication, cleaned cartridges were left to dry overnight under a laminar flow hood to force water evaporation. The inside of a cleaned and dried colour cartridge is shown in Figure 4.12. This also shows that a filter is present between the ink reservoir, to prevent any clots or particles present in the ink from clogging the nozzles. The presence of this filter is somewhat problematic if one intends to use the cartridge to deposit cells, as they might adhere to the fibres of the textile, although the filter could be removed to allow their passage. However, the filters were left in place for all printed work done in this project, to prevent the unnecessary clogging of nozzles. This process took 30 min to complete.



Figure 4.12: Cleaned colour cartridge

The process of filling a cleaned cartridge is comparatively simple. First, the nozzles are primed by adding 1 ml of deionised water to each ink reservoir and pressing the nozzles against paper towels until a wet mark can be seen spreading across the paper. Next, a sponge is placed in the reservoir and a hypodermic needle and syringe is used to deposit 3 ml of ink into the bottom of the sponge. Finally, the nozzles are again pressed against paper towels until it is observed that the new ink has reached the nozzles and has seeped into the paper. The nozzles are pressed against the paper towel in both instances to ensure that all of the nozzles are primed with either ink or water, preventing nozzles from being fired without some form of liquid present once installed in the printer. It is preferable to avoid doing this, as the resistors involved in firing each nozzle may burn out if no liquid is present due to the high temperature, compromising the cartridge.

4.6 Assessment of Modifications

Full characterisation of the printer is necessary before its applicability for the manufacture of biosensors can be established. The following section documents the procedures necessary to operate the printer, along with the three tests done to determine its viability for this project. The three tests consist of the following:

1. Testing of minimum printable resolution,
2. Testing of layer (mis)alignment, and
3. Testing if PEDOT:PSS can be printed effectively.

Following these steps it can be determined if the printer is suitable for the application of printing electronic devices, and more specifically, biosensors.

4.6.1 Printing Procedure

The procedure of printing an image or text has changed drastically due to the rearrangement of the printers mechanical components to serve the needs of this project. The most prominent change is the need to press a microswitch at a very specific moment during the process, which, if missed, causes the printer to halt and wait for the cycle to be restarted. After connecting a computer to the printer, the printing procedure is as follows:

- Step 1: Open the document to be printed on the computer,
- Step 2: Align the printing platform to the endstop blocks and ensure that the platform rests upon the first of the two rollers of the feed mechanism,
- Step 3: Position the substrate on the platform to align with the region where the ink will be deposited. It may be necessary to do a test print to determine this,
- Step 4: Issue the print command from the connected computer,
- Step 5: Wait for the printer to acknowledge the document and stand ready to press the microswitch,
- Step 6: Press the microswitch once the platform is seen to pause, and
- Step 7: Release the microswitch once the printer has begun depositing ink onto the substrate.
- Step 8: For multilayer structures this process will be repeated for each layer, with cartridges being exchanged as necessary.

This process, if followed closely, will result in successfully printed patterns with every attempt, although it may be necessary to practice activation of the microswitch at the appropriate time due to the briefness of the pause. Printing duration varies from image to image and is dependent on whether the printer is operating in rasterised- or vectorised mode, corresponding to raster- and vector format images, respectively.

4.6.2 Resolution Tests

As mentioned previously, the time taken to complete a print is dependent on the format of the image being printed - whether it is in a rasterised- or vector format. Rasterised formats, such as bitmaps (.BMP), store images as arrays of pixels, whereas vector formats, such as Scalable Vector Graphic (.svg), store images by describing them mathematically. Structures printed from vector format images tend to be completed in much less time than high-resolution rasterised images, but have other disadvantages.

The tests in this section were all done following the procedure described in Section 4.6.1. The first test done with the printer was to determine whether vector- or raster format images would be more suited to accurately realise structures on paper. This was done by designing similar structures in two formats - SVG was chosen for vector format, and XCF for raster format - and then comparing the realised structures. The structures in Figure 4.13(a) and Figure 4.13(b) show examples the types of patterns printed. All of the test patterns were printed using Silver Nanoparticle Ink (MBSIJ-MU01) onto resin-coated paper (NB-RC-3GR120) from Mitsubishi Paper Mills, using the colour cartridge (HP 652 Tricolor). The black cartridge was not used after it was found that it performed very poorly in initial tests, despite attempts at improvement.

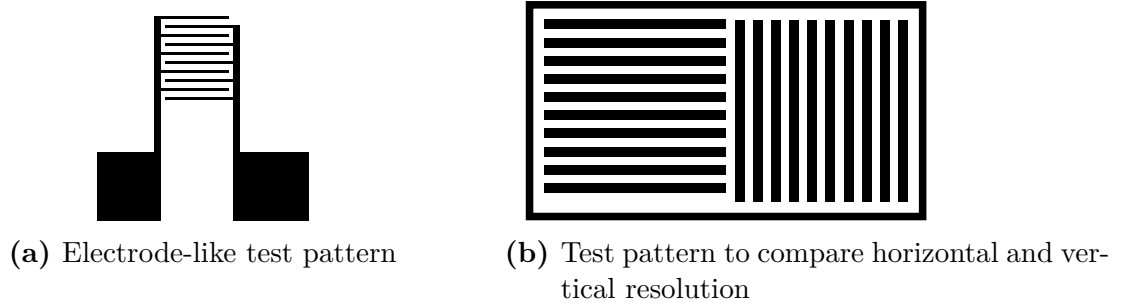


Figure 4.13: Test patterns for printer evaluation

The pattern in Figure 4.13(a) was designed to test the potential for the printer to realise interdigitated electrode-like patterns which are a popular method of maintaining a small size for high-performance transistors. It is therefore important for the printer to be capable of printing such structures. The second test pattern, shown in Figure 4.13(b), was used to evaluate the resolution of the printer in different directions - vertical and horizontal. This was done due to the reported resolution for the cartridges having different values in two directions. Variations of the patterns were done, and line lengths, widths, and gap widths were tested to determine the minimum resolution that can be printed by the printer.

All designs of vector format images shown here were done in the Inkscape graphical design application. It was found that patterns printed from designs in vector format performed unpredictably, with line widths varying across a group of printed tests. Figure 4.14 shows an example of the inconsistencies encountered while printing patterns from vector format designs. One can clearly see that there is almost no consistency between adjacent electrodes, and that there are also variations within individual electrodes.

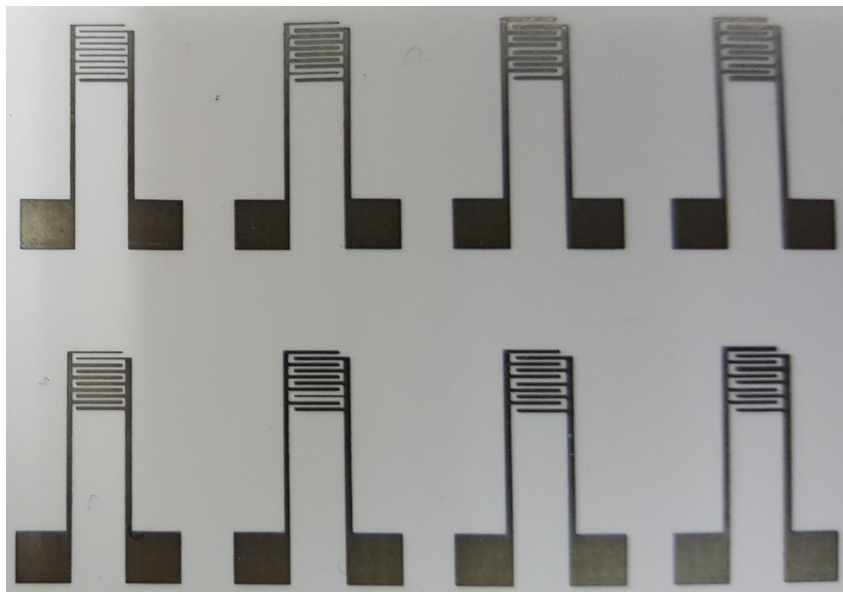
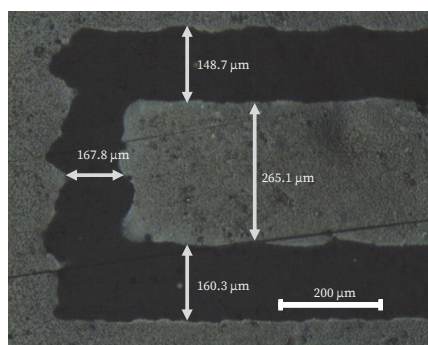


Figure 4.14: Inconsistencies in printed structures from vector format designs

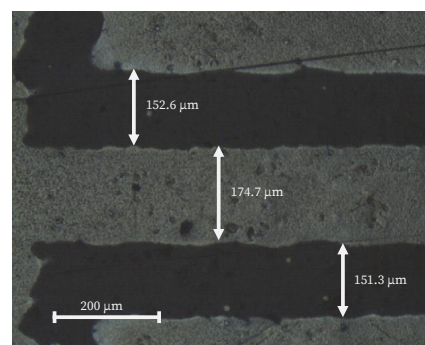
A possible reason for the inconsistencies in the results from the vector format designs is that the mathematical description of a structure has to be discretized before being printed

- often by the printer itself. This discretization process would then introduce errors in the printing process, and cause the inconsistencies seen in Figure 4.14.

Nevertheless, measurements were done of the patterns printed from vector format designs. Figure 4.15(a) shows electrodes printed from the first design, when viewed using a microscope. This image shows that the lines printed by the printer in vector mode are relatively straight, with very little sign of the original droplets. This means that the droplets are deposited in quick succession, before the individual droplets can dry and sinter, allowing them to merge into a single continuous structure, which should be beneficial to printed devices due to increased conductivity. Also present in Figure 4.15(a) is one of the other disadvantages of vector defined images: the printer does not realise vertical lines well, and the boundaries of vertical structures are poorly defined. This is probably due to the high speed of the carriage when printing vector format images, which may cause greater difficulty in alignment between adjacent horizontal lines. The high deposition rate of the droplets may also be contributing to this effect, causing the ink to spread around on the paper, but if this were the case one would expect to see the same in the vertical direction, which is not observed with any certainty.



(a) SVG-defined lines



(b) Minimum Line- and gap dimensions for SVG-defined structures

Figure 4.15: SVG-defined electrodes

Next, in Figure 4.15(b), the minimum line widths and gaps between lines for vector format images are shown. The minimum line width that could be reproduced with any consistency was $\approx 170 \mu\text{m}$, with gaps of $\approx 150 \mu\text{m}$ on either side, for both horizontal and vertical orientations. Increasing the width of the gaps between lines causes variation in the width of the horizontal lines, and decreasing the width of the lines causes the erratic behaviour seen in Figure 4.14.

The next test done was to determine the printer's performance using designs in raster format images. All designs for these tests were done in the GNU Image Manipulation Program (GIMP). It was found during the course of these tests that the specific configurations of the printer and application had a significant impact on the quality of structures deposited. GIMP has the added functionality that it has direct access to the printer drivers, which Inkscape did not. This means that GIMP could potentially realise structures in far higher resolution than Inkscape, if the correct configurations are used.

Initial tests were done with an image drawn at a resolution of 1200x1200 dpi, with GIMP set to print at normal resolution and the printer set to operate in high-quality mode. Figure 4.16 shows an example of the initial tests done using GIMP, where lines of $\approx 150\ \mu\text{m}$ could be printed, separated by gaps of $\approx 150\ \mu\text{m}$, but the lines seem to be composed of large droplets spaced far apart, causing lines to be poorly defined and inconsistent. The same performance was observed for both vertical and horizontal patterns. This is clearly unusable for the manufacture of electronic devices, and is far inferior to the performance of vector format images.

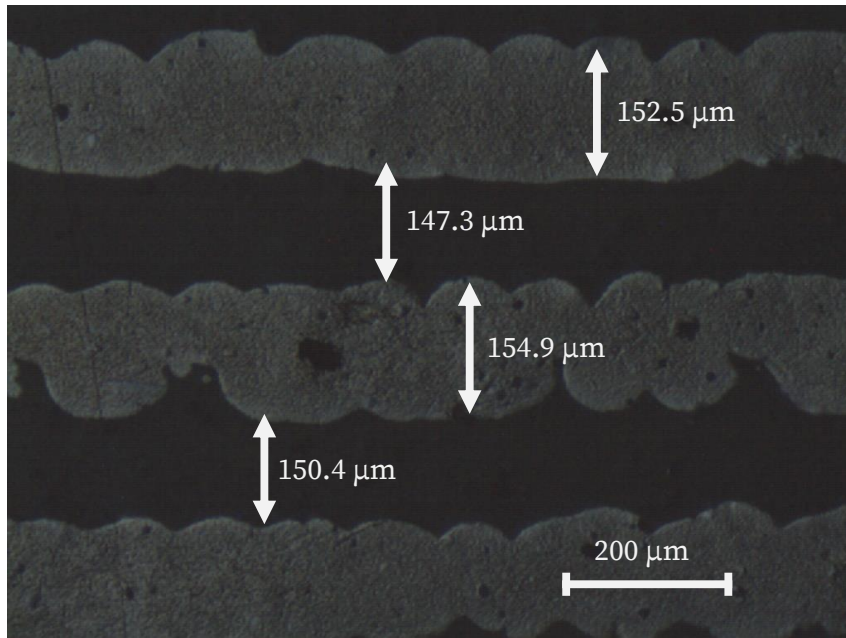


Figure 4.16: Initial GIMP-defined electrode dimensions

Next, GIMP was set to print at high quality, and the printer was left to operate in high-quality mode. The images in Figure 4.17 show the results of this test, with the minimum gap sizes in comparison with larger gaps. The pattern used in this test was an adapted version of Figure 4.13(b), where gaps of varying sizes were left in the middle of both the vertical and horizontal lines, to determine the size difference in horizontal and vertical resolutions for this particular configuration. This shows that the printer does have different resolutions in the two directions, as given by the manufacturer. Increasing the resolution settings in GIMP did not appear to offer any improvement in print quality. The minimum gap width that could be printed for horizontally defined gaps was $\approx 80\ \mu\text{m}$, in Figure 4.17(b), although the edges of these gaps can be seen to be somewhat irregular. For the vertically defined gaps, a minimum gap size of $\approx 30\ \mu\text{m}$ could be achieved, which corresponded to a single pixel width in GIMP, and a single droplet of ink on paper. The minimum width of a line that could be printed with this configuration, that remained conductive, was $\approx 100\ \mu\text{m}$. Thinner lines tended to become disconnected due to the gaps between droplets. Upon comparison of the general characteristics of the vertically- and horizontally defined gaps, it becomes clear that the printer has some limitations in terms of resolution. It would appear that lines in the horizontal direction are much more consistently printed with well-defined edges than is the case for vertically defined lines. This seems to be caused by the sequence in which the printer deposits the lines; the cartridges pass across the paper in the horizontal direction, while the paper moves in the vertical

direction (relative to the images). This may cause misalignment of horizontal lines, and allows horizontal lines to be deposited in one pass, while vertical lines must be built up in several steps.

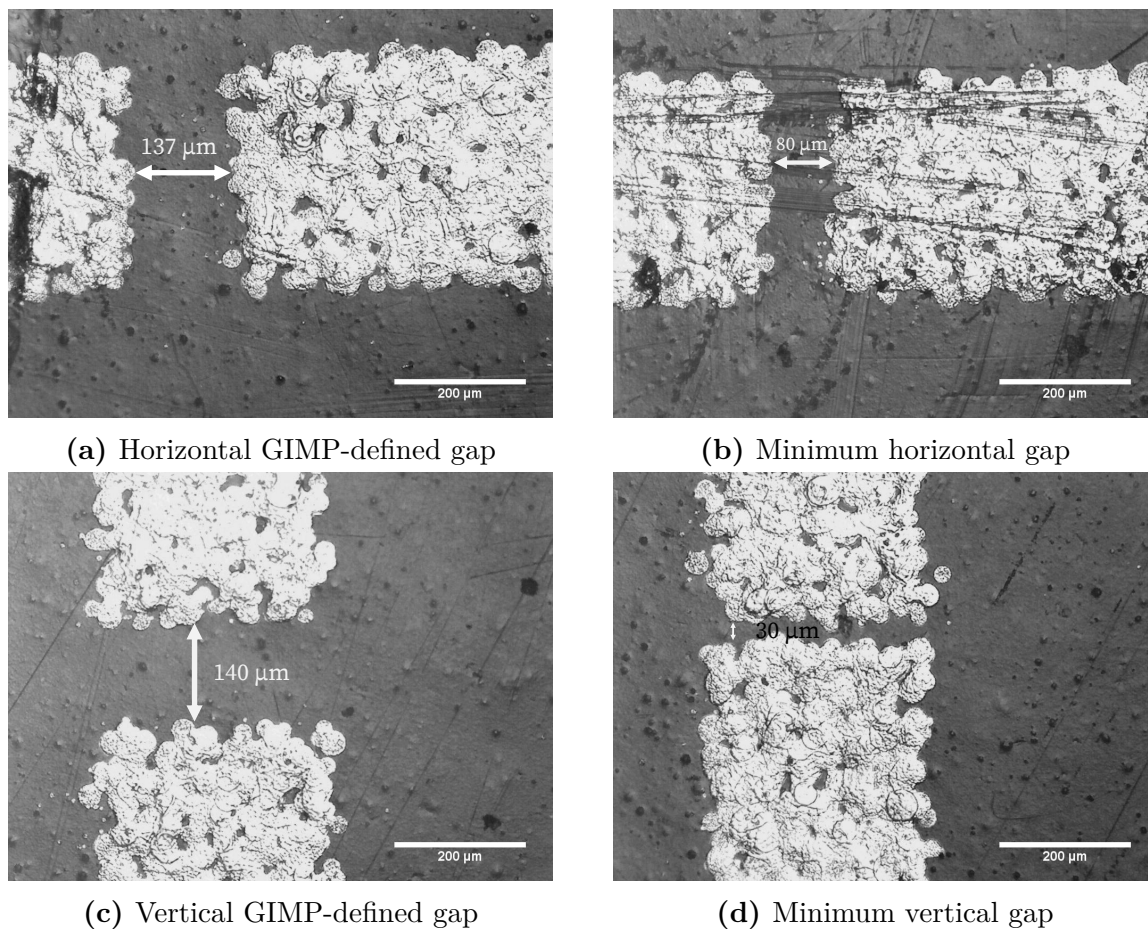


Figure 4.17: Comparison of printer performance in x- and y- directions

Further modification of the settings in GIMP, to printing in photo mode with full bleed enabled, improved the quality of printed structures. Shown in Figure 4.18 is the best performance realised with the printer, with both horizontal and vertical gaps reduced to $\approx 70 \mu\text{m}$. Smaller gaps were seen to become less consistent, with droplets often bridging the distance between silver regions. It is thought that this is caused by the higher density of droplets deposited when images are printed in photo-mode. The consistency of line edges had also been improved, as well as the coverage of silver over the desired regions - no gaps or voids can be seen in the silver layer, as was the case before. The minimum width of a line of silver that could be printed while remaining conductive was approximately $80 \mu\text{m}$, due to the conductivity of the silver becoming too low.

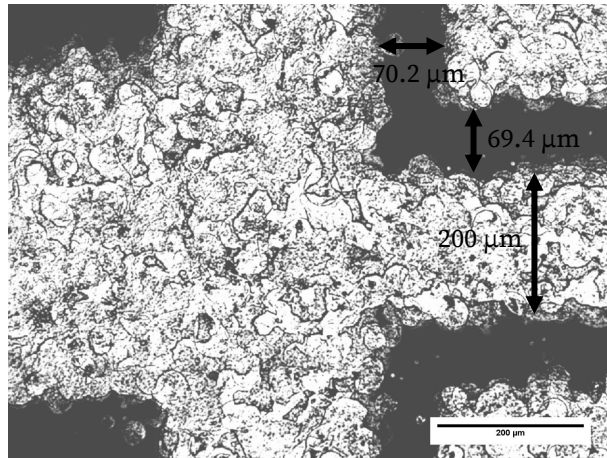


Figure 4.18: Printer resolution performance with improved configuration

Most of the tests shown above were repeated with higher resolution source images, specifically 1600x1200 dpi and 4800x1600 dpi, and no improvement could be seen in the structures printed from them. Table 4.1 shows a summary of the results of the tests done to determine the resolution of the printer.

Table 4.1: Summary of resolution test results

	Vector	Raster (initial)	Raster (intermediate)	Raster (final)
Minimum Gap (vertical) [μm]	150	150	30	70
Minimum Gap (horizontal) [μm]	150	150	80	70
Minimum Line [μm]	170	150	100	80

The results from the last group of tests show that, while the vector format designs have their advantages, the raster format designs, printed from GIMP, are clearly superior in the areas of consistency and resolution. Therefore it was decided to use GIMP for all subsequent tests done for this project. Table 4.2 shows the final configuration of both the printer and GIMP that was used for the rest of the project.

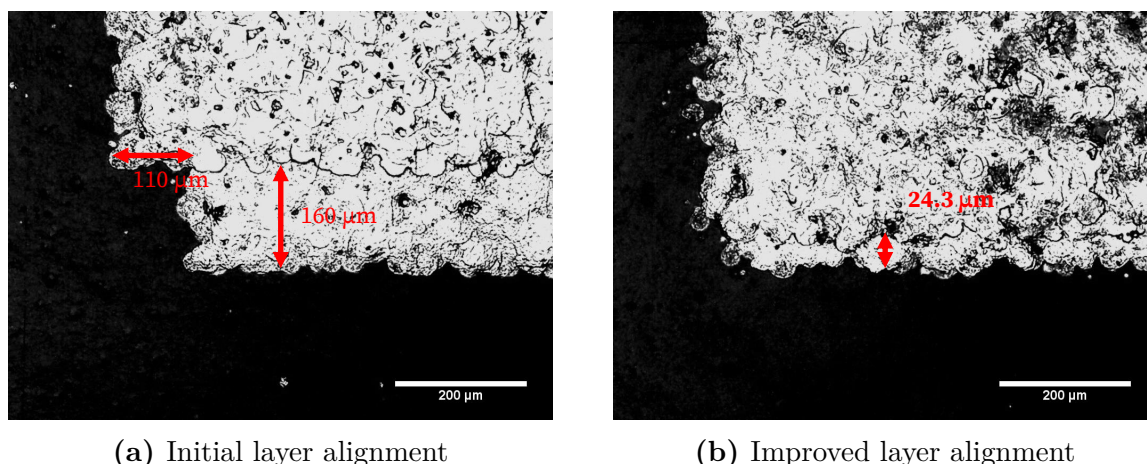
Table 4.2: Summary of parameters for printing

Name of Parameter	Value
Image resolution	1200x1200 dpi
Printout mode (in GIMP)	Photo on photo paper, full bleed, colour and black
Printout mode (on printer)	Photo
Paper type (on printer)	Plain paper

Paper type is a setting on the printer, not the actual paper type used. The Mitsubishi paper is closer to a high-quality photo paper than regular paper.

4.6.3 Layer Alignment Tests

After having determined that the printer can be used to successfully manufacture electrodes from silver nanoparticle ink, it was necessary to test the alignment of multiple layers printed onto the paper substrate. This was done by using the procedure described in Section 4.6.1. Initially, alignment between layers was poor, shown in Figure 4.19(a). The second layer was offset from the first by $\approx 110 \mu\text{m}$ and $\approx 170 \mu\text{m}$ in the x- and y- directions, respectively. This poor alignment was found to be caused by the printer platform not being aligned to the metal guides between layers, meaning that the starting position was different between layers.

**Figure 4.19:** Layer alignment tests

Following the observation above, the platform was aligned to both the endstop blocks and metal guides, with the resulting alignment shown in Figure 4.19(b). The printer was able to align two layers of silver to within $25 \mu\text{m}$ in the y-direction, and no difference could be measured in the x-direction. This alignment was found to be repeatable, with several subsequent prints being done with very similar alignments. There is, however, a limitation to this alignment system, and that is that the substrate must remain mounted to the platform at all times, as any movement will change the orientation of the substrate and cause misalignment between layers. This limits the processing methods that can be used between printed layers, and may prove problematic if it is not taken into account when the substrate must be removed between printed layers.

4.6.4 Comparison of Printed Structures on Different Paper Types

Following successful printing of small-scale structures onto the paper recommended by the ink manufacturer, a comparison was done to compare the performance of other types of paper to the results in the previous section. This is to ensure that the best paper type is used to manufacture sensors, and improve sensor performance if possible. The properties of interest are water resistance, as the sensors will be used in aqueous solutions, surface roughness, and mechanical stability. Surface roughness will have an effect on the performance of the transistors manufactured, and mechanical stability will determine whether the sensors are robust enough for general handling.

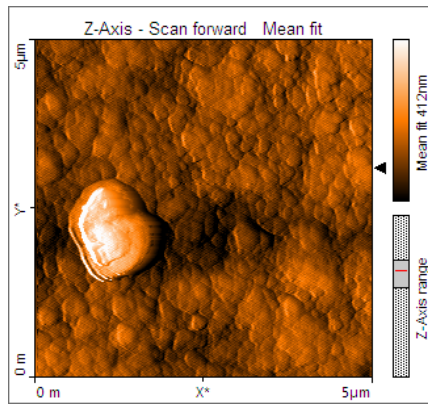
Photo papers are generally formulated to have a surface finish that is very smooth and slightly hydrophobic to allow printing of high-resolution images without the image being distorted due to ink spreading out through absorption by the underlying paper. It is for this reason that it was thought to compare three different photo papers to the resin-coated paper recommended by Mitsubishi Paper Mills for use with the silver nanoparticle ink. The three types of paper are shown in Table 4.3.

Table 4.3: Paper types chosen for comparison

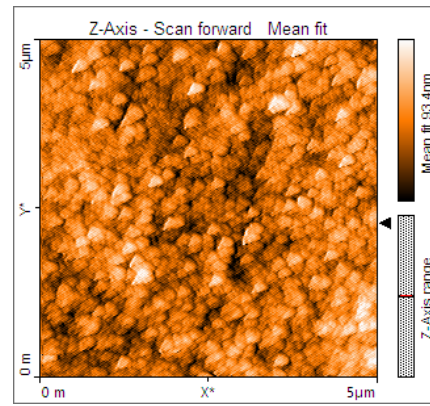
Paper Name	Paper Weight [g·m ⁻²]	Paper Type
Epson Premium Semigloss	251	Photo
Epson Ultra Glossy Photo Paper	300	Photo
JoJo Waterproof Glossy Inkjet Paper	230	Photo

The three types of paper were chosen for their very different surface coatings and capacity to absorb moisture. The Ultragloss paper should have a very smooth surface that is highly hydrophobic for ultra-high resolution images. The Semigloss paper should have a rougher surface finish for a matte-appearance, but the same hydrophobic coating as the Ultragloss. The final paper, with a waterproof coating, was chosen because the waterproof finish might be beneficial to sensors that are expected to function when submerged in aqueous solutions.

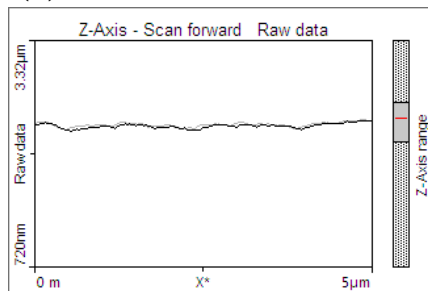
Following the choice of paper, samples of each type, including that from Mitsubishi, were imaged with an Atomic Force Microscope (AFM) (Nanosurf Easyscan 2) to compare their surface characteristics. The specific characteristics considered were surface area roughness and maximum surface deviation. Shown in Figures 4.20 and 4.21 are the images obtained for the four paper samples.



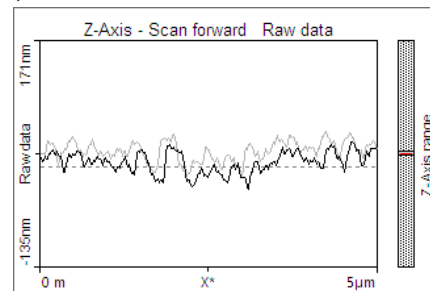
(a) Surface of Mitsubishi paper



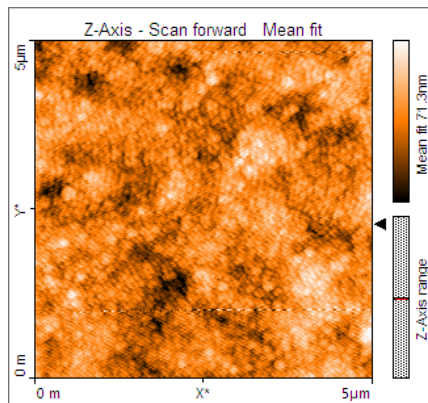
(b) Surface of Epson Semigloss paper



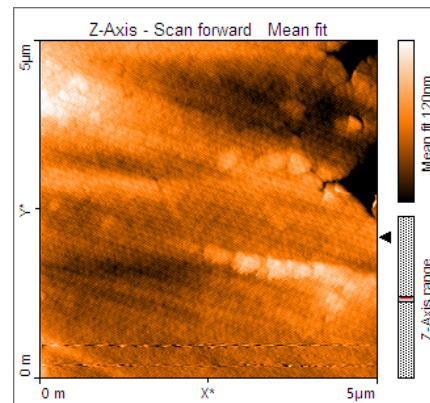
(c) Surface cross-section of Mitsubishi paper



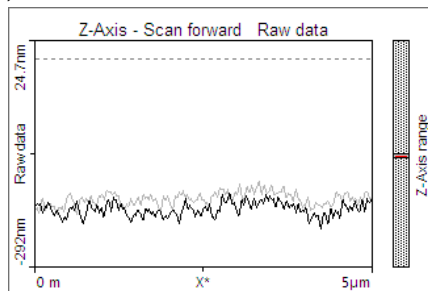
(d) Surface cross-section of Epson Semigloss paper

Figure 4.20: Surface properties of Mitsubishi and Semigloss papers

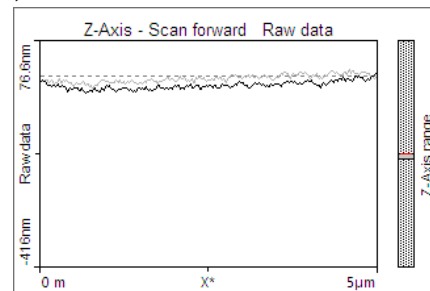
(a) Surface of Epson Ultragloss paper



(b) Surface of JoJo Waterproof paper



(c) Surface cross-section of Epson Ultragloss paper



(d) Surface cross-section of JoJo Waterproof paper

Figure 4.21: Surface properties of Ultragloss and JoJo Waterproof papers

From the results in Figures 4.20 and 4.21 it appears that the papers do differ substantially in terms of surface characteristics. The Mitsubishi paper, apart from the dust particle, appears to have a highly structured surface, with few peaks or valleys in the surface. The Semigloss and Ultragloss papers appear to have a highly granular surface, with many peaks and valleys. the waterproof paper appears to have a very smooth and uniform surface.

The measurements in Figures 4.20 and 4.21 were then used to calculate area roughness parameters for the paper samples, shown in Table 4.4, where S_a is the arithmetical mean height of the paper surface across the region of interest as measured by the AFM - calculations were done using the Nanosurf Easyscan 2 software. For the Mitsubishi paper, the value is calculated for a region that does not contain the dust particle seen in Figure 4.20(a).

Table 4.4: Calculated surface roughness for paper samples

	S_a [nm]
Mitsubishi	23.33
Semigloss	11.46
Ultragloss	8.73
Waterproof	12.98

This comparison shows that the Ultragloss paper has the lowest surface roughness of the four, followed by the Semigloss, Waterproof and Mitsubishi papers. This result is somewhat unexpected, as it appears to the naked eye that the Semigloss paper should have the highest surface roughness. From these results, it was expected that the Ultragloss and Semigloss papers would outperform the Mitsubishi in terms of printed resolution, as it was thought that the smoother surface would allow for finer control over where droplets are located when combined with the hydrophobic nature of photo paper.

Following comparison of surface parameters, the same pattern was printed onto each paper type. The image used was the same as in Figure 4.18, with the minimum gap size defined for both x- and y- directions. This pattern was chosen to evaluate the impact of the differing surface properties on on printing resolution, ink spread and the surface of printed silver layers. Shown in Figure 4.22 is the result of the printed patterns.

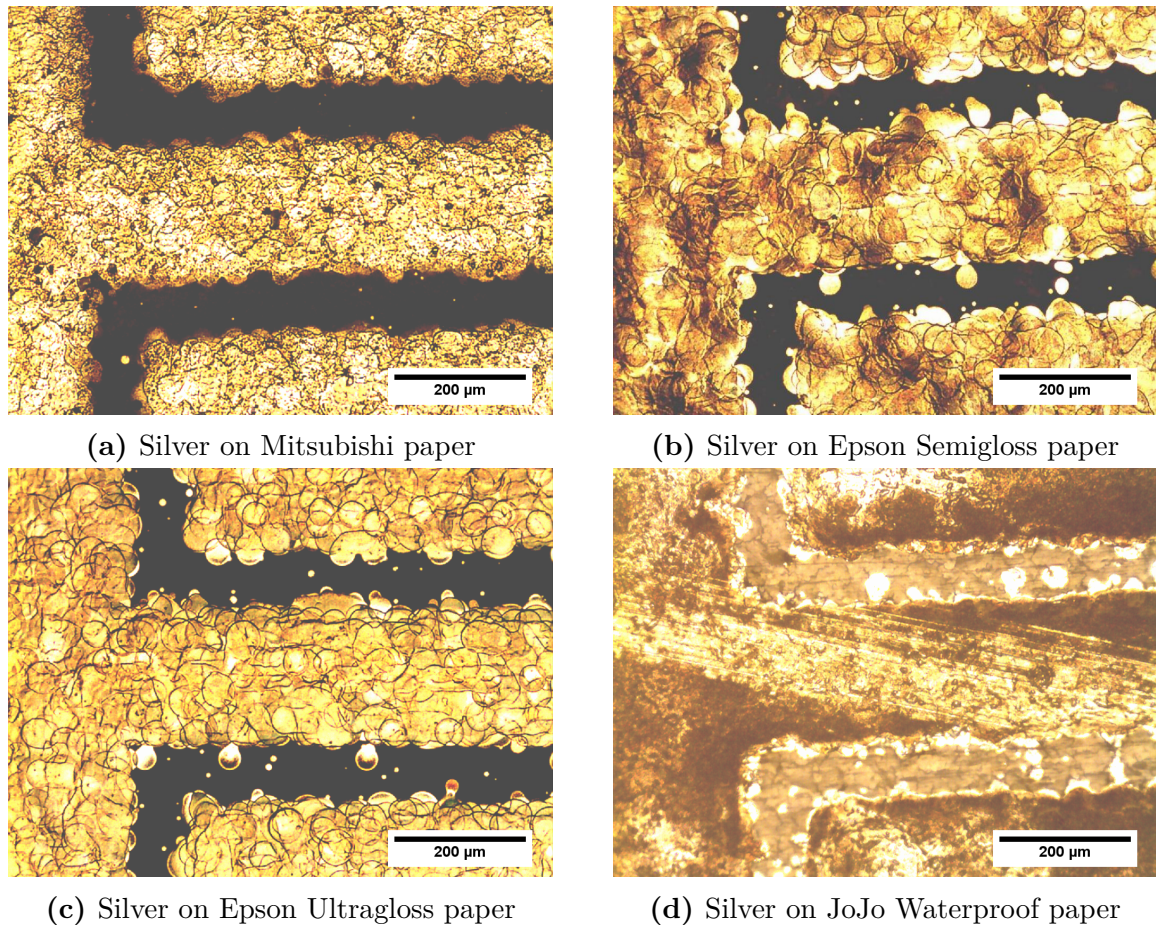
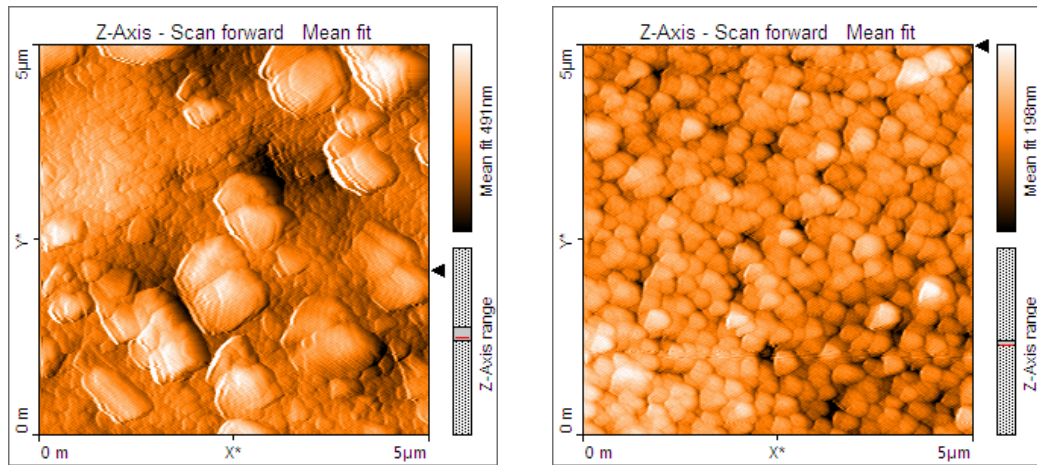
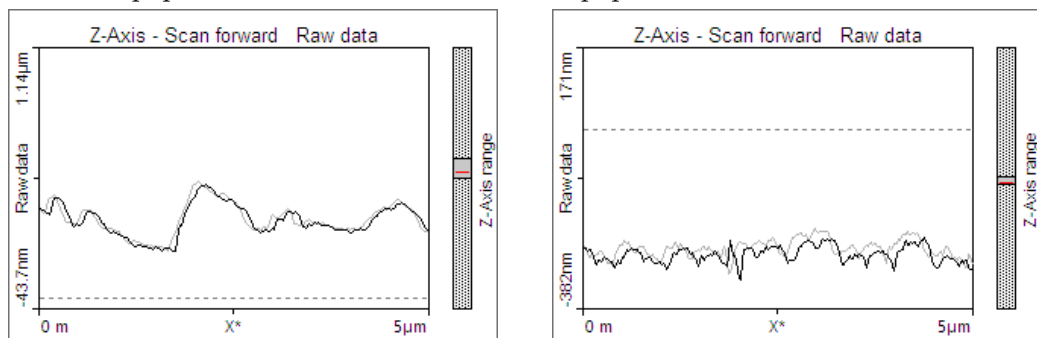


Figure 4.22: Comparison of printed silver on different paper types

These results clearly show that the choice of paper has a significant impact on ink and printer performance. Of the four tests, the Mitsubishi paper in Figure 4.22(a) appears to have performed the best, with the best-defined lines and most consistent gap widths. The appearance of the Semigloss paper is curious, as it seems to be midway between the Ultragloss and Mitsubishi papers, with the apparently rough surface of one and the errant droplets of the other. The Semigloss paper appears to have very well-defined individual droplets, which is due to the wicking properties of the photo paper - moisture is drawn away from the droplet by paper fibres and the porous surface coating to dry the ink as quickly as possible, while the hydrophobic coating keeps the droplet from spreading out while it dries. Unfortunately, this prevents the droplets from congealing, as seen in Figure 4.22(b). Comparison of Figure 4.22(c) with Figure 4.22(a) shows that the Ultragloss paper also has a higher incidence of satellite droplets than the Mitsubishi paper and fringing along edges, as also seen for the Semigloss paper. Again, this is thought to be due to the ink drying too quickly and not allowing the droplets to congeal during the process. As expected, the waterproof paper differs completely from the other papers. It appears that a dark layer of unsintered nanoparticles formed on the surface of the sintered silver, while the surface of the sintered silver closely resembles that of the Mitsubishi paper. Attempts at removing the dark layer by rubbing with gloves were met with limited success, as the lighter line through the image shows. Evaluation of the precise surface characteristics of the printed silver, in Figures 4.23 and 4.24 reveals that the paper has a high impact on the surface roughness of the printed silver.



(a) Surface of silver printed onto Mitsubishi paper (b) Surface of silver printed onto Semigloss paper



(c) Surface cross-section of silver printed onto Mitsubishi paper (d) Surface cross-section of silver printed onto Semigloss paper

Figure 4.23: Surface characteristics of silver printed onto Mitsubishi and Semigloss paper

For the Mitsubishi paper it appears that the printed silver sinters in a highly structured manner, with crystals or crystal-like structures forming on the surface and causing large bumps and troughs on the surface, seen in Figure 4.23(c). From Table 4.5 it can be seen that printed silver on the Mitsubishi paper has the second highest average surface roughness, S_a , of the four paper types, at 62.1 nm. Silver on the Semigloss paper has a much lower surface roughness than the Mitsubishi paper, with an average roughness of 21.6 nm, with smaller surface structures (Figure 4.23(d)), but the silver surface appears to be much less structured and has a more random appearance from Figure 4.23(b). The same can be said for the Ultragloss paper, where the surface structure is finer than for the Semigloss, but has the same pattern. The silver printed onto Ultragloss paper also has the lowest average surface roughness of the four paper types, 16.82 nm in Table 4.5, which might be beneficial to the creation of thin-film devices due to the constraints on electrode surface properties in such devices [163].

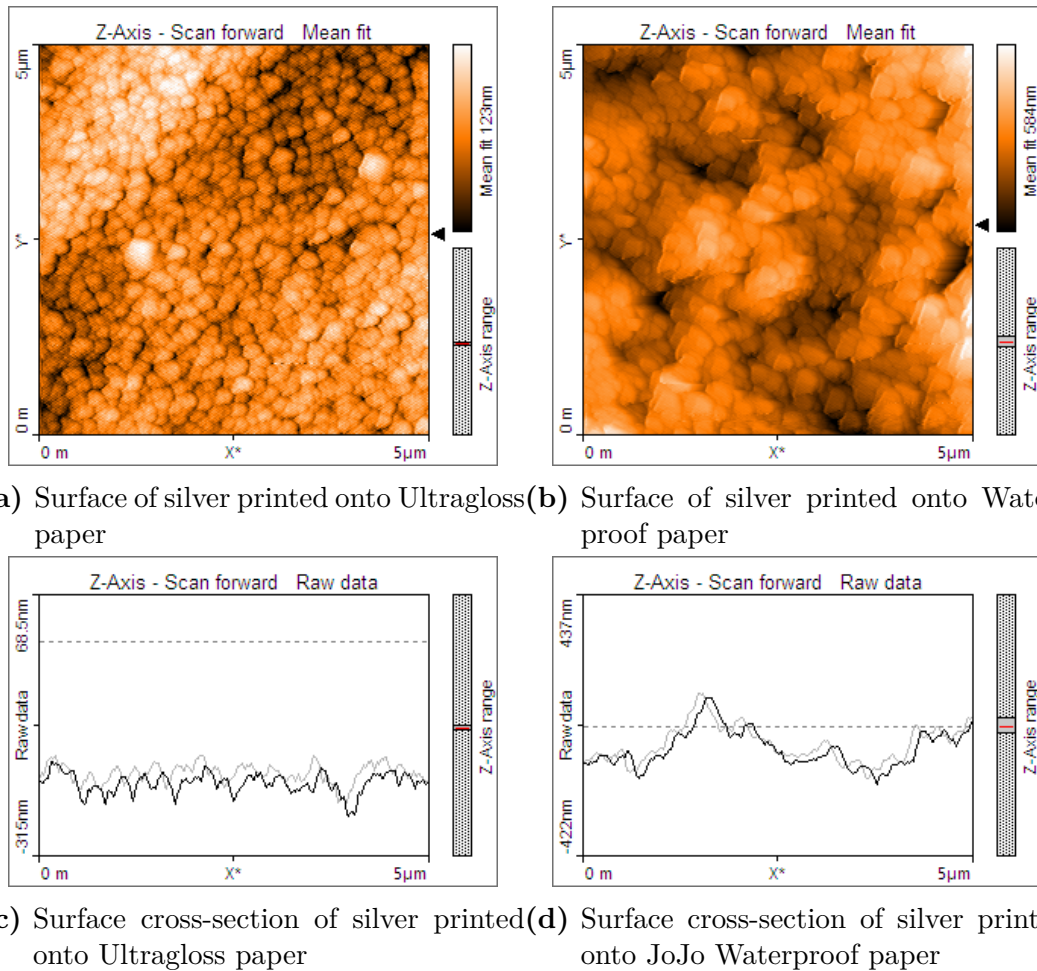


Figure 4.24: Surface characteristics of silver printed onto Ultragloss and JoJo Waterproof paper

The Waterproof paper is shown in figure 4.24(b) to have a similarly structured surface to the Ultragloss and Semigloss papers, but with much greater variation in height than either, shown in figure 4.24(d). As a result of this, the Waterproof paper has the highest average surface roughness of the four paper types, at 67.47 nm.

Table 4.5: Calculated surface roughness for silver on paper samples

	S_a [nm]
Mitsubishi	62.1
Semigloss	21.6
Ultragloss	16.82
Waterproof	67.47

Physical inspection of the printed silver revealed an additional piece of information: that the silver printed onto the Ultragloss and Semigloss papers adhered very poorly to the paper, and could be removed by bending the page very slightly. A possible cause for this

may be the surface coating of the photo papers - it may prevent the silver from penetrating into the paper and thereby adhering well. Another possible explanation may be the low surface roughness itself, which may mean that there are few locations for the printed silver to adhere to the paper surface, making delamination easier. The Mitsubishi and waterproof papers had no such problems and the silver remained stable when bent.

When taking into consideration all of the results from Figures 4.20, 4.21, 4.23 and 4.24, in combination with Tables 4.4 and 4.5, it would seem that the Mitsubishi paper is not the ideal substrate to manufacture thin-film devices with, due to the high average surface roughness. However, when the performance of the Mitsubishi paper in printing high-resolution structures and mechanical stability are taken into account it becomes clear that the Mitsubishi paper is better suited to sensor development, due to sensors requiring a high degree of repeatability and predictability.

4.6.5 Printing with PEDOT:PSS

After having shown that the printer is capable of both printing high-resolution electrodes and aligning multiple layers to high accuracy, the next step towards manufacturing biosensors is to formulate a mixture of PEDOT:PSS to print with in order to form the semi-conducting layer of the Organic Electrochemical Transistors (OECTs). To this end, a PEDOT:PSS solution was sought that was chemically compatible with the cartridges and had a low enough viscosity to enable it to be printed successfully without clogging the nozzles frequently. Viscosity requirements for thermal ink-jet mechanisms are known to be about 1.5-1 mPa·s [164], although it is dependent on manufacturer specifications and the shear rate at which the viscosity is measured. Therefore several iterations of ink dilutions were done, with each dilution lowering the viscosity of the mixture gradually. Care had to be taken to not dilute the proportion of PEDOT:PSS by a large factor, to maintain high conductivity for printed layers.

The PEDOT:PSS mixture known as Clevios PH1000, available from Heraeus, Germany, was used during these experiments, due to its high potential conductivity and well-known characteristics in literature [165]. Dimethyl Sulfoxide (DMSO) (Sigma-Aldrich, D5879-1L), ethylene glycol (Sigma-Aldrich, 102466-2.5L), glycerol (Sigma-Aldrich, G7893-1L), ethanol (17054, Cameron Chemical Consultants), and acetone (Protea Chemicals) were used during the process of refining the mixture. DMSO, ethylene glycol and glycerol are all well-known solvents for PEDOT:PSS and also act as secondary dopants to PEDOT:PSS [131], [166], [167]. Ethanol was evaluated due to its low viscosity and the potential for it to also act as secondary dopant, due to the alcohol groups present in its structure [110].

A set of colour cartridges were initially exposed to acetone, ethanol, DMSO, Ethylene Glycol (EG) and Glycerol to determine if any of these solvents would damage either the plastic housing of the cartridges, or cause damage to the printing mechanism. It was found that the plastic immediately reacted to Acetone exposure, turning white and eventually dissolving in the liquid. There was also a very slight whitening after several minutes of exposure to DMSO, but not to any of the other solvents. This test indicated that Acetone was not a suitable solvent for this application, but DMSO was still used in small quantities due to the long exposure necessary to react with the cartridge material.

A rheometer from Anton Paar, the MCR 502, was used to measure the viscosities of

each ink mixture. Unfortunately the rheometer in question had a known defect in that its measurements had a consistent error of 30%. Therefore a set of calibration measurements were done first, to determine what the exact error factor was. Tests were done of deionised water (MilliQ Millipore, $18\text{ M}\Omega$), DMSO and Ethylene Glycol to verify that their measured viscosities were measured correctly and could be calibrated for. Figure 4.25 shows the result of the calibration measurement, where the viscosities of water, DMSO and Ethylene Glycol are reported to be $1.0\text{ mPa}\cdot\text{s}$, $2.05\text{ mPa}\cdot\text{s}$ and $16.1\text{ mPa}\cdot\text{s}$ after calibration.

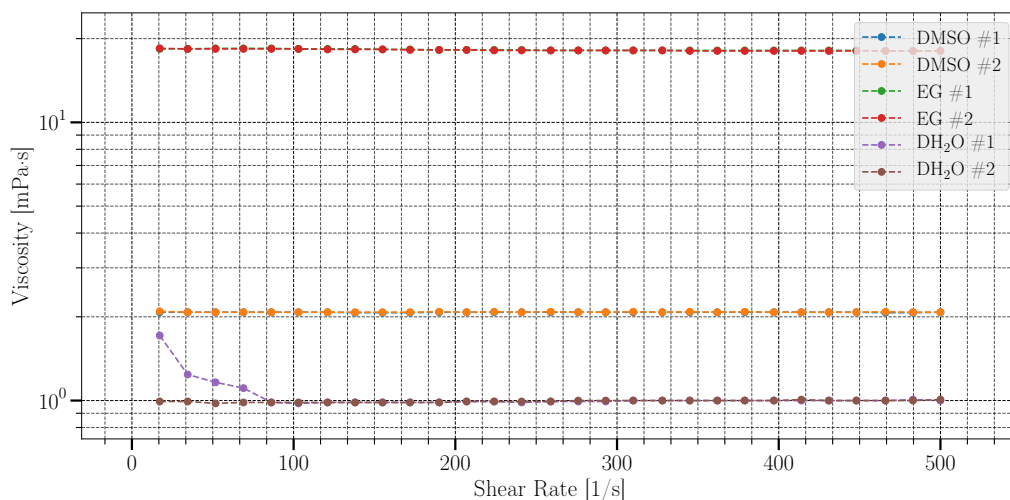


Figure 4.25: Viscosity calibration tests

Following calibration of the rheometer measurements, a series of tests were done to determine the viscosity of a set of initial PEDOT:PSS mixtures, shown in Figure 4.26. The first dilution consisted of equal parts PH1000 and deionized water, by volume, and had an initial viscosity of $16.04\text{ mPa}\cdot\text{s}$, which decreased to $9.79\text{ mPa}\cdot\text{s}$ at a shear rate of 500 s^{-1} . This behaviour was expected, as PEDOT:PSS solutions are known to be shear-thinning [129], and tend to have decreasing viscosities at high shear-rates. The second dilution contained PH1000, deionized water and DMSO in a volume ratio of 2:2:1. The viscosity of the mixture started at $15.73\text{ mPa}\cdot\text{s}$ and gradually decreased as a function of shear rate to $9.76\text{ mPa}\cdot\text{s}$. This result seemed to be contrary to what was expected, as the DMSO has a low viscosity and should have decreased the overall viscosity of the mixture. From these results it was determined that the PEDOT:PSS mixture would have to be diluted by a large factor to reach a workable viscosity. A summary of the results of these tests is shown in Table 4.6. The electrical properties of the dilutions were not assessed.

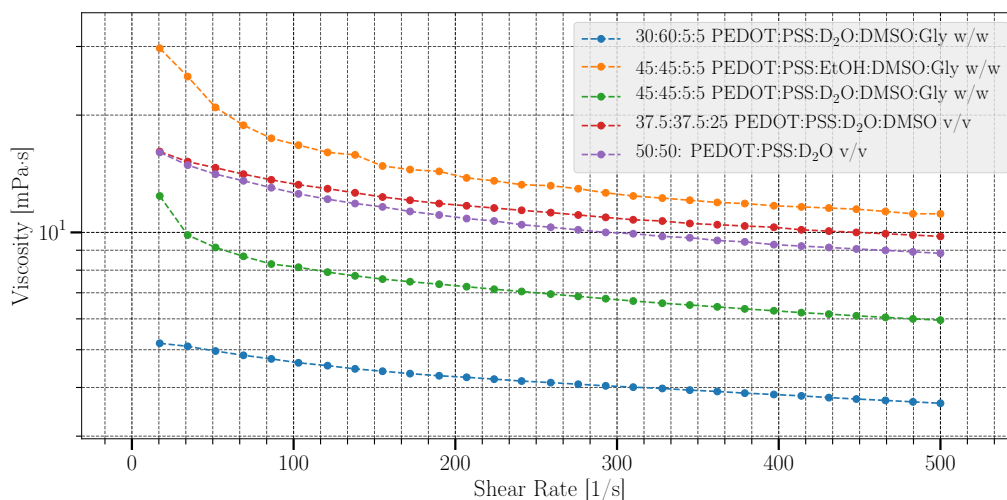


Figure 4.26: Viscosity tests of PEDOT:PSS dilutions

Table 4.6: Initial polymer ink dilutions

Label	PE- DOT: PSS %	H ₂ O %	DMSO %	Gly %	EtOH %	η -initial [mPa· s]	η -final [mPa· s]
Mix 1	50	50	0	0	0	16.04	9.79
Mix 2	37.5	37.5	25	0	0	15.73	9.76

All fractions given in %v/v. Gly = glycerol. EtOH = ethanol.

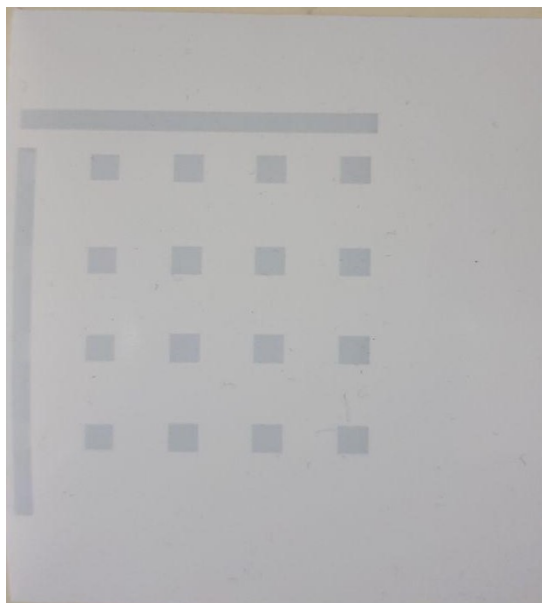
Further tests were done, some of which are shown in Figure 4.26, of mixtures containing varying combinations of PH1000, deionized water, ethanol and DMSO. A summary of the dilution results is also shown in Table 4.7. Two of the mixtures were tested in cartridges, containing ratios of 45:45:5:5 % (by weight) and 30:60:5:5 % (by weight) of PH1000:Ethanol:DMSO:Glycerol and PH1000:H₂O:DMSO:Glycerol, respectively. The ink mixtures were sonicated in an ultrasonic bath for 1 minute at a temperature of 30 °C to ensure even dispersion of the ink components before injection into a cartridge using a hypodermic needle, to improve ink uniformity and avoid clogging of nozzles due to clumping of ingredients. These two mixtures were found to be printable when used in a colour cartridge of the printer, despite their viscosities being higher than what was reported by some of the literature. The viscosity of the ethanol containing mixture was much higher than the suggested limit to be printable, of 1-10 mPa·s, which gave cause to test the other mixtures with viscosities thought to be too high. Those mixtures were found to not be printable, and it is not clear why the ethanol containing mixture did print successfully. It was however the least successful of the two dilutions, and leaked from the nozzles of the cartridge after some minutes of use, and could only be used to print once before causing the cartridges to become unusable by clogging nozzles and leaking uncontrollably.

Table 4.7: Refined Polymer Ink Dilutions

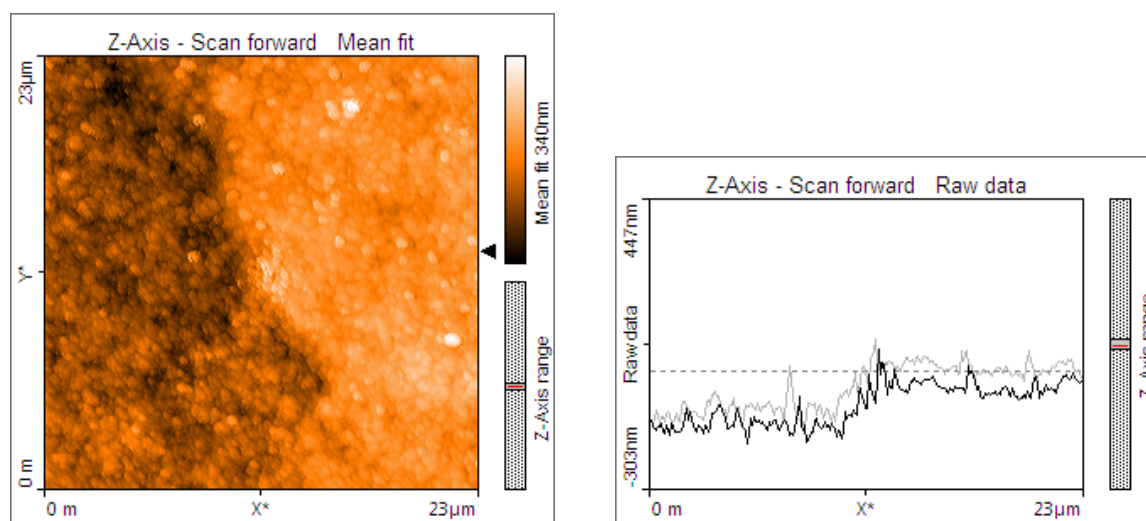
Label	PE- DOT: PSS %	H ₂ O %	DMSO %	Gly %	EtOH %	η -initial [mPa· s]	η -final [mPa· s]
Mix 3	45	0	5	5	45	29.68	11.16
Mix 4	45	45	5	5	0	12.4	5.95
Mix 5	30	60	5	5	0	5.19	3.64

All fractions given in %w/w. Gly = Glycerol. EtOH = Ethanol.

The dilution containing a mixture of PH1000:H₂O:DMSO:Glycerol was found to be printable with the colour cartridges without leaking from nozzles or clogging, and was found to print with more consistency than any of the many other dilutions that were tested. Shown in Figure 4.27 is a group of printed blocks of PEDOT:PSS ink, showing the characteristic blue colouring of the polymer.

**Figure 4.27:** Printed PEDOT:PSS blocks on paper

This shows that PEDOT:PSS ink can be successfully printed with the modified printer. Further investigation of the thickness of the printed PEDOT:PSS mixture, shown in Figure 4.28, revealed that the printed layer had a thickness of 140 nm relative to the top surface of the paper, which is significantly thinner than the 290 nm of the printed silver, which may mean that it would be necessary to print multiple layers of polymer solution to achieve functional transistors.



(a) PEDOT:PSS surface on Mitsubishi paper (b) Cross-section of PEDOT:PSS on Mitsubishi paper

Figure 4.28: Thickness of PEDOT:PSS printed on paper

4.6.6 Observations on Cartridge Longevity

A persistent problem that was encountered during the work done in this chapter was that cartridges become inoperable due to ink drying out in nozzles when the cartridges were stored between experiments. Cartridges filled with silver ink fared best, and lasted several days to a week or two, but had to be replaced periodically due to nozzles gradually clogging, in spite of the nozzles being covered by sealed containers when not in use.

The cartridges filled with PEDOT:PSS ink proved to be problematic due to their short lifespans. The cartridges were stored in sealed containers, with sealed coverings over the nozzles to prevent solvent evaporation during storage. In spite of these measures, a single cartridge was only useful for a week at most, usually less, due to ink drying in the nozzles when stored.

The short lifespans of the cartridges are not problematic for short-term research, but it becomes problematic when one considers that it may prevent the technology from being commercialized for large-scale sensor or electronics production.

4.7 Discussion

The printer performed better than expected, and patterns including feature sizes of 70 μm were successfully printed onto paper. The printer was also used to print aligned layers within 25 μm of one another. Some difficulties were experienced during the process of formulating PEDOT:PSS inks for printing with the printer, but that was also successfully completed. One disadvantage of the printer is the short lifetimes of the cartridges once filled with either silver or polymer ink. The cartridges did not last more than a week before having to be replaced due to ink drying in the nozzles and causing clogging.

The performance of the printer compares favourably with low-cost commercially produced material deposition systems, such as the Dimatix DMP-2800 series of printers. The Di-

matix printer can print structures with a resolution of 20 μm , with a repeatability of up to 25 μm between layers [168]. The Dimatix uses a camera system with printed fiducial markings [169] to align layers, which allows it greater flexibility in processing steps, as the substrate can be removed from the printer between printed layers for the application of other processing steps, such as plasma treatment.

The printer developed here is capable of printing with water-based inks, polymers and silver nanoparticle ink, as demonstrated previously. This capability is similar to that of commercial systems such as those from Dymatix, with the exception that the Dymatix printers have a very wide range of compatible viscosities and ink solvents, due to their use of a piezoelectric printing mechanism and chemically stable materials. This also makes the Dimatix printer more attractive for experiments regarding biological materials, but it has also been shown that thermal printing mechanisms do not necessarily damage sensitive materials during deposition [146].

Comparison of the relative cost of the printer to a system from Dimatix shows that there are two orders of magnitude of difference, with the Dimatix systems having a price around \$25 000 (R375 000) [170], while the whole process of modification cost approximately R5000.

The purposes of this project require the printer to satisfy three requirements: fast manufacturing of high-resolution electrodes onto paper, the alignment of printed layers, and printing of PEDOT:PSS on paper to manufacture printed transistors. All of these requirements have been shown to be satisfied, and the printer is suitable to be used for its intended purpose in this project.

4.8 Conclusion

This chapter set out to convert a regular desktop ink-jet printer, the HP DeskJet 4535, to become a material deposition device, capable of printing aligned layers of silver, through silver nanoparticle ink, and PEDOT:PSS, a semiconducting polymer mixture. This was done with the final goal of this project in mind, that of developing OEECT-based biosensors to aid in the differentiation between bacterial infections.

The printer was disassembled and its parts were evaluated, and it was found that the two main mechanical components, the feed mechanism and cartridge carriage, could be separated from the original chassis and reconfigured into a flatbed configuration. The modified printer was then subsequently used to print electrodes and other structures with silver nanoparticle ink. The printer was found to be capable of printing silver ink with a resolution of 80 μm , and printed layers could be aligned to within 25 μm of one another.

After the printer had been characterised, several attempts were made at formulating a mixture of PEDOT:PSS that could be deposited by the printer without regularly clogging the nozzles. The optimal composition of this mixture was found to be 30% PEDOT:PSS, 60% deionized water, and 5% each of DMSO and Glycerol, by weight, with a viscosity between 5.19 mPa·s and 3.64 mPa·s. The PEDOT:PSS mixture was then successfully printed without clogging the printer nozzles.

This chapter shows that it is entirely possible to construct a versatile material deposition system by modifying an existing desktop ink-jet printer, and that it can not only be used to print electrodes and semiconducting polymers, but also that it compares favourably to commercial systems, such as Dimatix DMP printers, at least superficially. Modification of the printer has therefore fulfilled all objectives for this part of the project, and the modified printer will be used in subsequent steps for rapid prototyping and the manufacturing of sensors.

Chapter 5

Transducer Development

The purpose of this chapter is to document the process by which OECTs were developed and functionalised for use in detecting and measuring CRP samples in buffer solutions. Three manufacturing methods were investigated for comparison, namely inkjet printing, spincoating and manual drop deposition. It was chosen to manufacture the final set of transducers for this project using the manual drop deposition technique. The manufactured transistors were then functionalised with APTES, and the functionalisation process was characterised using fluorescence microscopy and by comparison of transistor characteristics before and after functionalisation. An unexpected result from this chapter was the development of a spincoating method to selectively coat photoresist onto paper without coating silver electrodes printed onto the same sheet.

5.1 Introduction

After successful modification of the printer, the next step towards achieving the goal of this project was to manufacture OECTs. To this end, three possible manufacturing methods were investigated to determine which was more suited to this application. The three methods in question are inkjet printing, spincoating and manual droplet deposition. These three methods were chosen to provide effective comparison, due to their being very different in nature. The well-known standard method of manufacturing OECTs on glass and other rigid substrates is currently spincoating, combined with photolithography and other post-processing treatments, although it is not widely used for paper substrates. Inkjet printing is one of the methods being investigated in this project for the simplicity of the processing steps and the speed at which new iterations can be manufactured. Finally, as a benchmark for comparison of the first two methods, droplets of PEDOT:PSS were manually deposited onto electrodes to form transistors, as an extreme of simplicity in manufacturing method.

5.2 Transducer Layout

Typical OECTs consist of five main components: A substrate, metal electrodes, organic semiconducting material, electrolyte wells and a gate electrode. The proposed transducer layout for this project is shown in Figure 5.1, as discussed previously in Chapter 2.8.

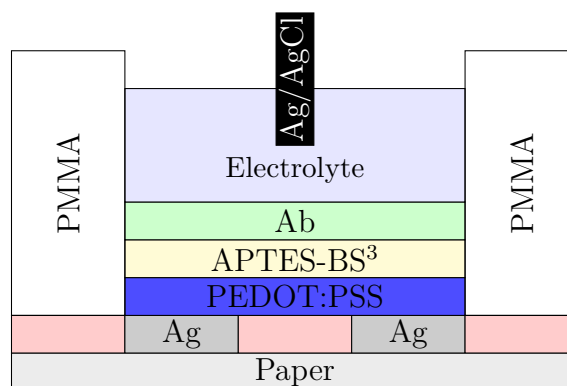


Figure 5.1: Proposed transducer layout

The transducer will consist of a bottom-contact, top-gated layout, with a layer of PEDOT:PSS mixture deposited on top of silver electrodes. Functionalisation of the transducer will be done by growth of an (3-Aminopropyl)triethoxysilane (APTES) monolayer on top of the PEDOT:PSS layer, whereafter the crosslinker known as BS³ will be used to covalently immobilise antibodies to the surface of the transducer. The electrolyte solution will be contained within walls of a PMMA container, and a strip of Silver/Silver Chloride will be used for the gate electrode.

5.3 Methods and Materials

Manufacturing of the functionalised transducers consisted of three steps. First, initial transducers were developed and evaluated, after which a functional layer was deposited onto the transducer surface. After functionalisation, validation of the correct functional surface groups had to be done to verify the preceding processing steps.

The materials used in this chapter for the transistors themselves were the same as in the previous chapter. Deionised water obtained from a laboratory supply was used, along with dimethyl sulfoxide (DMSO) and glycerol from Sigma-Aldrich. The PH1000 PEDOT:PSS solution from Heraeus was used alongside resin-coated paper and silver nanoparticle ink from Mitsubishi Paper Mills.

During functionalisation of the transistors, (3-Aminopropyl)triethoxysilane (APTES, from Sigma-Aldrich, 440140-100ML), bis[sulfosuccinimidyl] suberate (BS³, from Thermo Scientific, prod. num. 21580), anhydrous toluene (from Sigma-Aldrich, 244511-1L), fluorocein-isothicyanate (FITC, from Sigma-Aldrich, F3651- 100MG) and polyvinyl alcohol (PVA, MW 98 000, from Sigma-Aldrich, 341584-500G) were used. The previously developed inkjet printer along with a laboratory spincoater from Wetrak Systems and a precision mechanical pipette from Eppendorf AG were used to manufacture the transistors. Finally, Microposit S1818 photoresist (from MicroChem corp.) was used to improve water resistance of the paper substrate.

5.3.1 Improving Water Resistance of Paper

It became apparent during initial testing of the printed electrodes and transistors that the paper substrate was not ideal for paper-based electrochemical electronics, due to the

paper absorbing water over time and causing delamination of both the silver nanoparticle ink and printed PEDOT:PSS. The water also caused short-circuits between electrodes and prevented transistor operation. A possible solution to this problem was to cover the paper surface with a polymer coating that is not water permeable, such as photoresist, to prevent water from being absorbed into the paper, in a similar approach to that of [171], where SU-8 photoresist was inkjet printed. It was initially attempted to print a layer of S1818 photoresist using the printer, but the solvents necessary to dilute the photoresist sufficiently, namely propylene glycol monomethyl ether acetate (PGMEA) or acetone, proved to be incompatible with the cartridge construction and dissolved the plastic housing shortly after being introduced to a cartridge, which would not have been the case for a Dimatix printer. An alternative was sought by spincoating successive dilutions of S1818 onto paper with printed silver electrodes, and it was found that low-viscosity liquids would be absorbed by the paper, but would not coat the silver when spincoated at low speeds of 600 r/min. Slower speeds caused uneven coating of the paper, while higher speeds allowed the photoresist to spread across the silver electrodes. A dilution of 4:1 acetone:S1818 (w/w) was found to be optimal in selectively coating the paper substrate while leaving the printed silver exposed. Higher concentrations of S1818 coated the silver at all spin speeds tested.

The complete procedure for improving the water resistance of paper is as follows:

- Step 1: After printing silver structures onto the paper, the substrate is removed from the printer and placed into a spincoater,
- Step 2: 2 ml of diluted S1818 photoresist is deposited onto the paper while the paper is spinning at 600 r/min,
- Step 3: The coated paper is left to spin for 20 seconds,
- Step 4: To ensure that the photoresist is fully dried and any droplets adhering to the corners of the substrate are removed, the spin speed is increased to 1500 r/min for 15 s, and
- Step 5: The photoresist-coated paper is removed from the spincoater for further processing.

After spincoating, the three following methods were used to deposit PEDOT:PSS onto the electrodes.

5.3.2 Inkjet Printing of Transistors

The protocol to print transistors follows the printing process as developed in Section 4.6.1. First, a layer of silver electrodes was printed, then the paper was coated with photoresist, after which several layers of PEDOT:PSS ink was printed to form the semi-conducting region of the transistor structure. Tests were done for 1 to 10 layers of printed PEDOT:PSS. Following PEDOT:PSS deposition, the printed transistors were baked in a laboratory oven at 120 °C under atmospheric conditions for a minimum of 90 min to ensure that all deposited materials are fully dried before testing or further processing. The manufactured electrolyte wells were attached by using cyanoacrylate glue directly after baking.

5.3.3 Spincoating of Transistors

A simplified spincoating protocol was used to deposit PEDOT:PSS onto the printed electrodes. Usually, as in [123] or [126], the PEDOT:PSS layer would be patterned using photolithographic masks and wet-etching processes, but this type of processing becomes impractical for a paper substrate due to the absorbent nature of the paper. Specifically, the step of photolithographic patterning involving immersion in photoresist developer and subsequent rinsing in a solvent would make use of the paper substrate impossible. Therefore, an alternative was used. To prevent the PEDOT:PSS layer from completely covering the electrodes and contacts, a piece of adhesive tape was used to cover any areas that were required to remain uncovered by polymer. The standard spincoating technique for PEDOT:PSS was then used and individual electrode-pairs were coated with PEDOT:PSS by depositing 0.5 ml of PH1000 solution onto the substrate while spinning at a rate of 3000 r/min. After PEDOT:PSS deposition the adhesive tape was removed and the transistors were baked in a laboratory oven at 120 °C under atmospheric conditions for a minimum of 90 min to ensure that all deposited materials are fully dried before testing or further processing. The electrolyte wells were attached directly after baking.

5.3.4 Manual Drop Deposition of Transistors

The protocol for transistor manufacture by direct deposition of PEDOT:PSS droplets was developed in cooperation with Dean Bradford. The process is simple, and consists of using a precision mechanical pipette to deposit droplets of 5 μ l or 8 μ l onto the printed electrode area of a potential transistor. The substrate with deposited PEDOT:PSS droplets was then baked in a laboratory oven at 120 °C under atmospheric conditions for a minimum of 90 min to ensure that all deposited materials are fully dried before testing or further processing. The electrolyte wells were attached directly after baking.

5.3.5 Surface Functionalisation Protocol

Functionalisation of transistor surfaces with reactive amine (-NH₂) groups was done by growth of an APTES monolayer on the surface of the PEDOT:PSS semi-conducting layers. The following protocol was used during functionalisation, as described in detail in Chapter 3.4:

Step 1: 60 μ l of a 10% [w/w] APTES solution in anhydrous toluene was deposited into the electrolyte well of a transistor and left to incubate at room temperature overnight after being sealed with parafilm to prevent evaporation of the liquids, and

Step 2: After incubation, each well was rinsed 3x with 100 μ l of PBS (PH 7.4) and baked for 10 minutes at 100 °C to force evaporation of any residual water and toluene.

After baking, the functionalised transistors were either evaluated through fluorescent microscopy, or antibodies were immobilised onto the transducers for testing.

5.3.6 Functionalisation Validation Protocol

The functionalisation process had to be validated by verifying that the correct functional groups were presented on the transistor surface. This was done by adding a fluorescent

molecule, FITC, to the functionalised transducers, to bind to any potential -NH_2 groups present on the surface of a transducer, after which the surface was washed and imaged using a fluorescent microscope (Olympus IX81 Microscope). The protocol for FITC immobilisation is as follows:

- Step 1: FITC is dissolved in PBS(pH 7.4) at a concentration of $1 \text{ mg}\cdot\text{ml}^{-1}$,
- Step 2: $60 \mu\text{l}$ of FITC solution is added to the electrolyte well of a functionalised transistor,
- Step 3: The well is sealed with parafilm and left to incubate at room temperature in a dark environment for a minimum of 2 h, and
- Step 4: After incubation, the transistor is rinsed with PBS, and the well is again filled with PBS and kept in a dark environment before imaging.

After FITC incubation the transducer was taken to be imaged. All fluorescent imaging was done at Stellenbosch University Central Analytical Facilities' fluorescent microscopy unit in Stellenbosch, South Africa.

5.3.7 Electronic Measurement Configuration

Verification of transistor function was done by drawing of transistor transfer curves of the manufactured devices. This was done by utilising a Data Acquisition System (DAQ) from National Instruments, the NI cDAQ-9174 equipped with the NI 9206 Analog-to-Digital converter and NI 9264 Digital-to-Analog converter modules.

Shown in Figure 5.2 is the circuit used to characterise transistor devices, built by Dean Bradford. The DAQ was used to both generate the necessary voltages to activate the transistor devices and measure the resulting output voltages.

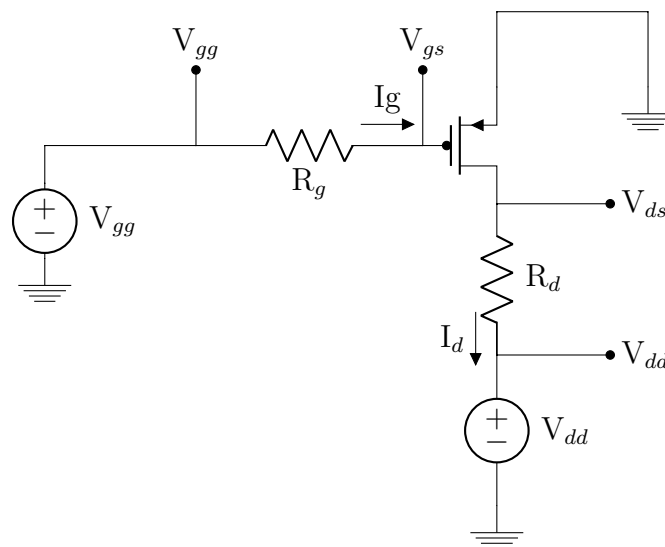


Figure 5.2: Configuration of measurements circuit

The measurement circuit is configured to place the source of the transistor on ground potential, to simplify the generation of voltages and measurement of currents, due to

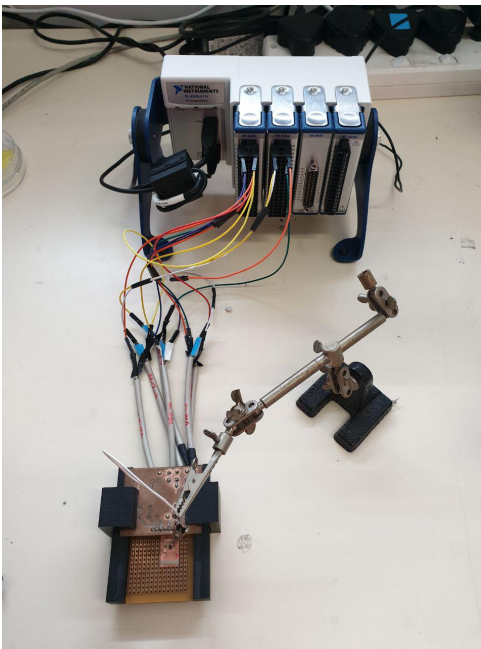
the p-type transistor then referencing all voltages to ground. The two voltage sources, indicated as V_{gg} and V_{dd} are outputs from the DAQ, and the four nodes indicated as V_{dd} , V_{ds} , V_{gg} and V_{gs} are measurement points connected to input channels of the DAQ. The currents flowing through the transistor, as measured by the DAQ are then given by

$$I_g = \frac{V_{gg} - V_{gs}}{R_g} \quad (5.1)$$

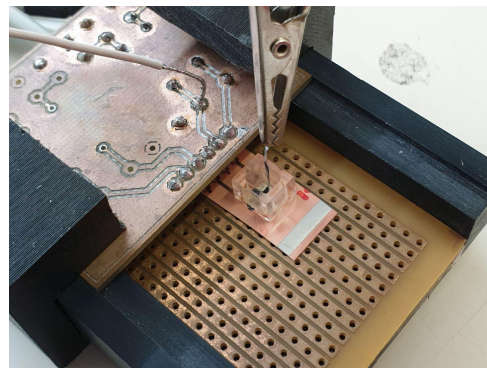
$$I_d = \frac{V_{ds} - V_{dd}}{R_d} \quad (5.2)$$

where $R_d = 147 \Omega$ and $R_g = 148 \Omega$.

Shown in Figure 5.3(a) is a photo of the measurement electronics, and in Figure 5.3(b) a closer perspective on the transducer mount can be seen, along with a transistor in the process of being tested.



(a) Measurement configuration



(b) Sample mount

The function of the measurement electronics was verified by generating transfer curves for a known transistor, namely the 2N2222 NMOS transistor. The result of this process is shown in Figure 5.4.

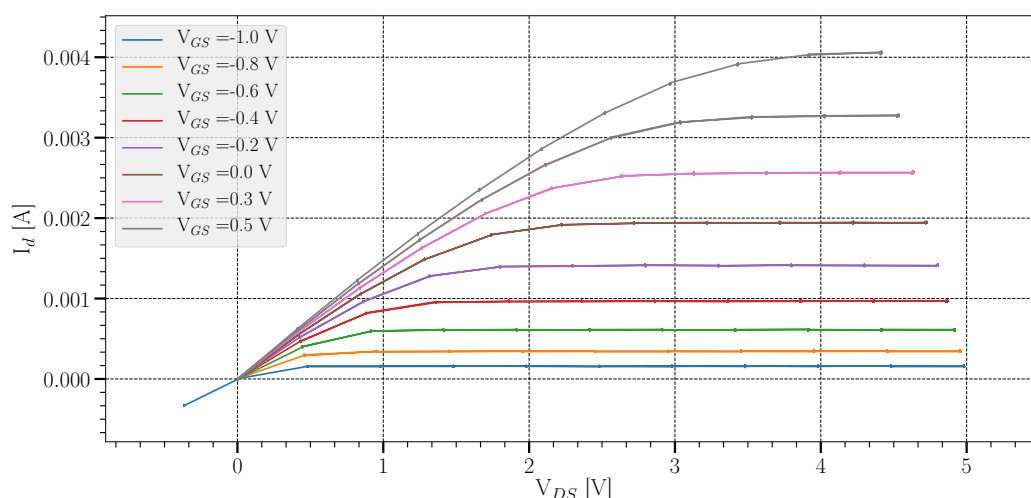


Figure 5.4: Verification of measurement electronics function

The NI DAQ was controlled from National Instruments' LabView 2015 software package, where the output voltages were directly manipulated. Data capture was also done through LabView, and the stored results were processed using the Python programming language.

The procedure for characterising transistors consisted of two types of measurements: First, the gate voltage, V_{gg} , was stepped from -1 V to 1 V in increments of 0.1 V , while the drain voltage V_{dd} was swept from 0 V to 0.5 V and back to 0 V in increments of 0.005 V for each gate voltage level. The gate voltage range was chosen because of the expected threshold voltage of -0.5 V . This was done to generate drain current transfer curves for the transistors. The second test done was a gate-voltage sweep, to quickly determine whether a device functions as a transistor and to quantify changes between transistors at different processing steps. For this test, the drain voltage was kept constant and the gate voltage was varied across a voltage range known to be in the transistor's saturation region, as determined from the previous test. The gate voltage sweep was also used to quickly characterise changes in transistor parameters between processing steps, or for verification of functionalisation.

As mentioned previously in Chapter 2.8 the gate consisted of a silver/silver chloride (Ag/AgCl) electrode, connected to the NI DAQ. An example of the electrodes used is shown in Figure 5.5. The silver was reacted with chloride ions in PBS by immersing the electrodes in a container filled with the liquid and then performing electrolysis by varying the voltage between the electrodes periodically from 0 V to 2 V . This allowed the reaction between silver and chloride ions to take place and form silver chloride on the surface of the electrode.



Figure 5.5: Silver/Silver chloride gate electrodes

The wells that the transistors were covered by were fabricated by using a 40 W TS4040 laser cutter (Transon CNC, China), and were cut from PMMA sheets. Shown in Figure 5.6 are two examples of the first version of the wells that were used.

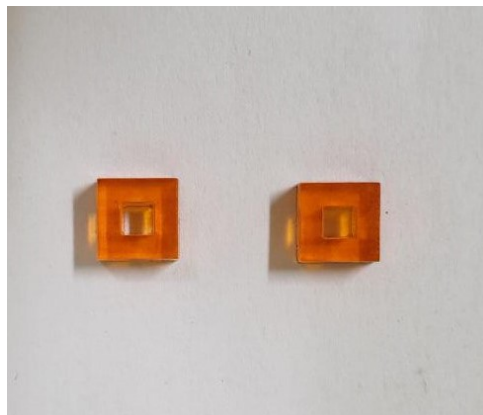


Figure 5.6: Electrolyte wells

The wells were 5x5 mm in size, with an inner opening of 3x3 mm. The wells could contain an electrolyte volume of 30 μ l.

5.4 Transducer Manufacture

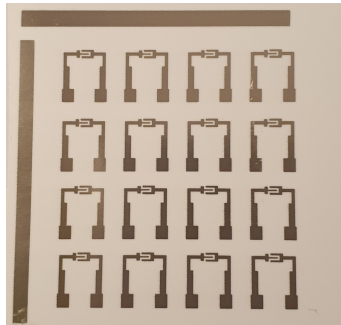
The first manufacturing method investigated was the inkjet printing of transistors. Thereafter spincoating was investigated. Finally, manual drop deposition was investigated and used to successfully manufacture transistors.

5.4.1 Printing Transistors

Figures 5.7(a), 5.7(b), and 5.7(d) show the different phases of the printing process followed to manufacture transistors, as discussed previously.

Figure 5.7(a) shows the first step of transistor preparation, where the silver electrodes have been printed onto the paper. The design shown here was the last to be tested, and has a channel width of ≈ 1000 μ m and a channel length of 300 μ m. The electrodes were printed on a sheet of paper 5x5 cm in size. The horizontal and vertical bars that can be

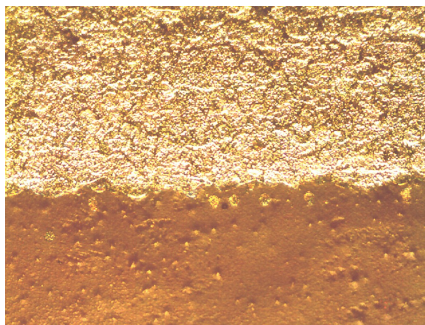
seen surrounding the electrodes were added due to unexpected behaviour of the printer - the left-most and top edge of any image would be badly-defined if it wasn't sure that the nozzles were filled with ink before the leading edge of an image was printed. Therefore a dark border was added to the top and left edges of any design printed with the printer, to ensure that the silver structures were realised as expected and that all edges were well-defined.



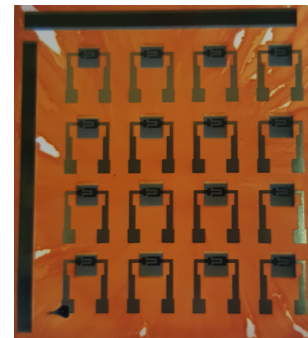
(a) Printed electrodes



(b) Printed silver electrodes on paper with photoresist spincoated to improve water resistance

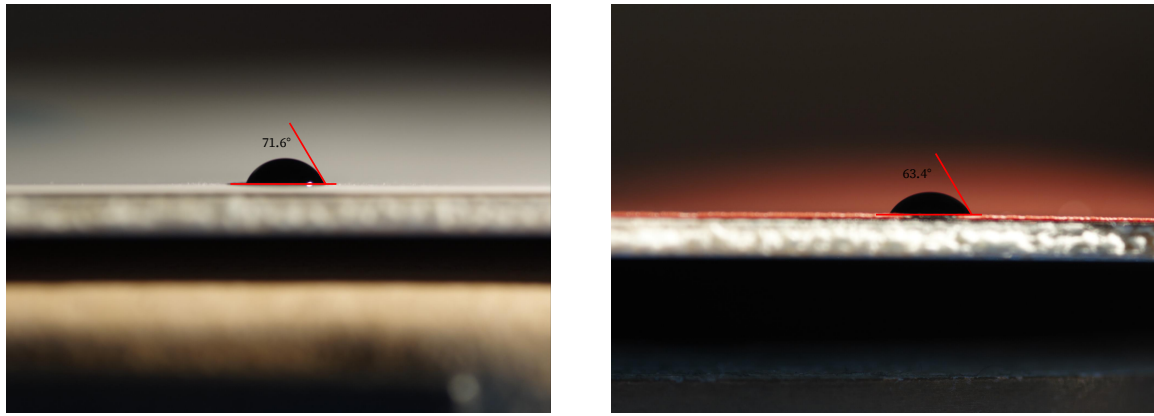


(c) Silver electrodes on paper with spincoated photoresist showing absence of photoresist from silver surface



(d) Silver electrodes with spincoated photoresist and 10 layers of PEDOT:PSS ink

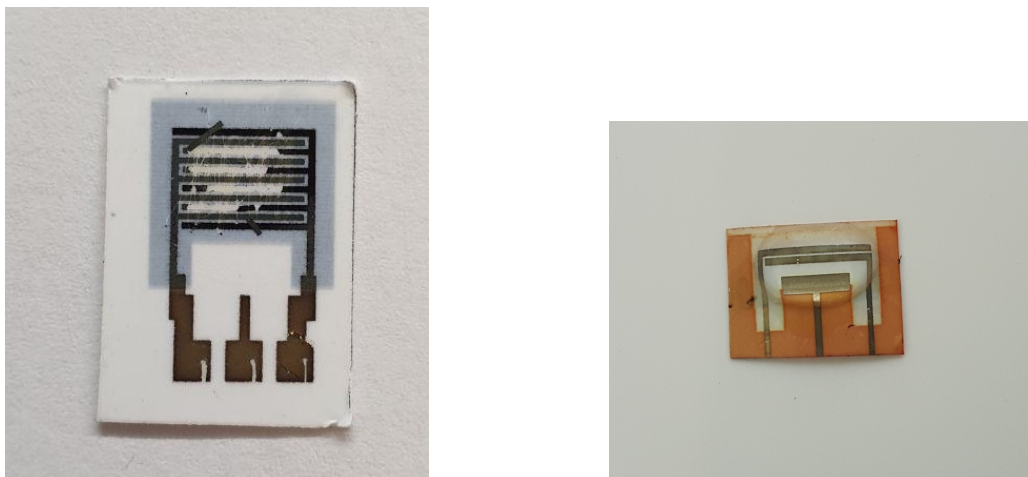
Figure 5.7(b) shows the result of spincoating photoresist onto paper, in order to prevent water from being absorbed into the paper. A water contact angle measurement was done, shown in Figure 5.8, to investigate the effect that the photoresist coating has on the paper. It was found that the coated paper was less hydrophobic than the uncoated paper, with a water contact angle of 63.4° , compared to 71.6° for the uncoated paper. This change in hydrophobicity might cause printed PEDOT:PSS droplets to spread out more, but this will be beneficial to the overall ink coverage, as it will be easier for adjacent droplets to merge and form a single continuous layer.



(a) Water contact angle measurement for clean Mitsubishi paper (b) Water contact angle measurement for Mitsubishi paper coated with diluted photoresist

Figure 5.8: Water contact angle comparison of before and after photoresist coating

Following the photoresist coating, a microscope was used to observe whether the photoresist covered the silver electrodes. Figure 5.7(c) shows how the spincoated photoresist layer on paper stops at the edge of the printed silver layer. Shown in Figure 5.9 is a comparison of two transistors, each printed with 5 layers of PEDOT:PSS and exposed to a droplet of water for 30 min. Figure 5.9(a) shows how the silver electrodes and polymer tend to delaminate after relatively short exposure to water, as opposed to the result in Figure 5.9(b), where a printed transistor is shown after an hour of being exposed to a water droplet. In the first case, the series resistance was measured to steadily decrease over time, until it suddenly became a short circuit, indicating that the water had penetrated into the paper and bridged the electrodes. The series resistance of the second case decreased for a time before stabilising, and remained stable for the duration of the test.



(a) Result of water exposure on printed transistor without photoresist treatment (b) Water resistance experiment with a printed transistor

Figure 5.9: Comparison of water resistance with and without photoresist treatment

Following the water resistance tests, a set of transistors were printed with 10 layers of PEDOT:PSS ink, shown in Figure 5.7(d), to lower series resistance and improve overall

performance. Table 5.1 shows the series resistances measured for selected layers, and indicates that additional layers only contribute to lowering the series resistance significantly up to five layers.

Table 5.1: Average series resistance of printed transistors

	1 layer	2 layers	3 layers	5 layers	10 layers
Average R_{ser} [Ω]	6.5	5.4	4.3	3.8	3.6

Testing of the transistors was done using the measurement configuration in Section 5.3.7.

Unfortunately, all tests done with printed transistors failed to produce any usable results. The device currents did not show any change due to a change in gate voltage, despite repeated attempts and variations on the designs and processes followed. Different electrode designs were evaluated, none of which were successful. Variations on the designs included changing the channel length between 70 μm and 300 μm , testing different numbers of electrodes in the interdigitated structure, various channel widths of between 200 μm and several mm, and printing up to 15 layers of PEDOT:PSS onto the channels for the different designs. The PEDOT:PSS mixture was also adapted to include a crosslinking agent, GOPTS, to decrease delamination of the printed polymer layers [126], but that did not have any effect other than to lower the series resistances to 1 Ω for a single printed layer. All of the 360 tests that were done showed that, while the devices were conductive, there was no relationship between the current flowing through the device and the gate voltage. It is thought that the thickness of the PEDOT:PSS film relative to the roughness of the silver surface might be a contributing factor, as the characteristics of thin-film devices are known to be highly dependent on the surface roughness of the metal electrodes, with high surface roughnesses causing high contact-resistances and preventing effective transistor function [163]. This was tested by attempting to print transistors onto Ultragloss paper, where the printed silver has a much lower surface roughness than the Mitsubishi paper that was used initially. Unfortunately use of the Ultragloss paper had the same results of the device current not being influenced by the gate voltage as was the case for the Mitsubishi paper.

It was decided to move on to the next manufacturing method after determining that it was not an effective use of time to continue attempts at printing transistors. Spincoating was attempted next.

5.4.2 Spincoating Transistors

Spincoating is the industry standard method of electronic device manufacture, and consists of coating a substrate with a substance, such as photoresist, by rotating the substrate at high speed while a set amount of the substance is decanted onto it. The process followed to manufacture transistors described in Section 5.3.3 was followed, and several mixtures of PEDOT:PSS inks were tested. Various electrode designs were tested with this manufacturing method, including those with channel lengths of 70 μm . The spincoated transistors typically had very high series resistances, typically 15 k Ω .

The devices manufactured using this method however had the same result as those for the inkjet printed devices, with no relationship between the gate voltage and device current observed at any time. Many tests were done, but none worked. It was then decided to move on to the last manufacturing method, that of manually depositing droplets of PEDOT:PSS onto printed electrodes.

5.4.3 Direct Drop Deposition

The method of manually pipetting drops of PEDOT:PSS ink was done as a simple alternative to the other two methods. There are almost no requirements in terms of viscosity or surface tension in order for them to be deposited by a mechanical pipette, and therefore a greater variety of ink mixtures is possible for this method than for inkjet printing.

The process for manufacturing transistors in this manner was followed by using the mixture of PEDOT:PSS that was also printed. This was chosen to determine if any mixture components may have been responsible for the transistors not functioning as expected. 5 μ l of the PEDOT:PSS mixture was deposited onto electrodes printed onto Mitsubishi paper, and subsequently baked to dry the droplets of ink. The result of the baking step can be seen in Figure 5.10(a), where the deposited droplets can be seen to have spread out to form dark circular spots on the paper.



(a) Manually deposited drops on electrodes after baking (b) Transistors with electrolyte wells attached after baking

Figure 5.10: Manufactured transistors

After baking, the series resistance of the transistors were measured, and it was found to have an average value of 5.63 Ω , with a maximum value of 7 Ω . Next, the transistors were tested to determine if they did function as transistors. The result of one of these measurements is shown in Figure 5.11(a), where the gate and drain currents are shown for different gate voltages.

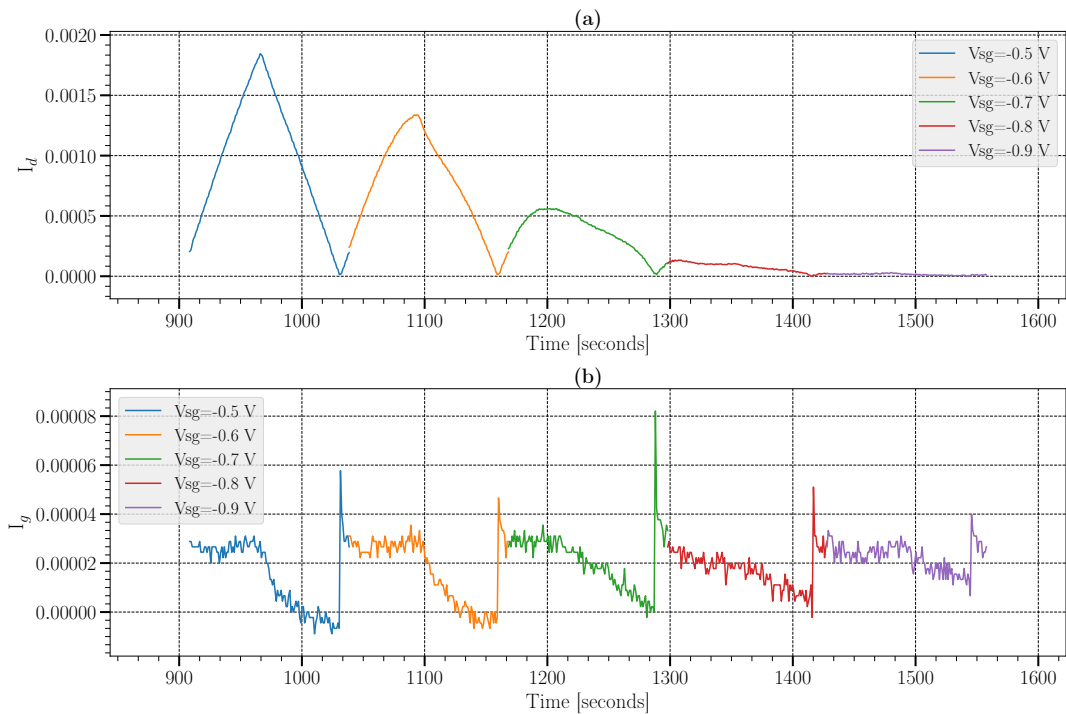


Figure 5.11: Current through Transistor for drain voltage sweeps over time (a) Drain current and (b) Gate current

This shows that the manufactured devices do exhibit a transistor-like behaviour, with the drain current increasing for increasing values of the gate voltage, which ranges here from -0.9 V to -0.5 V . Ten of these devices were tested and exhibited the same behaviour, although the results for only one are presented for readability. The graph shown in Figure 5.11(b) shows the gate current for the transistors, which is measured to remain less than 10^{-2} of the total current, or rather, the contribution of the gate current is less than 1% of the total current, and decreases to 0 when the transistor switches off. Therefore the dominant contribution to the measured current is from the drain and not the gate, as could have been the case if there had been a significant leakage current. Reorganising the measured currents to construct an output curve, Figure 5.12(a) shows that there is some hysteresis in the transistor function. This type of behaviour is typical of what is observed when charge-trapping at the interface between the semiconductor and electrodes causes an increase in contact resistance [172]–[174].

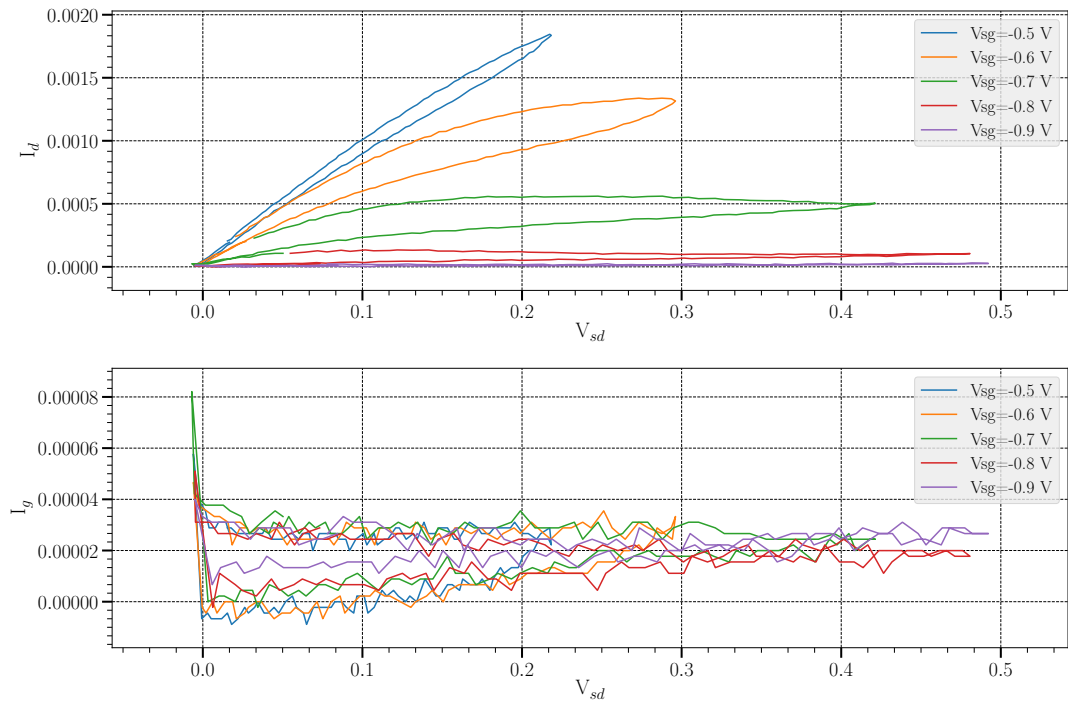


Figure 5.12: (a) Output curve and (b) Reverse transfer curve for manufactured transistor

Following the normal transfer curve, a gate voltage sweep was done to determine the turn-on voltage of the transistor, as well as to gauge the sensitivity of the transistor to changes in the gate voltage, which would give an indication as to the applicability of this type of transistor for a sensor. The resulting transfer curve is shown in Figure 5.12.

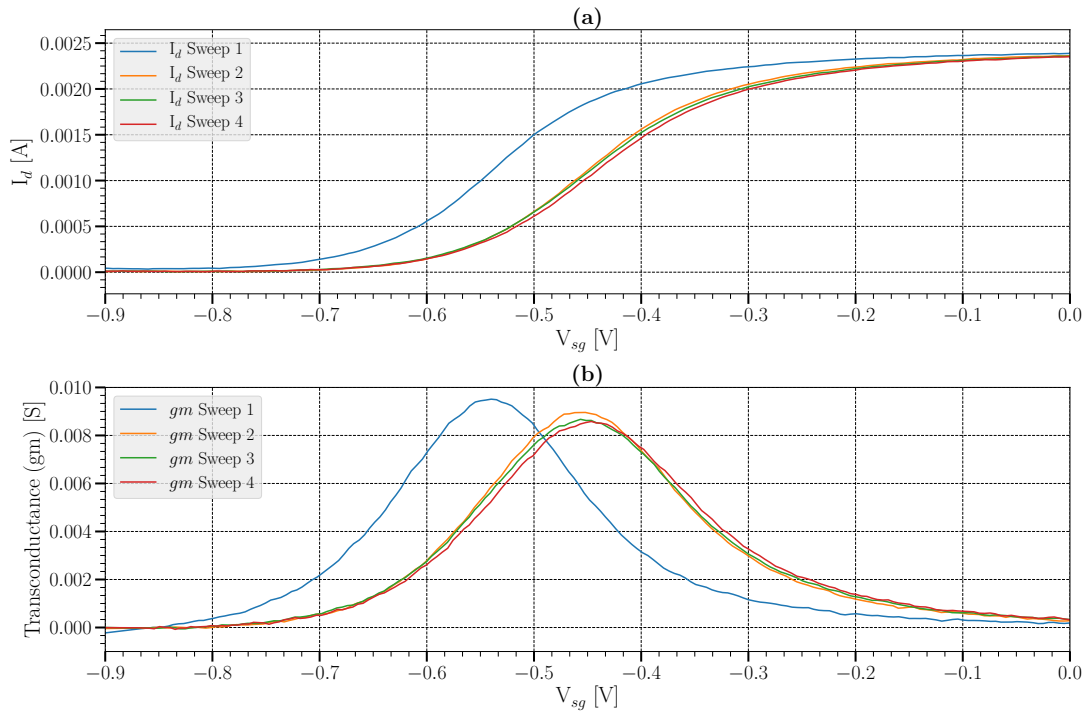


Figure 5.13: (a) Current vs. gate voltage sweep (b) and Transconductance vs. gate voltage

For the test done in Figure 5.13, V_{dd} was kept constant at -0.4 V to allow the transistor to switch on when necessary, where the hysteresis in the previous figure seems to be at a minimum. The transfer curve shows that the transistor characteristics change when the gate current is varied over time through the NI-DAQ, but stabilises after one or two sweeps. The time elapsed for each sweep was 10 seconds. It can be seen that the transistor initially switches on at a voltage of $V_{sg} = -0.8$ V, which changes to -0.7 V, and the peak transconductance of the transistors is situated at $V_{sg} = -0.45$ V, which is the voltage at which a sensor must be biased to achieve maximum sensitivity [126]. The consistent turn-on voltage, V_{tp} of -0.7 V, after stabilisation is similar to those of [173] and [175], where threshold voltages of -0.5 V were reported for PEDOT:PSS-based transistors.

After showing that the fabricated devices function as transistors, verification of the immobilisation method was done. The PEDOT:PSS ink was adjusted to the final mixture, containing PVA, as discussed in Section 2.8. The PVA was added as part of the functionalisation process to provide surface oxygen groups for the process of antibody immobilisation in an adapted version of the protocol developed by Strakosas [110].

5.5 Transducer Functionalisation

After successfully verifying that the manufactured devices function as transistors, the method of functionalising their surfaces with amine groups was applied. Thereafter fluorescent microscopy was used to verify that the correct functional groups were present on the transducer surface. The transistors tested here are those manufactured with the final ink mixture containing PVA for antibody immobilisation.

5.5.1 Functionalisation with Amine-groups

The result in Figure 5.14 shows that the APTES immobilisation protocol was successful, and that the FITC bound to the available amine groups.

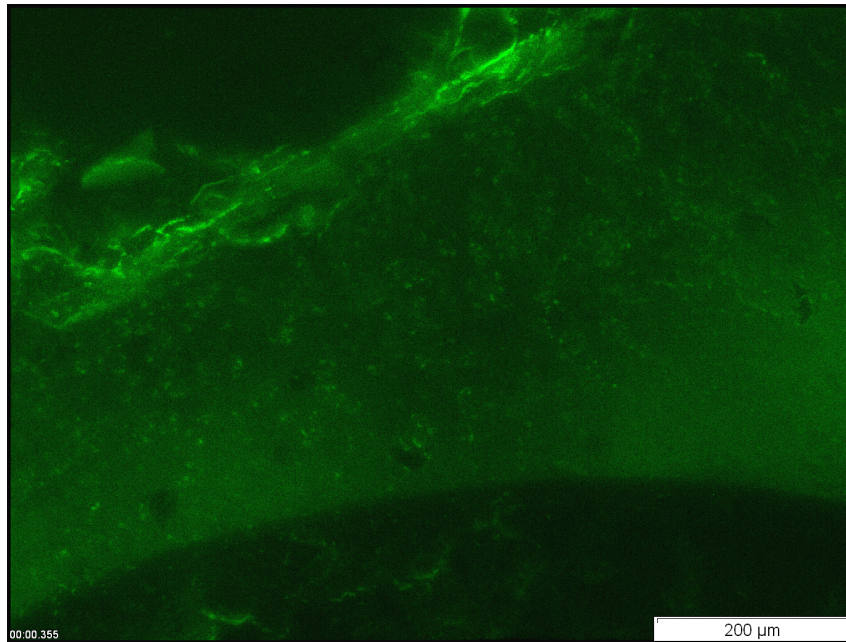


Figure 5.14: Fluorescent microscopy image of APTES functionalised PEDOT:PSS, labelled with FITC

The dark part of the image in the foreground shows a region of PEDOT:PSS glowing brightly, but the contrast of the image had to be reduced due to the brightness of the sample, because of the high concentration of bound FITC. The bright line in the upper-left corner is the location where the electrolyte well would have been, had it not been removed to position the sample in the microscope. The region beyond the line where the well stopped can be seen to be devoid of FITC, and green structures.

5.5.2 Characterisation of Functionalised Transistors

The PEDOT:PSS mixture with which the transistors were manufactured was adjusted to the final mixture after verification of transistor function.

Transfer curves were drawn for the new transistors, and they were found to function as expected. Shown in Figure 5.15(a) is a transfer curve for a transistor before being exposed to APTES, with V_{dd} again biased at -0.4 V.

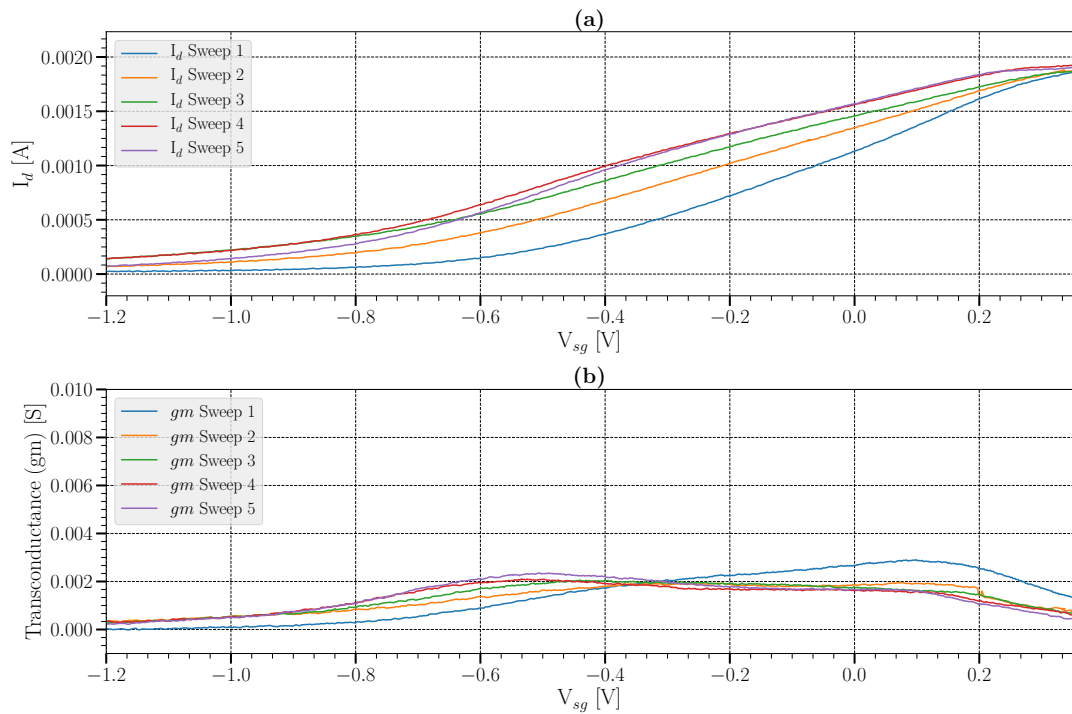


Figure 5.15: (a) Current vs. gate voltage sweep (b) and Transconductance vs. gate voltage of transistors manufactured with high-PVA content before APTES treatment

The transistors with the adjusted PEDOT:PSS mixture appear to also change for repeated gate voltage sweeps, gradually stabilising towards a threshold voltage of $V_{sg} = -1.15$ V, with a very wide distribution in transconductance, which peaks at -0.53 V for the transfer curves after stabilising.

Following verification that the transistors function as transistors, the functionalisation procedure was once again performed, and a transfer curve was drawn for the same transistor as before, after APTES monolayer growth, shown in Figure 5.16. This graph shows that the transistor remains functional after APTES addition, but that the peak current at saturation had been reduced from 1.8 mA to 1 mA, and the peak in transconductance had shifted from $V_{sg} = 0.53$ V to -0.06 V. The threshold voltage had also changed to -1 V, from $V_{sg} = -1.15$ V.

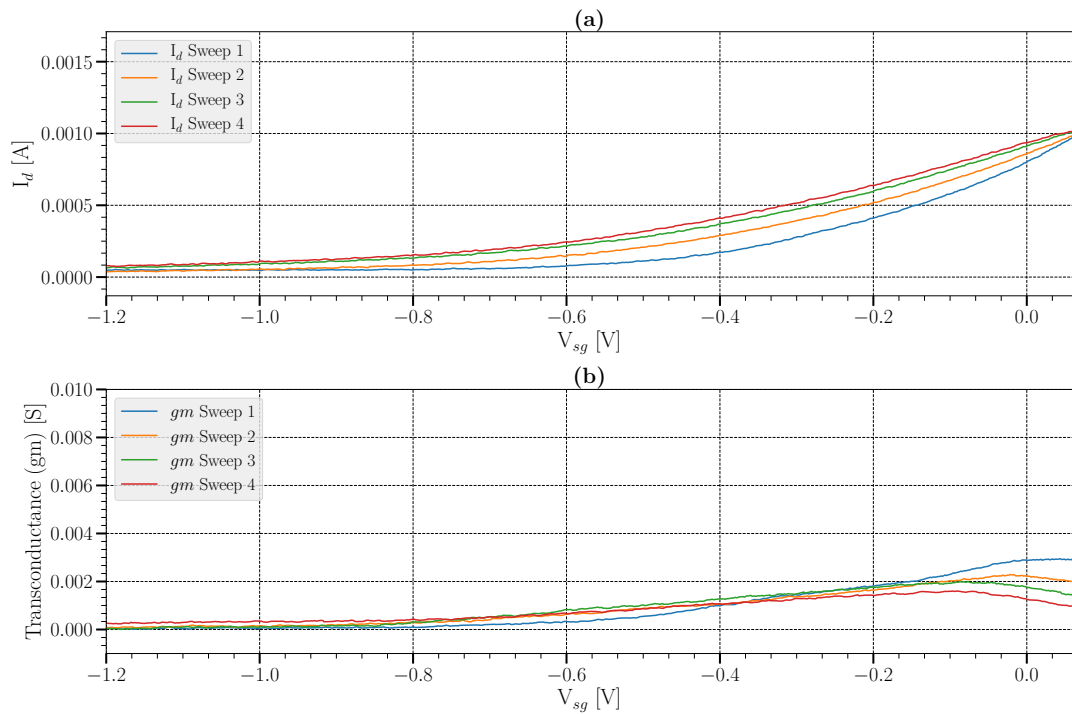


Figure 5.16: Transfer curves for transistors with high PVA content after APTES treatment

The same transistor was then used to verify whether the functionalised transducers would react to a substance binding to the amine groups on the surface. The transistor was therefore tested after having been incubated in a solution containing FITC at a concentration of 1 mg/ml. The result of this test is shown in Figure 5.17, which appears markedly different from the previous transfer curves. The peak current had not decreased, but the threshold voltage had clearly shifted to -0.8 V, from -1 V. The peak in transconductance had also shifted past $V_{sg} = 0$ V, which shows that the transistor reacts to binding occurring on its surface.

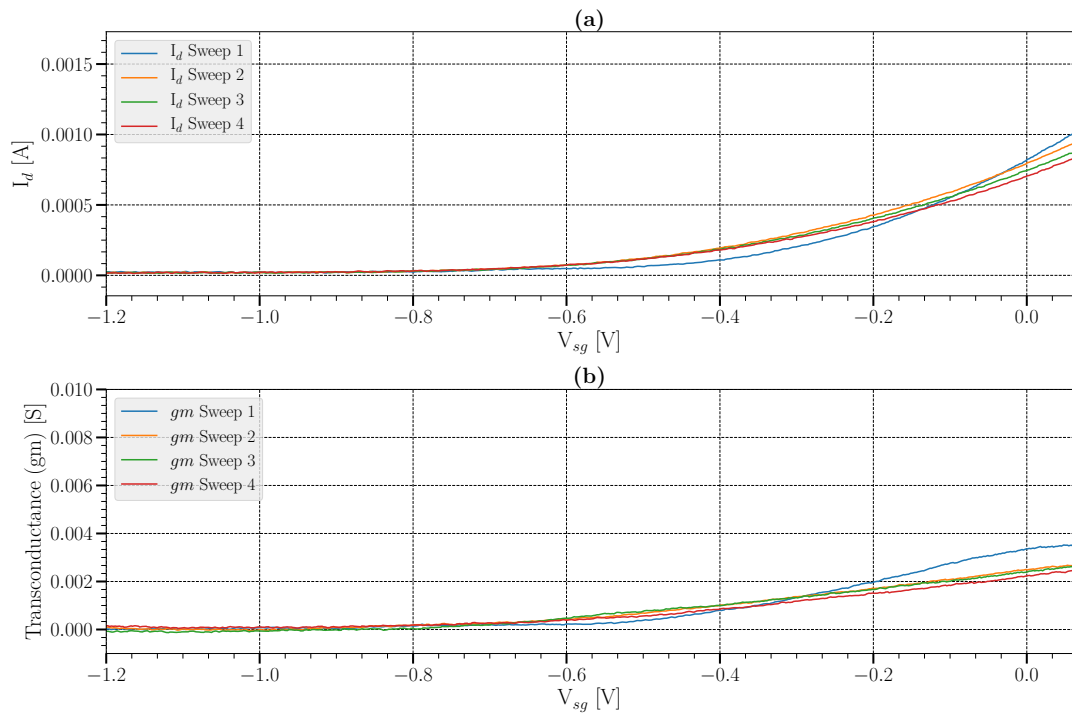


Figure 5.17: Transfer curves for transistors with high PVA content after FITC addition

As a second verification of this principle, two tests were done during which transistors were biased at $V_{dd} = 0.4$ V and $V_{sg} = -0.1$ V, which is where the peak in the post-APTES functionalised transistor's transconductance was. These tests were done to evaluate the effect of FITC binding on the transistors over time, and gain an understanding of the behaviour that could be expected from the sensors. The two graphs shown in Figure 5.18 shows that the drain current remained stable for the first 100 seconds, after which the FITC solution in PBS was added, and the current increased slightly due to the added PBS, after which it steadily decreased over the next 10 minutes, and then becoming slightly erratic.

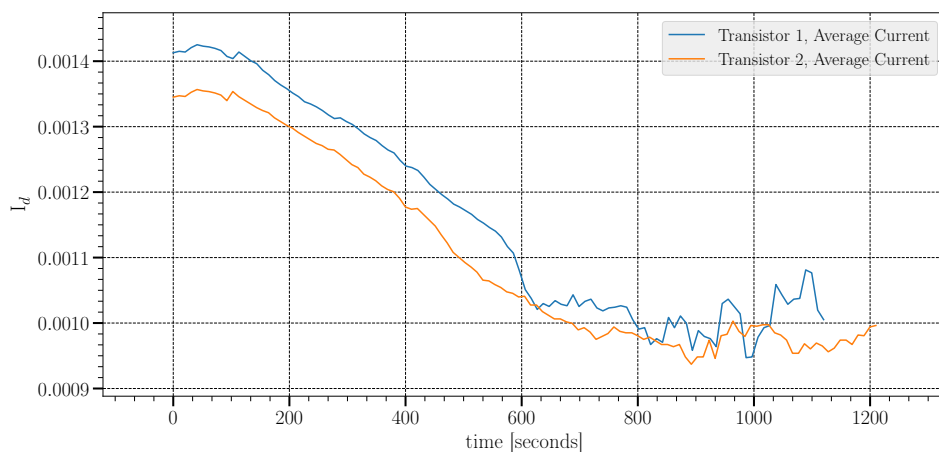


Figure 5.18: Verification of sensor principle by addition of FITC to functionalised transistors

The current for transistor 1 decreased from 1.35 mA to 0.5 mA, a change of 29.63 % relative to the initial value. The current through the second transistor changed in a similar manner, and decreased by 31.76 %, and shows that the binding of molecules to the surface functional groups has an effect on the transistor characteristics.

5.6 Conclusion

The goal of this chapter was to fabricate a working transducer that would be capable of detecting and measuring a target protein in buffer solution, with the eventual goal of contributing towards combating the rising problem of antimicrobial resistance. Three manufacturing methods for organic electrochemical transistors were investigated with the goal of comparing their results, namely inkjet printing, spincoating and manual drop deposition.

Of the three manufacturing methods that were investigated, only manual drop deposition was successful in manufacturing working transistors. Inkjet printing and spincoating did not produce any functioning transistors on the paper substrate. The manufactured transistors were then characterised by generation of their transfer curves, and the functionalisation method chosen for this project was validated, namely growing an APTES monolayer onto the surface of a transistor by using a modified version of the process developed by [110]. The effect of the immobilisation method on the manufactured transistors was investigated, and it was found that there was a clear difference in a single transistor between each of the subsequent steps of APTES incubation and FITC binding. After having shown that the transistors could be effectively functionalised and may be suitable for use as biosensors, two transistors were tested with a dummy analyte in the form of FITC, the fluorescent marker used to validate the functionalisation process. The transistors were observed to react to the FITC binding as expected, and the transistors will next be implemented as biosensor transducers.

Chapter 6

Biosensor Tests

The goal of this chapter is to document the processes followed during the final experiments of this project. The functionalised transistors from the previous chapter were used to form biosensor transducers by immobilising monoclonal anti-CRP antibodies onto their surfaces using the crosslinker known as BS³. After antibody immobilisation the transducers were successfully tested and shown to have concentration dependent behaviour, although not in the manner that was expected. The reduction in transducer drain current was found to be independent of concentration, although the rate at which the current decreased was. This was thought to be due to the large surface area of the sensors. Finally, the results were processed to show the relationship between current decrease and protein concentration.

6.1 Introduction

The next step in the process to manufacture a transducer with the necessary characteristics to detect and measure CRP concentrations in buffer solutions is to immobilise anti-CRP antibodies onto the functionalised transistors developed in the previous chapter. Many immobilisation methods exist, and can be divided into two categories [176], [177]: non-covalent and covalent methods. Of the non-covalent methods two are widely used, namely physical adsorption and biotin-streptavidin conjugation. Covalent methods have more variation, but the ubiquitous NHS-EDC strategy is most widely used today. In this project a variant of the NHS-ester interaction was chosen as immobilisation strategy, and the crosslinker known as BS³ was chosen for the reduced number of processing steps required, while retaining the effectiveness of NHS-ester groups binding to primary amine functional groups.

A set of 60 transistors were manufactured to do 6 tests per concentration in the protein dilution series. After immobilisation of the biorecognition elements, the transducers were tested using a testing methodology that combines AC- and DC- measurement strategies to compare whether either is more effective in determining analyte concentration.

6.2 Biorecognition Element Immobilisation

The methodology that was used to immobilise the antibodies onto the transducer surface was loosely based on a testing methodology used by Synexa Life Sciences, a company that develops and performs various analytical tests, including immunoassays. The antibody

immobilisation methodology documented in Section 3.4 was used to covalently attach polyclonal capture antibodies (Ab31156, AbCam Inc, USA) to the sensor surface, by first binding BS³ to the APTES-functionalised surface, after which the antibodies were added to the transducers. In summary, the following process was followed:

- Step 1: Transistors were manufactured according to the process documented in Chapter 5, by using the manual drop deposition method,
- Step 2: Following transistor manufacture, 60 μl of a solution consisting of 10% (w/w) APTES in anhydrous toluene was incubated on the transducers overnight to grow an APTES monolayer on the transistor surface,
- Step 3: After amine-functionalisation of the transistors, the transistors were rinsed 3x with PBS(pH 7.4) to remove any unbound APTES and baked for 10 mins at 100 °C,
- Step 4: Next, 60 μl of a solution of BS³ in PBS with a concentration of 0.6 $\text{mg}\cdot\text{ml}^{-1}$ was added to the transistors and incubated at room temperature for 2.5 h,
- Step 5: Following BS³ linking, the transducers were rinsed 3x with PBS,
- Step 6: After rinsing, 40 μl of the capture antibody solution, at a concentration of 4 $\mu\text{g}\cdot\text{ml}^{-1}$ in PBS, was added to the transducers and incubated at room temperature for 2.5 h,
- Step 7: After antibody incubation, the transducers were rinsed 3x with washing buffer, consisting of 0.0005 % (v/v) Tween20 in PBS,
- Step 8: Next, 100 μl of blocking buffer (3% BSA w/w) was added to the transducers and incubated for 1.5 h at room temperature, and
- Step 9: Finally, after blocking the transducers were rinsed again with PBS before testing.

Shown in Figure 6.1 is one of the final set of transducers, with the electrolyte well attached to the paper with cyanoacrylate glue, which was chosen for its mechanical stability and water resistance - the glue would not dissolve or otherwise allow water to escape and cause short-circuits in the electrodes outside the well. The final transistors consisted of IDE's, with a single electrode on one side and two on the other. The electrodes were separated by a space of 300 μm on all sides and had a length of 2 mm.

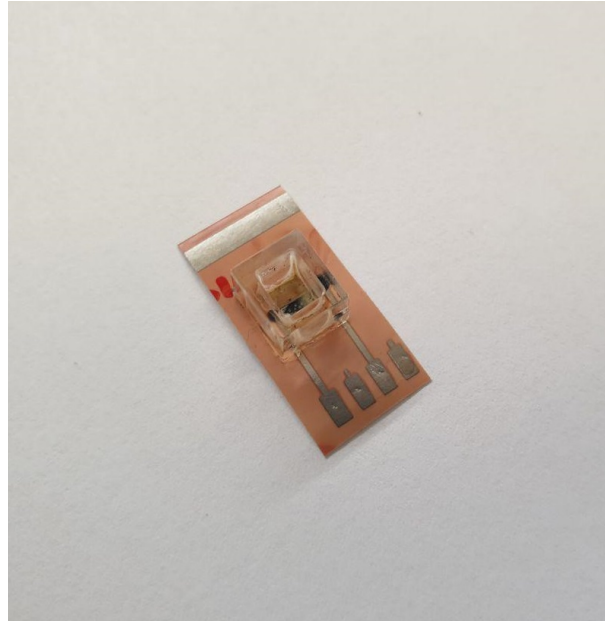


Figure 6.1: Final transistor configuration with electrolyte well attached

Following successful antibody immobilisation, each transducer was tested using the testing methodology proposed in Section 3.5.

6.3 Test Procedure

Testing was done with the measurement configuration shown in Figure 5.2, where the NI DAQ was configured to generate the necessary input voltages to perform the required tests.

As observed from the results in the previous chapter, the addition of PBS to a functioning transistor may cause an increase in drain current due to the influx of ions to the solution, which then changes the doping concentration in the channel region without having an effect on the gate voltage. This is problematic for the function of the sensors, as this increase in drain current may prevent the results from reflecting the change in current due to the binding of proteins to their corresponding antibodies. To this end several tests were done to determine the effect of PBS addition and removal on transistor function, and to determine the initial volume of electrolyte necessary to minimise the effect of the addition of protein-containing buffer to the well. This was done by successively adding 20 μl of PBS to the well of a transistor, or alternating between adding and removing the same volume, starting with a volume of 30 μl of electrolyte in the well.

Figure 6.2 shows the result of alternating between adding and removing PBS, where PBS is added at the first decrease in current, removed at the following increase and again added for the last decrease. This shows that both the drain current and transconductance are affected, with a decrease in drain current and increase in transconductance when PBS is added, and the opposite when removed. The process is not fully reversible, as can be seen by the difference in current after the first removal, which is slightly greater than the original steady-state value. This difference is thought to be due the amount of ions that have migrated into the PEDOT:PSS region without being removed with the PBS: the

result is that the doping concentration is not maintained between addition and removal of PBS.

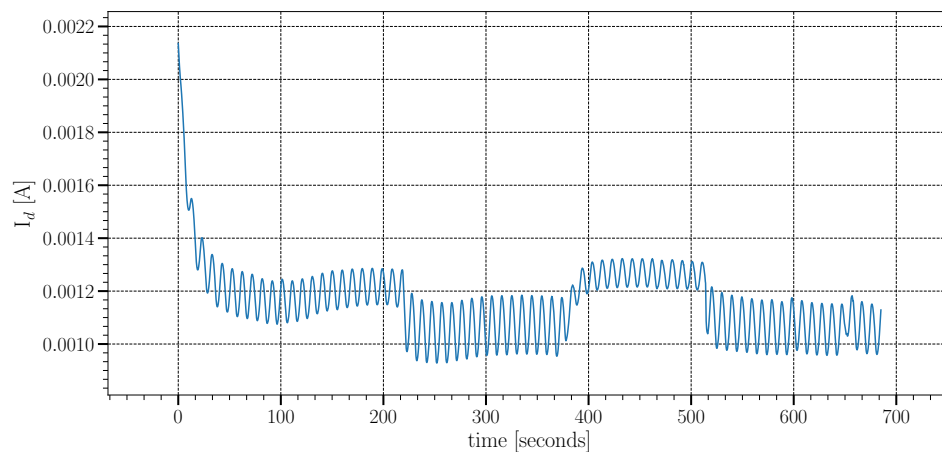


Figure 6.2: Effect of PBS addition and removal on transistor function

It was determined that a minimum well volume of 60 μl was necessary to prevent the addition of PBS from having an effect on the drain current. This volume was larger than the original well size, and new wells were cut from 5 mm thick PMMA sheets to take this into account. The new electrolyte wells were 8x9 mm in size, with an inner opening of 4x3 mm, shown in Figure 6.3. The wells were designed for a total volume of 120 μl to take the addition of protein solution into account.



Figure 6.3: Larger electrolyte wells for final experiment

Shown below, in Figure 6.4 is a histogram representing the series resistances of the 60 transistors that were manufactured for the final series of tests, before APTES treatment. This graph shows that there is some variation between transistors, with an average resistance of 70.54Ω and standard deviation of 31.2Ω .

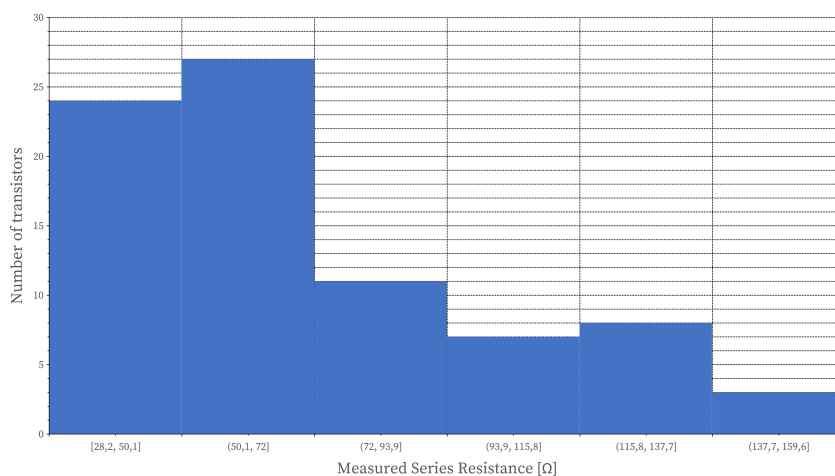


Figure 6.4: Series resistance before APTES functionalisation

After APTES functionalisation the average series resistance of the transistors were found to have increased by a factor of 9.3. The average resistance had changed to 655.6Ω , with a standard deviation of $1.2 \text{ k}\Omega$ and two outliers with series resistances of 22 and 11 $\text{k}\Omega$. The rest of the functionalisation procedure was carried out nonetheless, but no further series resistance measurements were done to prevent any applied voltages from potentially altering the transistors in a significant manner.

The testing procedure for the final experiments was done according to the methodology proposed in Section 3.5. The transistors were connected to the NI DAQ after antibody attachment and incubation in the blocking buffer. Then, $60 \mu\text{l}$ of PBS was added to the electrolyte well, and the preconfigured testing program was started from LabView. The drain supply voltage, V_{dd} of the transistors were biased at -0.4 V , to ensure that the transistor is biased at the point where hysteresis in the transfer curves is at a minimum. The gate supply voltage, V_{gg} was biased at -0.05 V to ensure that the transistors were biased at the point where they are most sensitive to changes in effective gate voltage, to more effectively detect protein bindings. A triangular waveform with an amplitude of 0.05 V and frequency of 0.1 Hz was superimposed on the gate voltage to evaluate any change in transconductance that may occur due to protein binding and the subsequent change in drain current.

After activation of the excitation voltages and verification that all measurements were correct, the transistors were left until the drain current was observed to have stabilised from any transient behaviour directly after activation. Once the drain current had been observed to have stabilised, the concentration series of CRP protein were added to subsequent transistors and left until the drain current had again been observed to have stabilised, or the transistors became non-functional.

The protein concentrations tested were $10 \mu\text{g}\cdot\text{ml}^{-1}$, $5 \mu\text{g}\cdot\text{ml}^{-1}$, $2.5 \mu\text{g}\cdot\text{ml}^{-1}$, $1.2 \mu\text{g}\cdot\text{ml}^{-1}$, $0.625 \mu\text{g}\cdot\text{ml}^{-1}$, $0.31 \mu\text{g}\cdot\text{ml}^{-1}$, $0.078 \mu\text{g}\cdot\text{ml}^{-1}$ and $19.53 \text{ ng}\cdot\text{ml}^{-1}$. The concentrations were chosen to be lower than the clinically relevant range of CRP in patients, to ensure that the sensors are not saturated by the high concentrations usually observed for CRP ($\approx 100 \mu\text{g}\cdot\mu\text{l}^{-1}$). The dilutions were made by adding $5.76 \mu\text{l}$ of stock protein solution at a concentration of $1 \text{ mg}\cdot\text{ml}^{-1}$ to $474 \mu\text{l}$ of assay buffer (1% BSA in PBS), to achieve the

first protein concentration of $10 \mu\text{g}\cdot\text{ml}^{-1}$. Next, $240 \mu\text{l}$ of the first solution was removed and added to the same volume of assay buffer for the next dilution. The mixture was then gently pipetted up and down to mix thoroughly before the process was repeated for the next dilutions in the series, as discussed in Section 3.5.1. The protein used was recombinant C-reactive protein, Ab167710 from AbCam Inc, USA.

The measurements for each concentration were then taken and processed by calculating the average current over time and transconductance over time to determine if any relation between concentration and transistor behaviour was present.

6.4 Results

The above methodology was followed to test the transistors and determine if any relationship exists between their behaviour and the concentration of analyte present in the sample added during the test. First, a negative control was done with a single transistor, with antibodies immobilised, using PBS spiked with a concentration of 3% BSA (w/w) to determine if the transistors had any reaction to unwanted proteins. Following the negative control, the full set of transistors were tested with protein solutions and the results were processed.

6.4.1 Negative Control

The raw result of the single negative control test is shown in Figure 6.5, where the top graph represents the drain current measured over time, and the bottom graph represents the transconductance as calculated from the drain current and variation in gate voltage.

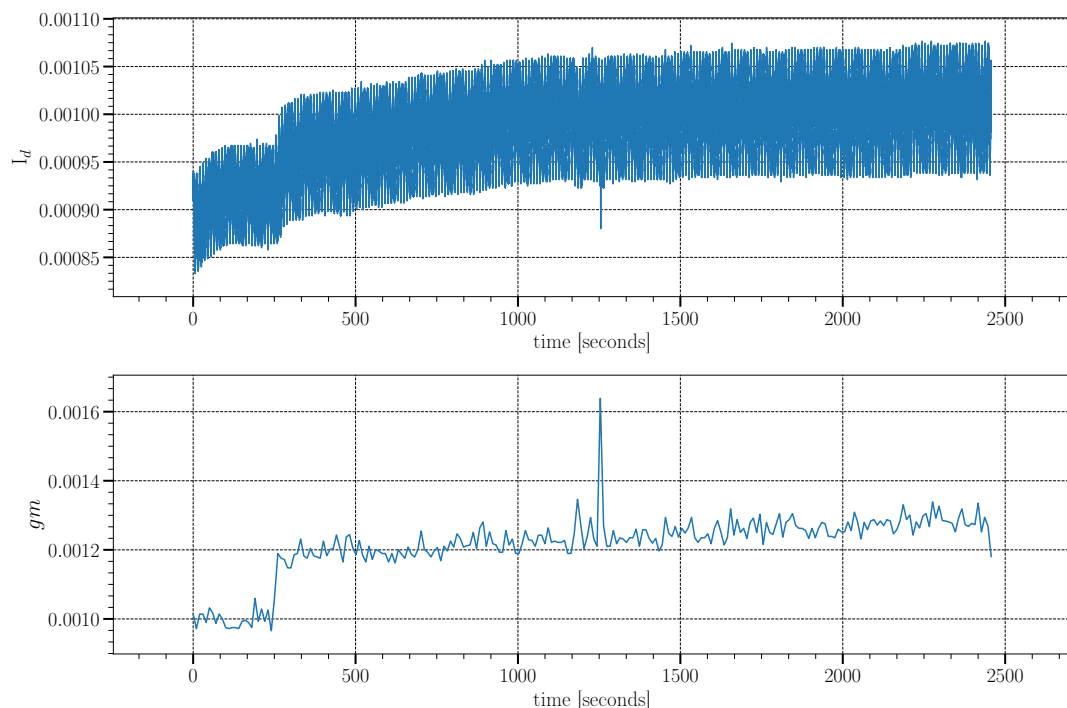


Figure 6.5: Negative control tests results, current over time

This shows that the transistor drain current immediately increased from 0.925 mA to 0.95 mA upon the addition of PBS, instead of decreasing as seen in previous tests, where the initial volume of PBS in the electrolyte well was lower. The drain current then steadily increases for 16 minutes before stabilising at 1.1 mA. The calculated transconductance follows a similar pattern of an initial spike, gradual increase and eventual stabilisation. This behaviour was unexpected, as tests had been done to prevent the addition of PBS having a direct effect on the transistor current. The increase in current however was probably not caused by the adsorption of BSA onto the transducer surface, due to the isoelectric point of BSA being at a pH of 5.4, meaning that BSA would be negatively charged and binding to the sensor surface would cause a decrease in current. This result shows that the transistor current does not decrease for a high concentration of an unwanted analyte, and a response for CRP itself can be interpreted as such, as it is expected to cause a decrease in drain current due to the addition of negative charge at the transistor surface when bound to an antibody [178], which should then decrease the carrier concentration in the channel region and reduce the drain current.

6.4.2 Protein Dilutions

The testing procedure discussed earlier was followed to test the transducers for the dilution series, and selected results of these tests are shown below. The results were chosen for three concentration tests that were identified as being representative of their group of results.

Not many of the transistors remained functional after antibody immobilisation, and only 32% (19) of the transducers were found to act as transistors. Table 6.1 shows the number of transistors that remained functional per concentration test, whose results were then processed, although all of the transistors onto which antibodies were immobilised were tested and went through the complete procedure.

Table 6.1: Number of functional transistors per concentration test

Concentration [$\mu\text{g}\cdot\text{ml}^{-1}$]	Number of functional transistors
10	2
5	3
2.5	2
1.2	4
0.625	1
0.31	3
0.078	2
19.53	2

This small sample size for the tests means that any results cannot be statistically significant, and that the results should be interpreted as such.

For one of the tests done for the concentration of $10\ \mu\text{g}\cdot\text{ml}^{-1}$ the raw measured data

is shown in Figure 6.6, along with the calculated transconductance over time. The first cyan arrow on the graph indicated when protein solution was added to the well, and the second arrow indicates when the drain current stabilised. The average current through the device increased slightly when the protein solution was added, with a corresponding increase in transconductance. The current then steadily declines until it stabilises after approximately 10 minutes. The decrease in current was calculated to be $242 \mu\text{A}$, and the change in transconductance between protein addition and stabilisation was $-327 \mu\text{S}$. The time taken for the current to stabilise was measured to be 10.4 min.

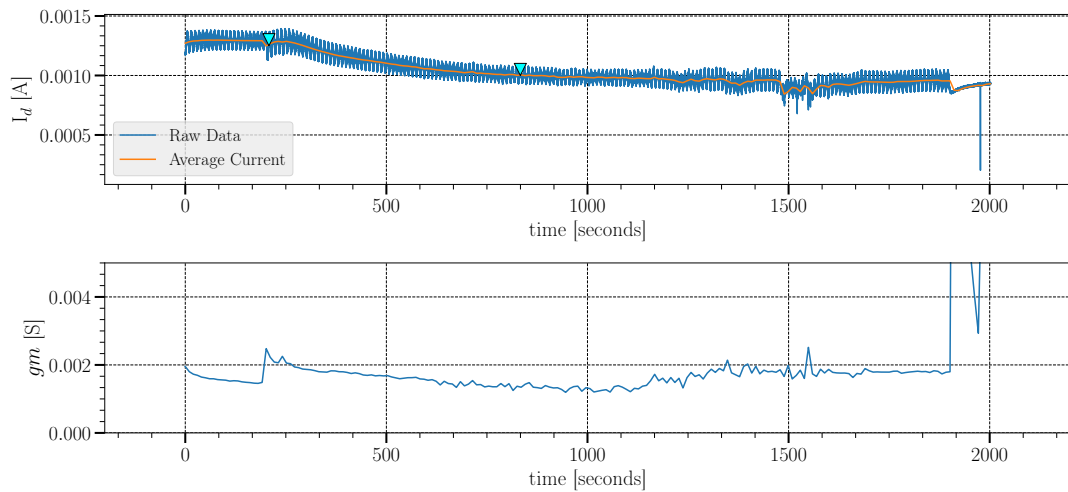


Figure 6.6: Raw measurement data for test 4 - concentration = $10 \mu\text{g}\cdot\text{ml}^{-1}$

For the response in Figure 6.7, which was for protein concentration of $0.31 \mu\text{g}\cdot\text{ml}^{-1}$, the current once again steadily decreased from the initial steady-state value towards a new value. The transconductance in this case did not suddenly increase when the protein sample was added, but rather increased gradually before decreasing again to a value $312 \mu\text{S}$ larger than the initial value. The decrease in current was $267 \mu\text{A}$. For this test the time taken for the current to stabilise was 25.8 min.

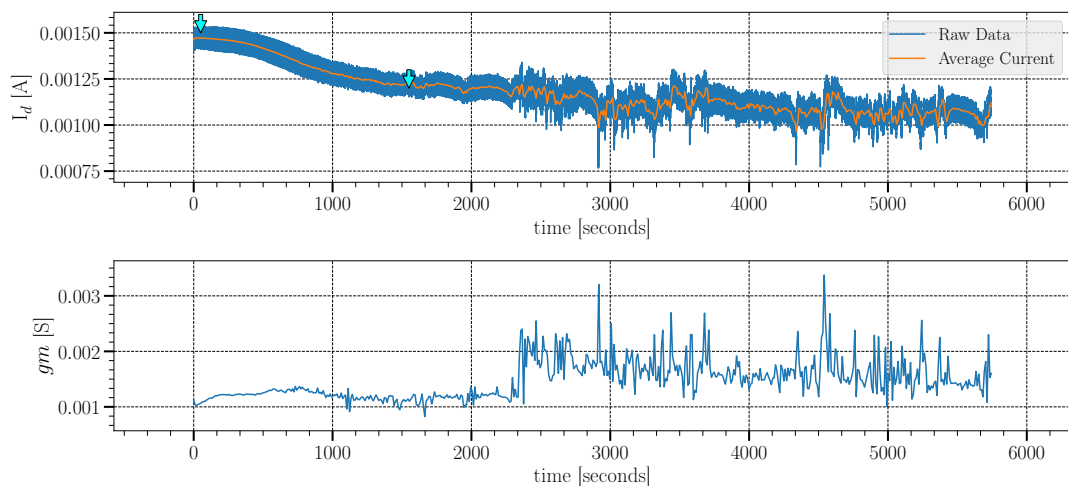


Figure 6.7: Raw measurement data for test 25 - concentration = $0.31 \mu\text{g}\cdot\text{ml}^{-1}$

For the test in Figure 6.8, there was once again a sudden increase in both current and transconductance when the protein solution sample was added to the electrolyte well. The current once again steadily decreased before stabilising, and the transconductance decreased to a value $0.11 \mu\text{A}$ lower than the initial value. The time elapsed before the current stabilised in this case was 37.4 min.

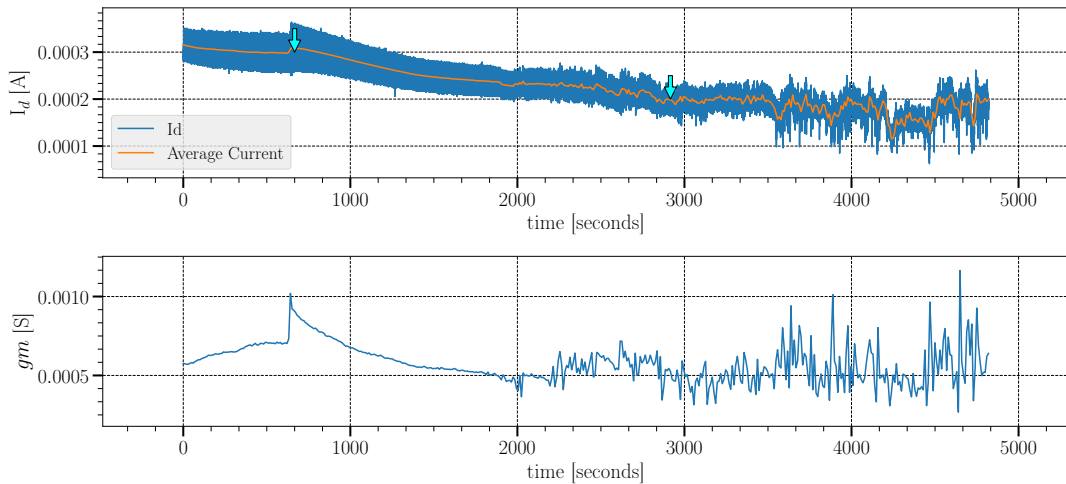


Figure 6.8: Raw measurement data for test 56 - concentration = $0.078 \mu\text{g}\cdot\text{ml}^{-1}$

Plotting the three graphs on the same axis in Figure 6.9 however reveals that the absolute change in current had no relationship with the protein concentration - the currents start at very different values due to the poor repeatability of the transistors themselves. The change in transconductance is similarly not of any use, as some transistors shows a nett increase in gm after protein addition and others a nett decrease.

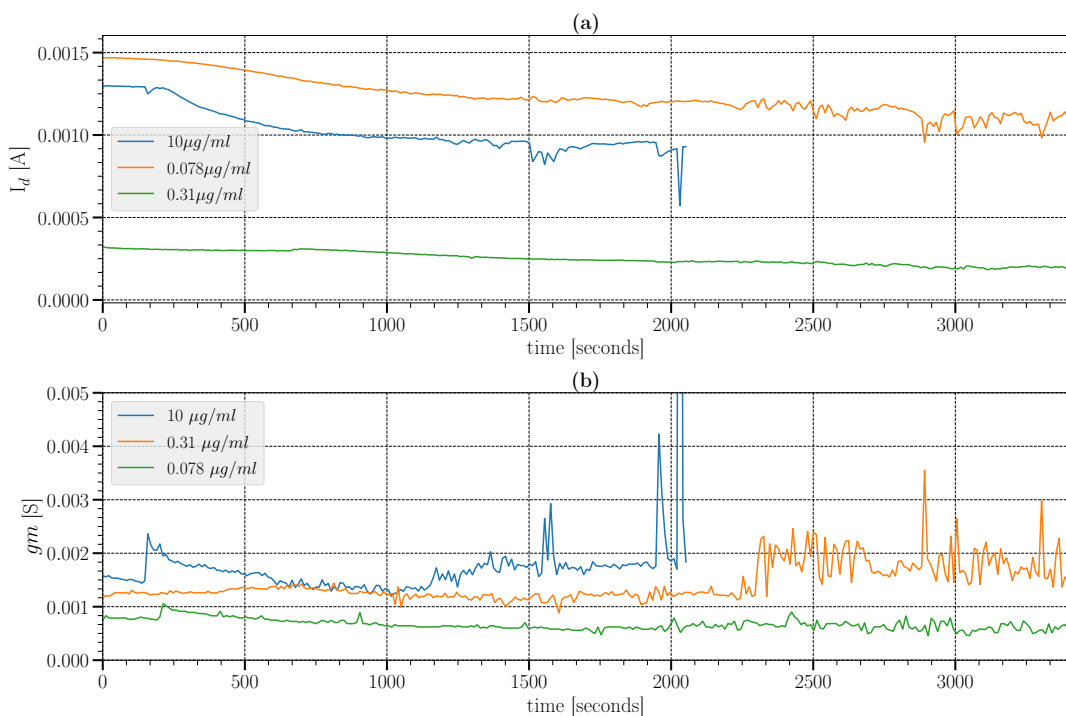


Figure 6.9: Comparison of absolute current change over time

Normalising the current shows that the proportional decrease per test is similar and that it seems that the rate at which the current decreases may have some correlation to the protein concentration - shown in Figure 6.10 are the three tests normalised to their current values immediately before protein addition and shifted in time to align the time at which protein is added.

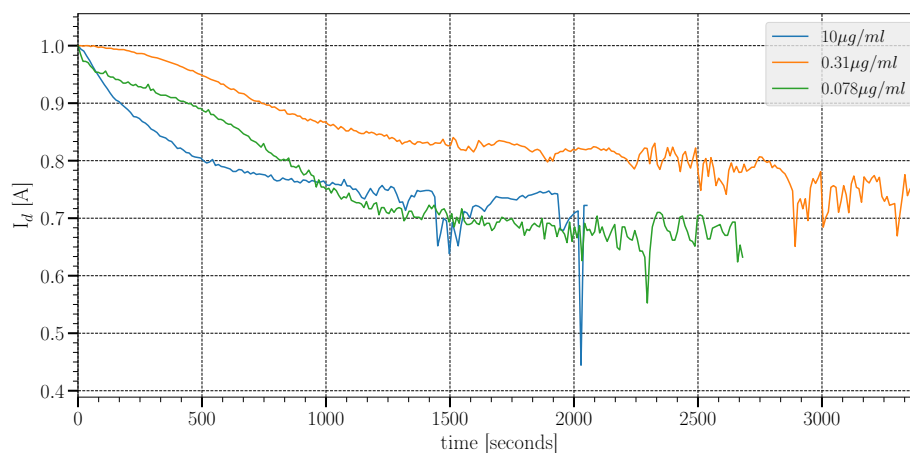


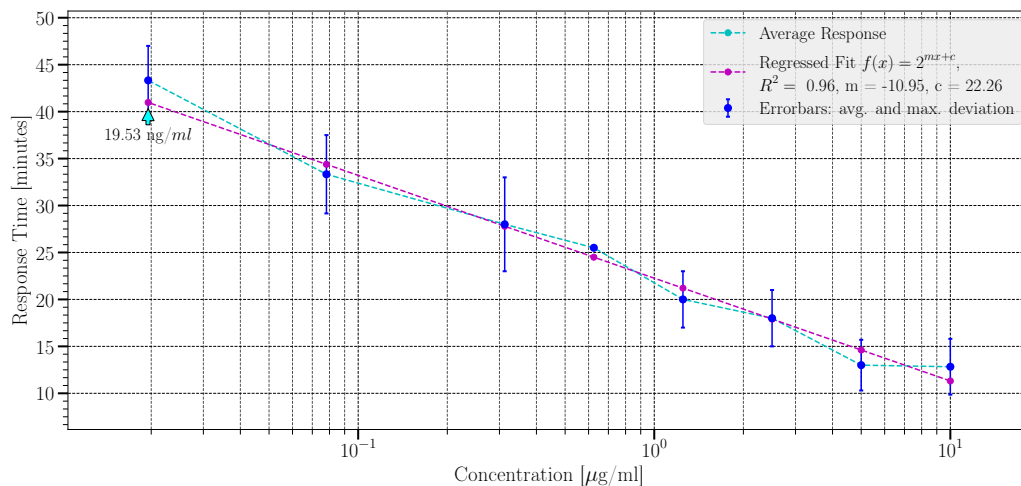
Figure 6.10: Normalised change in current over time

The first two tests show a decrease to 75% and 70% of the initial value, while the third settles at a value 80% of the initial current. In the three tests shown above, the current of the highest protein concentration settles much faster than the other two. The second concentration to stabilise is that of the $0.31 \mu\text{g}\cdot\text{ml}^{-1}$ protein concentration, followed by the test of $0.078 \mu\text{g}\cdot\text{ml}^{-1}$. From this observation a method of calculating the time elapsed for each concentration test to reach a steady-state current was developed. Each measurement was normalised to its value at protein addition after which the time elapsed until the current reaches steady-state was calculated. The result of this process is shown in Table 6.2, where the average time taken to reach steady-state for each concentration is shown. The proportional decrease in drain current for the tests with antibodies is very similar to the results from the previous, specifically Figure 5.18, where the current decreased by $\approx 30\%$ for binding due to a very high concentration of FITC, suggesting that the transducers are being eventually saturated for every concentration, and that the difference in response time is due to the lower concentrations needing more time to bind to all of the available antibodies.

Table 6.2: Average response time per concentration

Concentration [$\mu\text{g}\cdot\text{ml}^{-1}$]	Average response time [minutes]
10	12.8
5	13.1
2.5	18.2
1.25	20
0.625	25.5
0.31	28
0.078	33.3
0.0195	43.3

The results from Table 6.2 was then plotted against concentration, along with the deviation from the average for that concentration. A semilog x-axis was used to plot the results due to the exponential decrease in concentration to display the results in a readable manner. The method of linear regression was also used to determine the linearity of the results, and an equation of the form $f(x) = 2^{mx+c}$ was fitted to the calculated average response times. The result of this calculation was an R^2 value of 0.95, for $m = -10.99$ and $c = 23.07$. It seems that the linear range for these transducers is for concentrations between $19.5 \text{ ng}\cdot\text{ml}^{-1}$ and $2.5 \mu\text{g}\cdot\text{ml}^{-1}$, due to the ambiguity in the response times for the first two concentrations.

**Figure 6.11:** Plot of average response time over concentration

6.5 Discussion

It can be seen from the results of measuring the series resistances of the transistors before functionalisation that the manufacturing method is somewhat flawed. The variation between individual transistors is too high for the transistors to be acceptable in an industrial or commercial setting, but the devices function as intended. It would be necessary to

improve the consistency of such sensors before application on any scale can be considered.

The manufacturing method has two main disadvantages, with regards to repeatability: the exact area covered by the PEDOT:PSS droplet is not controllable to any reasonable precision, as the droplet spreads out on the paper during the pipetting and baking steps. The second source of variation is the number of processing steps necessary to manufacture a single transistor: first, silver is printed onto paper, then photoresist is spincoated onto the paper, after which the PEDOT:PSS is deposited and baked. Any and all of the above steps could introduce variations to manufactured transistors. Therefore the number of processing steps must be reduced, and simplified to limit the sources of contamination and variation. Inkjet printing would be ideal to eliminate some of the sources of variation, due to the advantages of inkjet printing previously discussed. Screen printing, gravure printing or physical vapour deposition would also be viable alternatives, but all require costly equipment and facilities to implement.

While the functionalisation process was successful, it was not ideal, and rendered many transducers inoperable after antibody immobilisation. This may be due to the nature of the APTES interaction, which was seen to react with silver nanoparticle ink and render it non-conductive. This may be part of the reason for the many transistors becoming inoperable, as it could be seen that the solution of APTES in toluene could, infrequently, penetrate into the photoresist coated paper and reach the silver outside the electrolyte well or under the PEDOT:PSS layer.

As biosensor transducer, the transistors manufactured in this chapter performed very differently from what was expected, and neither of the two expected performance metrics were of any use. It was found that the change in drain current did not exhibit a correlation to concentration - tests for two very different concentrations showed nearly the same proportional decrease in current, while a third test decreased by a different proportion. The change in transconductance was similarly inconsistent, increasing after protein addition for some tests and decreasing for other. It was however observed that the time necessary for each concentration to reach a steady-state current after protein addition was related to the concentration of protein present in the sample.

It is thought that the cause of this seemingly bizarre result may be the large surface area of the transistors, as the final designs were manufactured with PEDOT:PSS regions with a size of 4x3 mm, with an estimated thickness of several hundred micron, which is considerably larger than many of the designs found in the literature, such as [179] or [126], although not the largest - the sensors developed by Currano *et al.* [119] are centimetres in length. The large surface area of the transistors, combined with the large volume of the electrolyte wells could allow all of the protein present in the well to bind to the antibodies, and thereby saturate the sensor for all of the concentrations that were tested.

Finally, the protein concentrations that were tested covered the complete clinically relevant range for most individuals [158], [159], but the response time measured for all of the concentrations would be too slow to be used as part of a quantitative point-of-care device - typical doctor appointments only last 15 minutes, although it might be of use in hospital settings when a patient is admitted to monitor the progression of symptoms and effectiveness of treatment. Alternatively the transducers can be used in a qualitative capacity, where a confirmation is sought for the CRP concentration being within a specific

concentration range.

The concentrations of interest for CRP in individuals with an unknown infection are above $25 \mu\text{g}\cdot\text{ml}^{-1}$ for acute inflammation due to infection, as shown by [180], which is outside of the linear range of the transducer. This can be remedied by testing dilutions of patient samples to lower the effective concentration. The dilution factor can then be used to calculate the original concentration of protein in the sample.

6.5.1 Cost Estimation

A simple cost-estimation was done to determine a lower-limit to the cost of manufacturing such sensors on large-scale. The amount of antibody immobilised, along with the amount of BS³ and CRP used was calculated using the protocol used to manufacture the sensors, in combination with the documented concentrations of the reagents. Labour cost was estimated as the cost of a low-skilled factory worker producing 80 sensors per 8.5 hours, as was the case during completion of this project, [181], [182], where the average wage for such a factory worker is given as R4500 per month, or R35 per hour. Other costs were taken to be negligible, as the paper, APTES and other materials used can be manufactured at large scale and low cost, keeping their contribution to the total cost of a transducer to a minimum. The antibodies and proteins however are more difficult to manufacture at large scale and will always have a dominant contribution to the cost of a transducer.

Table 6.3: Cost estimation for sensors

Component	Cost per Unit [R/ μg]	Units per Transducer [μg]	Cost per Sen- sor
Capture Anti- bodies	39.17	0.192	7.52
Recombinant CRP Protein	33.84	0.192	2.44
BS ³	0.043	30	1.29
Labour	R35/hour	0.10625	3.71
Total:			R15.2

The total cost of such a transducer would then be calculated to be R15.2 excluding equipment costs, such as for ovens, pipettes, sterile workstations, etc. If the cost per sensor is doubled, or even tripled, to take profit, equipment and property, logistical costs and FDA certification costs into account, the cost of a transducer or test utilising the transducer would be R45 to an end-user. Current prices for CRP tests done at pathology laboratories, such as PathCare [38], are R202.70.

The lower potential cost of a test utilising one of the transducers developed in this project would mean that CRP, and other, tests would become more accessible to the general public, and could potentially enable wider use of such sensors in secondary healthcare settings, such as clinics and government healthcare installations.

6.6 Conclusion

This chapter set out to evaluate the function and applicability of the manufactured transducers for their intended purpose: to detect and measure the concentration of CRP in buffer solution, to eventually contribute towards combating antimicrobial resistance by simplifying the diagnosis of infections of unknown origin.

The transducers were functionalised with biorecognition elements by covalently linking polyclonal anti-CRP antibodies to the sensor surface by linking the amine groups on the Fc region of the antibodies to amine groups grown on the transducer surface.

After characterisation of the transducers by evaluation of the resulting change in current and transconductance over time, it was found that the rate at which the transducer current decreased was proportional to analyte concentration, but that the specific proportion of current reduction was not. The sensors were successful in detecting CRP concentrations between $2.5 \mu\text{g}\cdot\text{ml}^{-1}$ and $19.53 \text{ ng}\cdot\text{ml}^{-1}$, which covers the clinically relevant range for healthy individuals [158], [159], and the range of detectable concentrations can be extended by diluting samples to lower the effective concentration, as is often done in ELISA or MSD protocols for samples with unknown concentrations of analyte.

The transducers fulfilled their goal, but there is room for improvement in both the manufacturing method and immobilisation method.

Chapter 7

Discussion

The goal of this chapter is to provide an overview of the results obtained from this project, and to provide discussion on the subjects treated therein. The project consisted of three main phases, each determining the direction of the next. The first part concerned the modification of a commercial desktop inkjet printer into a flatbed configuration. The second part of this project concerned the development and functionalisation of organic electrochemical transistors. The third and final part of the project consisted of the final experiment, which was conducted to determine whether the manufactured transducers reacted to C-reactive protein in buffer solution.

7.1 Printer Development

The first part of this project was primarily focussed on modifying an inkjet printer to become a material deposition system. The goal of this part of the project was to investigate whether a modified inkjet printer would be capable of printing metal nanoparticle and polymer inks at high resolution with any degree of repeatability. Modification of the printer was done by first disassembling the chassis and removing all of the functional mechanisms, including the cartridge carriage and feed mechanism. The feed mechanism and cartridge carriage were then installed into a new chassis designed to allow printing onto substrates of different height and alignment of multiple printed layers. Performance of the printer was evaluated by doing three tests. The first test was to determine the minimum resolution of structures that could be printed. Initial results showed that the printer performance varied wildly depending on the specific configurations of both the printer and the application controlling it, but a combination was eventually found that would deliver consistent results. With this optimal configuration it was found that the printer could print structures of silver nanoparticle ink with a resolution of 70 μm . The second test done with the printer was to attempt alignment of multiple printed layers of ink on top of one another. Multilayer alignment was made possible by adding endstop blocks to the printer guides, to force the substrate platform to start at the same position for each subsequent printed layer. It was found that the alignment of layers could be manipulated by exploiting a brief pause in the printer's printing process, and the final tests done showed that layers could be aligned to within 25 μm of one another.

The third test done was to compare the performance of different types of paper to the one suggested by the manufacturer of the silver nanoparticle ink, Mitsubishi Paper Mills.

Four types of paper were evaluated: Mitsubishi paper, Epson Semigloss paper, Epson Ultragloss paper, and JoJo Waterproof paper. The types of paper were compared in terms of printed resolution and performance, surface roughness of the clean paper, and the surface roughness of silver printed onto the paper. The tests made it clear that the Mitsubishi paper was indeed the best option for the silver nanoparticle ink, and that the others had certain incompatibilities with the ink that made them unsuitable for sensor manufacturing. The Ultragloss paper, for example, had a low surface roughness, but the silver adhered very poorly to its surface and easily peeled off when the paper was bent slightly. Lastly, the printer was also used to print PEDOT:PSS ink, which was intended to be used to print semiconducting regions for OECT biosensors. Several ink dilutions were made and the viscosities thereof tested, and eventually a mixture containing PEDOT:PSS, DMSO, deionised water and glycerol in a ratio of 30:60:5:5 % (w/w) was successfully printed onto paper without immediately clogging the cartridge nozzles. However, the cartridges did not last more than a week before having to be replaced due to ink drying in the nozzles and causing clogging. Comparison of the performance of the printer developed during this part of the project with a Dimatix system, the DMP-2800, reveals that the Dimatix is capable of printing structures with a resolution of up to 20 μm , with a repeatability of up to 25 μm between layers [168], which is very close to what can be achieved with this low-cost modified printer - alignment of 25 μm and print resolution of 70 μm .

The modified printer exceeded all expectations of what it would be capable of doing, and this part of the project was successful in achieving its goals.

7.2 Transducer Development

The second part of this project consisted of the process by which transistors were manufactured and eventually functionalised with surface amine groups. The chapter investigated three methods of transistor manufacturing, namely inkjet printing, spincoating and manual drop deposition. The method of inkjet printing was investigated due to its novel nature, and potential for rapid prototyping. Spincoating was chosen due to its being the standard manufacturing method of organic electrochemical transistors, and manual drop deposition was chosen as a contrast in simplicity to the other two methods.

Many attempts were made to print transistors, but none were successful. Variations on electrode designs, ink composition, the number of PEDOT:PSS layers printed and the type of paper were investigated, but to no avail. It was then decided to attempt spincoating, but that did not work either. Finally, manual drop deposition was attempted, and was successful.

Two of the three manufacturing methods investigated in this chapter did not succeed in forming functional transistors of any sort. The manufactured devices were very conductive, but it seemed that there was some factor of either the electrode designs, the paper, the printed silver or a combination of all three (or more factors that were not considered, such as secondary dopants or impurities in the polymer mixture) that caused the thin-film transistors to fail. Tests were done to determine whether it was the surface roughness of the printed silver that had an unintended effect on the function of the transistors, but

this also did not deliver any useful information.

Transistors manufactured with the manual drop deposition method were verified to function as transistors, and transfer curves were drawn for these devices. The first group of transistors, manufactured without addition of PVA, had threshold voltages of -0.7 V . PVA was then added to the PEDOT:PSS ink mixture to provide surface alcohol groups for the surface functionalisation method chosen for this project. Fluorescence microscopy was used to verify that APTES bound to the transistor surfaces, and transfer curves were drawn for transistors at the different stages of functionalisation, from which a clear difference was visible between processing steps. Finally, the transistors were tested by adding the fluorescent marker FITC to the amine-functionalised surfaces and the current through the devices was measured to determine whether a molecule binding to the amine groups would cause a change in the drain current of the transistors. It was found that the drain current of the functionalised transistors consistently decreased for five devices when exposed to FITC, showing that the working principle of the transducers was sound.

7.3 Protein Measurements

The third and final part of this project was the final experiment consisting of sets of manufactured transistors being exposed to a series of protein dilutions to determine whether their response has any relationship to protein concentration.

The transistors were functionalised with antibodies by using the crosslinker known as BS³, which uses two sulfo-NHS groups to link primary amine groups on either end with a spacer length of 11.4 \AA . The transistors were found to have a low repeatability in terms of series resistance after APTES functionalisations, which goes contrary to the results reported by Strakosas [110] for a very similar reaction where the APTES was replaced by GOPTS. This may be due to the APTES/Toluene solution penetrating into the paper substrate and causing unknown interactions with the silver electrodes under the PEDOT:PSS layer, as it was observed that the toluene could penetrate the photoresist layer from time to time. This would seem to explain the observations of large and unpredictable variation between groups of transistors.

The final experiment was executed, and it was found that there was too much variation between individual transistors to compare the drain current as-is, but an attempt was made to normalise the current measurements to the value at the time of the protein sample being added, and the aligning the responses over time. It was then discovered that the time elapsed between the addition of protein and the drain current reaching a steady-state value was directly proportional to the concentration of the protein.

The sensors could detect protein values as low as $19.5\text{ ng}\cdot\text{ml}^{-1}$, with a maximum measurable value of $2.5\text{ }\mu\text{g}\cdot\text{ml}^{-1}$, which is inside the clinically relevant range of CRP protein in healthy individuals.

7.4 Limitations of Study

The limitations of the work in this project were largely related to limited repeatability in the sensors manufacturing process, which were caused by a combination of the manufacturing method and antibody surface functionalisation method. The manufacturing methods introduced variation between devices, which were amplified by the process of functionalising the surface with APTES and subsequently immobilising antibodies to the surface. The large number of processing steps, from printing and spincoating to antibody incubation and blocking, had a total duration of 8.5 hours to complete the 12 distinct processing steps. This large number of processing steps could also be a source of variation, as each step would introduce slight variations between transducers, with the end-result compounding to form a set of very different transducers. The inconsistent performance of the transducers themselves prevented use of the usual performance metric of absolute change in drain current from being used to determine protein concentration, and likely also prevented the transconductance measurement from being of use, resulting in the comparison of transistor response-time as a measure of protein concentration. A correlation was established between this metric and protein concentration, although many more tests would need to be done to determine its validity; a sample size of 12 transistors is not quite enough to be statistically significant.

7.5 Conclusion

The original goals of this project were to develop a sensor to distinguish between bacterial and viral infections by measuring the concentration of CRP in solution. The objectives along the way were divided into three distinct stages, that of printer development, transducer development and finally transducer evaluation. All three of the objectives were met, although the last two were not achieved in the manner that was originally expected.

It had been expected to be able to print the transistors and in so doing accelerate the development process of iterating through transistor designs to find one with optimal parameters as a sensor. This was, however, not the case, as no printed transistor showed any sign of the drain current being dependent on the gate voltage. This was thought to have been caused by any of several parameters of the printing process, but variation of most of them revealed no insights. It could be a simple case of the thin-film transistors being too large for them to function effectively.

The reason for the transducers working as well as they did might be easier to explain, and is thought to be caused by a high affinity of the antibody for the CRP protein in combination with the high surface area of the sensors compared with the well surface area. The protein simply has to settle down onto the transistor surface to bind to an antibody, which will readily happen when the antibody has a high affinity for the protein. This means that the transducers will effectively continue being saturated over time due to the high affinity and large surface area. The results from the previous component, that of FITC labelling, supports this hypothesis, showing the same proportional decrease in drain current over a much shorter amount of time, due to the very high concentration of FITC used for the test.

Regarding the comparison of the AC and DC measurement techniques, there was a clear tendency for the transistors to stop functioning after some time, as seen in the raw mea-

sured data, when the measured response from the transistors spontaneously becoming very noisy in nature. Closer inspection of the voltage output at these points reveal that the current starts behaving probabilistically, varying at random between the expected distorted sinusoid to jagged edges. This is a similar behaviour to that observed for charge-trapping in large-scale MOSFETS [183], and may have implications for water penetration into the PEDOT:PSS layer.

More work needs to be done to determine why these transistors work in the manner that they do, and why they are as sensitive as they are. An alternative manufacturing method must also be found, as the manual drop deposition technique is not suited to production of any scale, and introduces variation between devices instead of decreasing it.

Chapter 8

Conclusion

Antimicrobial resistance is a growing problem in the world, with increasing numbers of highly drug-resistant strains of bacteria being reported every year. Conversely, pharmaceutical companies are spending less on developing antibiotic substances every year due to the effective lifetime of antibiotics becoming so short as to no longer be profitable. The main cause of the growth in AMR is the indiscriminate use of antimicrobial medications in human patients and livestock for agricultural use, and more effective methods of antimicrobial stewardship are necessary to address the problem.

To this end, the World Health Organisation has issued a call for the development and investigation of new technologies to combat the problem of AMR. One of the suggested strategies is to identify novel biomarkers, or use ones that are already known, that can be used to better distinguish between the possible causes on infection in patients presenting with ambiguous symptoms.

Three potential biomarkers have been identified that, when used in combination with one another, have potential to provide information regarding the cause of infection. The three biomarkers are: human myxovirus resistance protein-A, or MxA, procalcitonin, or PCT, and C-reactive protein, or CRP. Of the three markers, CRP is the second largest molecule and already widely used by primary healthcare professionals to aid in diagnostic decisions.

With the goal of eventually contributing towards a management strategy for AMR, it was decided to develop a paper-based biosensor transducer to detect and measure CRP in buffer solutions, as a first step towards developing a biosensor for this purpose.

8.1 Review of Aims and Objectives

This project had three initial goals, of which all three were achieved. The first objective was to develop a low-cost inkjet printing system with which rapid prototyping could be done during the development of a biosensor transducer. This was achieved through extensive modification of a commercial desktop inkjet printer, the HP DeskJet 4535, which was converted into a flatbed printer. The printer was configured to allow alignment between subsequent printed layers, and to print with silver nanoparticle ink alongside an ink formulated using the conducting polymer known as PEDOT:PSS. The printer could print small-scale structures with a resolution of 70 μm , and layers could be aligned to within

25 μm of one another.

The second objective of the project was to manufacture electrochemical transistors, with which the transducer would be constructed. Three manufacturing methods were investigated to this end; inkjet printing, spincoating and manual drop deposition were investigated to compare transistor characteristics between the three methods. Of the three, only manual drop deposition was successful in manufacturing transistors. After having successfully manufactured transistors, the functionalisation strategy with which antibodies would be immobilised onto the transistors was validated, and was found to be successful by a combination of fluorescence microscopy and comparison of transistor characteristics at various points of the manufacturing process.

After successful transistor manufacture, the third goal of the project was attempted: measuring CRP protein in buffer solution. This was done by immobilising anti-CRP antibodies onto the transistor surfaces by linking amine groups on the Fc region on the antibodies to amine groups on the transistor surface through BS³. This goal was also successfully achieved, but not in the manner expected.

8.2 Findings

The method of sensor evaluation was chosen to be a combination of AC and DC measurements, to compare the effectiveness of the two methods in reflecting the change in transistor characteristics. The measurement method superimposed a small AC signal on top of a DC biasing voltage for the transistors, in an attempt to evaluate both changes in DC current and in small-signal transconductance due to protein binding to the surface of the transistor sensors. The results from these tests did not reveal any relationship between the magnitude or proportion of current change or transconductance variation and the protein concentration present in samples added to the transducers during the test procedure. Re-evaluation of the measured responses revealed a correlation between the rate of change in drain current, and the time necessary for the current to reach a steady-state value after protein addition. Protein concentrations between 19.53 $\text{ng}\cdot\text{ml}^{-1}$ and 10 $\mu\text{g}\cdot\text{ml}^{-1}$ were tested using the sensors, and the response time remained linearly related to protein content for concentrations between 2.5 $\mu\text{g}\cdot\text{ml}^{-1}$ and 19.5 $\text{ng}\cdot\text{ml}^{-1}$, with response times between 20 and 43 minutes. The time-based measurement done for the transducers has the implication that a likely application would rather be in quantitative diagnostics than qualitative, although qualitative results are also possible if a fast result is not necessary to the user. A cost estimation was done for the transducers, and it was found that, if commercialised, a single transducer might cost an end-user R45, which is much less than the current cost of CRP tests.

The results of this project show that a low-cost paper-based transducer could be manufactured to detect and measure protein concentrations in buffer solutions, and that there is potential for such a transducer to be integrated into a biosensor system to aid in the differentiation between bacterial and viral infections, thereby aiding in the management of antimicrobial resistance.

8.3 Recommendations and Future Work

Further work that should be pursued with relation to this project can be divided into three categories: improvement of repeatability, preprocessing and system integration. The main difficulty encountered during this project was that of repeatability in manufacturing methods, and the implications thereof for the manufactured transistors. Further, integrated preprocessing techniques would be necessary for the transducer to be integrated into a complete biosensor system. Lastly, the practical implications of integrating the transducers with a biosensing system would need to be investigated, as factors such as data processing and hardware configurations would have an impact on the applicability of the transducer to any practical situation.

8.3.1 Manufacturing Methods

The three manufacturing methods investigated in this project should all have been successful, but only one could be successfully implemented, and it was the method with the worst potential for repeatability

8.3.2 Preprocessing

Several preprocessing methods have been successfully used in biosensing applications, and it is well known that such steps are necessary to implement such a system successfully due to the complex mixtures of proteins, ions, cells and other materials present in biological samples [184]. Two preprocessing techniques would be of interest to this application: the use of nanofibre filters to separate cells and other large particles from samples and allow proteins to reach the transducer, and the integration of the transducer into a lateral-flow assay type test. The first method would be aimed towards reducing the probability of unexpected interactions between the sensor and other materials present in blood, where CRP is primarily found. Companies such as Stellenbosch Nanofibre Company currently have the capabilities to manufacture such filters.

Integration into a lateral flow assay would potentially allow the sensor to integrate pre-concentration of antibodies and proteins and implementation of a sandwich-type assay to increase the sensitivity of the sensors. This improvement of sensitivity would then allow the sensor to be used for a large number of other proteins, such as PCT and MxA that are present at much lower concentrations than CRP.

8.3.3 System Integration

Several improvements can be made to the overall system configuration by which the transducers were evaluated. first of all, the measurement methodology can be improved for greater sensitivity by optimising the sensor layout and signal processing chain. The data processing procedure can also be improved, as much of the data interpretation for this project was done on a case-by-case basis due to the poor repeatability between sensors. Furthermore, machine learning can be integrated with the data processing stage to offer more effective interpretation of results. Finally, multiplexed simultaneous sensing of multiple biomarkers can be implemented to achieve the eventual goal of such a sensor system: a comprehensive diagnostic system capable of aiding healthcare professionals in making better, more accurate decisions regarding patient diagnosis and treatment.

8.3.3.1 Measurement Methodology

The measurement methodology used in this project showed that the indirect measurement of small-signal transconductance had little to no value to the evaluation of protein concentrations, possibly due to the large transducer size limiting the effect that protein binding can have on carrier mobility. Therefore the more effective measurement was the average DC current, and a measurement methodology can be developed to take advantage of this.

One of the current standards in resistance measurement is known as a resistive bridge, or Wheatstone bridge. A manner could be found to integrate such a differential bridge measurement technique to improve noise rejection and overall sensitivity of a transistor or resistance-based sensor system. An example of such a measurement configuration is shown in Figure 8.1, where a pair of transistors could be functionalised with antibodies, while the other acts as reference to subtract any effects of nonspecific interaction from the measured output.

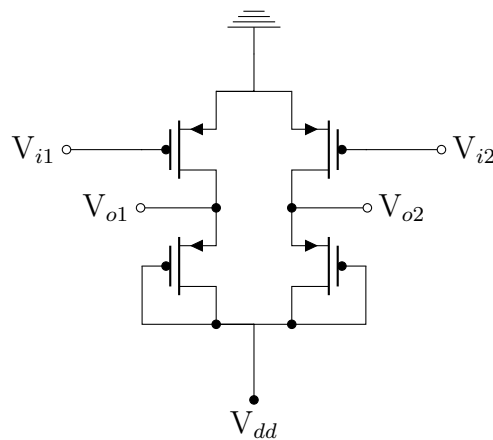


Figure 8.1: Proposed bridge configuration circuit

8.3.4 Other Applications

Other applications are possible for the transducers developed in this project, such as in the field of home-use biomonitoring devices. A current trend in public health awareness is the fitness revolution, where individuals extensively monitor parameters such as heart-rate and cadence to better understand the impact of exercise on their bodies. Measurement of CRP, an inflammatory marker, would be of benefit to these individuals due to its correlation with muscle damage and other inflammatory responses.

Another field that this transducer would be of interest to is the agricultural sector, where large amounts of antibiotics are used to improve overall animal health and yield. Effective monitoring of animal health through low-cost sensors could lower the amounts of antibiotics consumed by this industry, and in so doing avoid unnecessary use of antimicrobials.

The printer has functionality that could also be used in applications of printed electronics, such as flexible or wearable monitoring systems. High-frequency electronics such as antennas could also be developed using such a system, greatly reducing the cost of manufacturing simple structures and accelerating the development process.

Appendices

Appendix A

Datasheets and Technical Information

BioVision

12/16

For research use only

C-reactive/CRP Monoclonal Antibody

CATALOG NO:	A1208-100
ALTERNATIVE NAMES:	CRP, PTX1, C-reactive protein
AMOUNT:	100 µg
IMMUNOGEN:	Human CRP Protein
HOST/ISOTYPE:	Mouse IgG
SPECIES REACTIVITY:	Human
PURIFICATION:	>95%, Protein G purified
FORM:	Liquid
FORMULATION:	In NaCl with 15 mM NaN ₃ (pH 7.4)
STORAGE CONDITIONS:	For long term storage store at -20°C in small aliquots to prevent freeze-thaw cycles.
DESCRIPTION:	C-reactive protein (CRP) is an annular (ring-shaped), pentameric protein found in blood plasma, the levels of which rise in response to inflammation (i.e., C-reactive protein is an acute-phase protein of hepatic origin that increases following interleukin-6 secretion from macrophages and T cells). Its physiological role is to bind to lysophosphatidylcholine expressed on the surface of dead or dying cells (and some types of bacteria) in order to activate the complement system via the C1q complex. CRP is synthesized by the liver in response to factors released by macrophages and fat cells (adipocytes). It is a member of the pentraxin family of proteins. It is not related to C-peptide (insulin) or protein C (blood coagulation). C-reactive protein was the first pattern recognition receptor (PRR) to be identified.
APPLICATION:	ELISA, LEITA, LFIA

Note: This information is only intended as a guide. The optimal dilutions must be determined by the user.

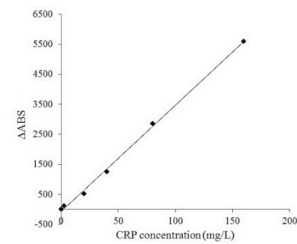


Fig1. Calibration curve for CRP in latex-enhanced turbidimetric immunoassay (LEITA): CRP proteins react with anti-CRP antibody precoated onto latex beads to form insoluble complex, resulting in turbidity increasing with was then detected by automatic biochemical analyzer.

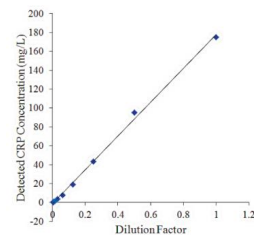


Fig2. Determination of the CRP concentration by serial dilution of clinical serum: The high value CRP serum was 2-fold serially diluted with physiological saline and measured on LETIA platform showed decline in CRP concentrations along with serial dilution of blood samples

RELATED PRODUCTS:

- Human CellExp™ C-reactive/CRP, human recombinant (Cat. No. 7242-100)
- CRP, human recombinant (Cat. No. 4864-250, -1000)

FOR RESEARCH USE ONLY! Not to be used on humans.



Product datasheet

Recombinant Human C Reactive Protein ab167710

1 Image

Overview

Product name	Recombinant Human C Reactive Protein
Protein length	Full length protein

Description

Nature	Recombinant
Source	HEK 293 cells

Amino Acid Sequence

Accession	P02741
Species	Human
Sequence	FGQTDMSRKA FVFPKESDTS YVSLKAPLTK PLKAFTVCLH FYTELSSTRG YSIFSYATKR QDNEILIFWS KDIGYSFTVG GSEILFEVPE VTVAPVHICT SWESASGME FWVDGKPRVR KSLKKGTVG AEASIIIGQE QDSFGGNFEG SQSLVGDIGN VNMWDFVLSP DEINTMLGG PFSPNVLNWR ALKYEYVQGEV FTKPQLWP

Molecular weight	23 kDa including tags
Amino acids	17 to 224
Tags	His tag C-Terminus

Specifications

Our [Abpromise guarantee](#) covers the use of **ab167710** in the following tested applications.

The application notes include recommended starting dilutions; optimal dilutions/concentrations should be determined by the end user.

Applications	SDS-PAGE
Endotoxin level	< 1.000 Eu/μg
Purity	>95% by SDS-PAGE .
Form	Lyophilised



Product datasheet

Anti-C Reactive Protein antibody ab31156

★★★★★ 2 Abreviews 3 References 1 Image

Overview

Product name	Anti-C Reactive Protein antibody
Description	Rabbit polyclonal to C Reactive Protein
Host species	Rabbit
Tested applications	Suitable for: ELISA, WB, Immunoelectrophoresis, Immunodiffusion, IHC-P
Species reactivity	Reacts with: Human
Immunogen	Full length native protein (purified) (Human).
Positive control	This antibody gave a positive result in IHC in the following FFPE tissue: Human normal liver.

Properties

Form	Liquid
Storage instructions	Shipped at 4°C. Store at +4°C short term (1-2 weeks). Upon delivery aliquot. Store at -20°C long term.
Storage buffer	pH: 7.20 Preservative: 0.02% Sodium azide Constituents: 0.0268% PBS, 0.812% Sodium chloride
Purity	Protein A purified
Purification notes	Purity was determined by SDS PAGE (blue stain), showing that the IgG constitute was greater than 90% of total protein.
Clonality	Polyclonal
Isotype	IgG

Applications

Our [Abpromise guarantee](#) covers the use of **ab31156** in the following tested applications.

The application notes include recommended starting dilutions; optimal dilutions/concentrations should be determined by the end user.

Application	Abreviews	Notes
ELISA	★★★★★	Use at an assay dependent concentration.

*Heraeus Deutschland GmbH & Co. KG
Leverkusen*

Number 81076212
Issue 2016-09-13

CLEVIOS™ PH 1000

Description of Product Aqueous dispersion, blue liquid

Synonyms / Abbreviations PEDT / PSS, PEDOT / PSS

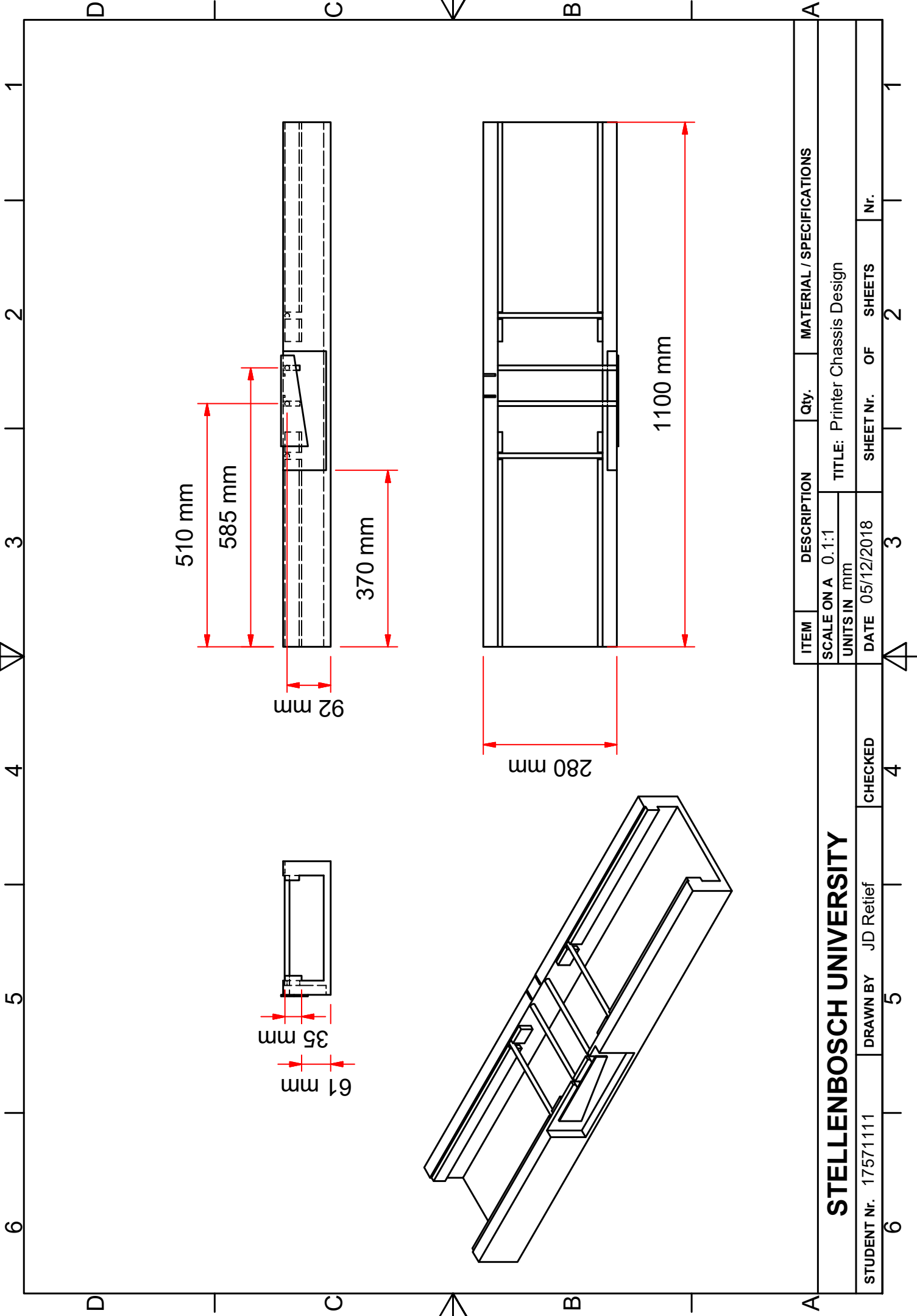
Physical Characteristics¹⁾

	Min		Max	Unit
Solid content	1.0	-	1.3	%
Specific conductivity*	850			S/cm
Viscosity	15	-	60	mPas

*After the addition of 5% Dimethyl sulfoxide. Measured on the dried coating.

Appendix B

Technical Drawings



ITEM	DESCRIPTION	Qty.	MATERIAL / SPECIFICATIONS
SCALE ON A	0.1:1		TITLE: Printer Chassis Design
UNITS IN	mm		
DATE	05/12/2018	SHEET Nr.	Nr.

STELLENBOSCH UNIVERSITY

STUDENT Nr. 17571111 DRAWN BY JD Relief CHECKED

OF SHEETS 2

3

4

5

6

Bibliography

- [1] H. C. Neu, “The Crisis in Antibiotic Resistance”, *Science*, vol. 257, no. 5073, Aug. 1992.
- [2] W. Witte, “BIOMEDICINE: Medical Consequences of Antibiotic Use in Agriculture”, *Science*, vol. 279, no. 5353, pp. 996–997, Feb. 1998, ISSN: 00368075. DOI: 10.1126/science.279.5353.996.
- [3] F. C. Tenover and J. E. McGowan, “Reasons for the Emergence of Antibiotic Resistance”, *Am. J. Med. Sci.*, vol. 311, no. 1, pp. 9–16, Jan. 1996, ISSN: 00029629. DOI: 10.1016/S0002-9629(15)41625-8.
- [4] M. Brooks, “Public Confused About Antibiotic Resistance, WHO Says”, 2015.
- [5] WHO, “Antimicrobial Resistance: Global Report on Surveillance”, World Health Organisation, Geneva, Switzerland, Tech. Rep., Jun. 2014.
- [6] —, “Worldwide country situation analysis: response to antimicrobial resistance”, World Health Organisation, Geneva, Switzerland, Tech. Rep., Apr. 2015.
- [7] WHO/EMP/IAU, “Global Framework for Development & Stewardship to Combat Antimicrobial Resistance”, WHO/EMP/IAU, Geneva, Switzerland, Tech. Rep., 2017.
- [8] S. Dittrich, “Meeting of Experts on Biomarkers to Discriminate Bacterial From Other Infectious Causes of Acute Fever”, WHO, ReAct, MSF Access Campaign and FIND, Geneva, Switzerland, Tech. Rep. September, Sep. 2015, pp. 1–28.
- [9] P. Lin and F. Yan, “Organic thin-film transistors for chemical and biological sensing”, *Adv. Mater.*, vol. 24, no. 1, pp. 34–51, Jan. 2012, ISSN: 09359648. DOI: 10.1002/adma.201103334.
- [10] D. Elkington *et al.*, “Organic Thin-Film Transistor (OTFT)-Based Sensors”, *Electronics*, vol. 3, no. 2, pp. 234–254, Apr. 2014, ISSN: 2079-9292. DOI: 10.3390/electronics3020234.
- [11] J. Hamilton-Miller, “Antibiotic resistance from two perspectives: man and microbe”, *Int. J. Antimicrob. Agents*, vol. 23, no. 3, pp. 209–212, Mar. 2004, ISSN: 09248579. DOI: 10.1016/j.ijantimicag.2003.12.001.
- [12] N. Waglechner and G. D. Wright, “Antibiotic resistance: it’s bad, but why isn’t it worse?”, *BMC Biol.*, vol. 15, no. 1, p. 84, Dec. 2017, ISSN: 1741-7007. DOI: 10.1186/s12915-017-0423-1.
- [13] American Chemical Society International Historic Chemical Landmarks, *Discovery and Development of Penicillin*.

- [14] E. P. Lesho *et al.*, “The Antimicrobial Resistance Monitoring and Research (AR-MoR) Program: The US Department of Defense Response to Escalating Antimicrobial Resistance”, *Clin. Infect. Dis.*, vol. 59, no. 3, pp. 390–397, Aug. 2014, ISSN: 1058-4838. DOI: 10.1093/cid/ciu319.
- [15] WHO, “Seventeenth World Health Assembly: A70/12 - Antimicrobial resistance”, World Health Organisation, Geneva, Switzerland, Tech. Rep., Apr. 2017.
- [16] B. T. Tadesse *et al.*, “Antimicrobial resistance in Africa: a systematic review”, *BMC Infect. Dis.*, vol. 17, no. 1, p. 616, Dec. 2017, ISSN: 1471-2334. DOI: 10.1186/s12879-017-2713-1.
- [17] T. Wi *et al.*, “Antimicrobial resistance in *Neisseria gonorrhoeae*: Global surveillance and a call for international collaborative action”, *PLOS Med.*, vol. 14, no. 7, e1002344, Jul. 2017, ISSN: 1549-1676. DOI: 10.1371/journal.pmed.1002344.
- [18] Y. Wang *et al.*, “Emergence of *Salmonella enterica* serovar Indiana and California isolates with concurrent resistance to cefotaxime, amikacin and ciprofloxacin from chickens in China”, *Int. J. Food Microbiol.*, vol. 262, pp. 23–30, Sep. 2017, ISSN: 01681605. DOI: 10.1016/j.ijfoodmicro.2017.09.012.
- [19] WHO/EMP/IAU, “Antibacterial agents in clinical development: an analysis of the antibacterial clinical development pipeline, including tuberculosis.”, World Health Organisation, Geneva, Tech. Rep., 2017.
- [20] WHO, “Biomarkers and Risk Assessment: Concepts and Principles”, World Health Organisation, Geneva, Switzerland, Tech. Rep., 1993, p. 11.
- [21] K. Strimbu and J. A. Tavel, “What are biomarkers?”, *Curr. Opin. HIV AIDS*, vol. 5, no. 6, pp. 463–466, Nov. 2010, ISSN: 1746-630X. DOI: 10.1097/COH.0b013e32833ed177.
- [22] A. J. Kapasi *et al.*, “Host biomarkers for distinguishing bacterial from non-bacterial causes of acute febrile illness: A comprehensive review”, *PLoS One*, vol. 11, no. 8, pp. 1–29, Aug. 2016, ISSN: 19326203. DOI: 10.1371/journal.pone.0160278.
- [23] L. Mchugh *et al.*, “A Molecular Host Response Assay to Discriminate Between Sepsis and Infection- Negative Systemic Inflammation in Critically Ill Patients: Discovery and Validation in Independent Cohorts”, *PLOS Med.*, vol. 12, no. 3, pp. 1–35, Dec. 2015. DOI: 10.1371/journal.pmed.1001916.
- [24] V. Chieux *et al.*, “MxA protein in capillary blood of children with viral infections”, *J. Med. Virol.*, vol. 59, no. 4, pp. 547–551, 1999, ISSN: 01466615. DOI: 10.1002/(SICI)1096-9071(199912)59:4<547::AID-JMV20>3.0.CO;2-B.
- [25] R. Sambursky and N. Shapiro, “Evaluation of a combined MxA and CRP point-of-care immunoassay to identify viral and/or bacterial immune response in patients with acute febrile respiratory infection.”, *Eur. Clin. Respir. J.*, vol. 2, no. 5, p. 28245, 2015, ISSN: 2001-8525. DOI: 10.3402/ecrj.v2.28245.
- [26] S. Dittrich *et al.*, “Target Product Profile for a Diagnostic Assay to Differentiate between Bacterial and Non-Bacterial Infections and Reduce Antimicrobial Overuse in Resource-Limited Settings: An Expert Consensus”, *PLoS One*, vol. 11, no. 8, C. Yansouni, Ed., e0161721, Aug. 2016, ISSN: 1932-6203. DOI: 10.1371/journal.pone.0161721.

- [27] L. Ashkenazi-Hoffnung *et al.*, “A host-protein signature is superior to other biomarkers for differentiating between bacterial and viral disease in patients with respiratory infection and fever without source: a prospective observational study.”, *Eur. J. Clin. Microbiol. Infect. Dis.*, vol. 37, no. 7, pp. 1361–1371, Jul. 2018, ISSN: 1435-4373. DOI: 10.1007/s10096-018-3261-3.
- [28] C. Horlock. (2018). Enzyme linked immunosorbent assay, [Online]. Available: <https://www.immunology.org/public-information/bitesized-immunology/experimental-techniques/enzyme-linked-immunosorbent-assay>.
- [29] Bosterbio.com. (2018). Four Types of ELISA Assay, [Online]. Available: <https://www.bosterbio.com/newsletter-archive/20170728-which-elisa> (visited on 12/06/2018).
- [30] Bio Rad Antibodies. (2018). Types of ELISA | Bio-Rad, [Online]. Available: <https://www.bio-rad-antibodies.com/elisa-types-direct-indirect-sandwich-competition-elisa-formats.html%7B%5C#%7DIndirect> (visited on 12/07/2018).
- [31] R. Panda *et al.*, “Validated Sandwich-type ELISA for Detection of Buckwheat Protein Residues in Processed Foods”, *J. Allergy Clin. Immunol.*, vol. 125, no. 2, AB86, Feb. 2010, ISSN: 00916749. DOI: 10.1016/j.jaci.2009.12.337.
- [32] B. Pang *et al.*, “Development of a low-cost paper-based ELISA method for rapid Escherichia coli O157:H7 detection”, *Anal. Biochem.*, vol. 542, pp. 58–62, Feb. 2018, ISSN: 0003-2697. DOI: 10.1016/J.AB.2017.11.010.
- [33] C.-Y. Lu *et al.*, “A highly specific ELISA for diagnosis of 2009 influenza A (H1N1) virus infections”, *J. Formos. Med. Assoc.*, vol. 111, no. 12, pp. 693–697, Dec. 2012, ISSN: 09296646. DOI: 10.1016/j.jfma.2011.11.029.
- [34] Y. Chen *et al.*, “Mimotope ELISA for Detection of Broad Spectrum Antibody against Avian H5N1 Influenza Virus”, *PLoS One*, vol. 6, no. 9, T. Kimman, Ed., e24144, Sep. 2011, ISSN: 1932-6203. DOI: 10.1371/journal.pone.0024144.
- [35] Y. Wu *et al.*, “Fluorescence ELISA based on glucose oxidase-mediated fluorescence quenching of quantum dots for highly sensitive detection of Hepatitis B”, *Talanta*, vol. 181, pp. 258–264, May 2018, ISSN: 00399140. DOI: 10.1016/j.talanta.2018.01.026.
- [36] A. Nakatsuma *et al.*, “Detection of HIV-1 p24 at attomole level by ultrasensitive ELISA with Thio-NAD cycling”, *PLoS One*, vol. 10, no. 6, pp. 1–10, 2015, ISSN: 19326203. DOI: 10.1371/journal.pone.0131319.
- [37] Synexa Life Sciences, *Synexa Life Sciences*, 2018.
- [38] PathCare. (2018). Fees Lookup | PathCare, [Online]. Available: <https://www2.pathcare.co.za/fee-lookup-2/> (visited on 12/03/2018).
- [39] C. L. Wong and M. Olivo, “Surface Plasmon Resonance Imaging Sensors: A Review”, *Plasmonics*, vol. 9, no. 4, pp. 809–824, Aug. 2014, ISSN: 1557-1955. DOI: 10.1007/s11468-013-9662-3.
- [40] M. Zourob *et al.*, “Principles of Bacterial Detection”, *Princ. Bact. Detect. Biosensors, Regognition Recept. Microsystems*, pp. 255–291, 2008, ISSN: 0090-4481.
- [41] S. Sabban *et al.*, “Development of an in vitro model system for studying the interaction of Equus caballus IgE with its high-affinity receptor FcεRI”, 2013, pp. 10–16. DOI: 10.1016/j.vetimm.2013.01.008.

- [42] P. Damborsky *et al.*, “Optical biosensors”, *Essays Biochem.*, vol. 60, no. 1, pp. 91–100, Jun. 2016, ISSN: 0071-1365. DOI: 10.1042/EBC20150010.
- [43] D. S. Wang and S. K. Fan, “Microfluidic surface plasmon resonance sensors: From principles to point-of-care applications”, *Sensors (Switzerland)*, vol. 16, no. 8, 2016, ISSN: 14248220. DOI: 10.3390/s16081175.
- [44] BioNavis. (2018). BioNavis: Life science applications, [Online]. Available: <http://www.bionavis.com/en/life-science/applications/> (visited on 12/09/2018).
- [45] FortéBio. (2018). FortéBio, [Online]. Available: <https://www.fortebio.com/> (visited on 12/09/2018).
- [46] Biosensing Instrument Inc. (2018). Biosensing Instrument Inc., [Online]. Available: <http://biosensingusa.com/technologies/bi-spr-technology/> (visited on 12/09/2018).
- [47] RPS. (2018). FebriDx product brochure, [Online]. Available: https://www.rpsdetectors.com/wp-content/uploads/2018/11/FRM-MKT-361.5%7B%5C_%7DFebriDx-Brochure%7B%5C_%7DFinal.pdf.
- [48] K. M. Koczula and A. Gallotta, “Lateral flow assays”, *Essays Biochem.*, vol. 60, no. June, pp. 111–121, Jun. 2016. DOI: 10.1042/EBC20150012.
- [49] Abionic. (2018). The abioSCOPE® The diagnostic platform for medical practice, [Online]. Available: https://abionic.com/wp-content/uploads/2017/03/D4baabba%7B%5C_%7D170310%7B%5C_%7DEnglish%7B%5C_%7DabioSCOPE%7B%5C_%7DBrochure%7B%5C_%7DJGA.pdf.
- [50] C. B. van Houten *et al.*, “A host-protein based assay to differentiate between bacterial and viral infections in preschool children (OPPORTUNITY): a double-blind, multicentre, validation study”, *Lancet Infect. Dis.*, vol. 3099, no. 16, pp. 1–10, 2016, ISSN: 14733099. DOI: 10.1016/S1473-3099(16)30519-9.
- [51] MeMed. (2018). MeMed | MeMed Key, [Online]. Available: <https://www.memed.com/memed-key> (visited on 12/06/2018).
- [52] R. R. Miller *et al.*, “Validation of a Host Response Assay, SeptiCyte LAB, for Discriminating Sepsis from Systemic Inflammatory Response Syndrome in the ICU”, *Am. J. Respir. Crit. Care Med.*, vol. 198, no. 7, pp. 903–913, Oct. 2018, ISSN: 1073-449X. DOI: 10.1164/rccm.201712-24720C.
- [53] Collins Dictionary. (2018). Biosensor definition and meaning | Collins English Dictionary, [Online]. Available: <https://www.collinsdictionary.com/dictionary/english/biosensor> (visited on 12/04/2018).
- [54] N. Bhalla *et al.*, “Introduction to biosensors.”, *Essays Biochem.*, vol. 60, no. 1, pp. 1–8, 2016, ISSN: 1744-1358. DOI: 10.1042/EBC20150001.
- [55] MBL Life Science. (2018). Types of antibodies | MBL Life Science, [Online]. Available: <http://ruo.mbl.co.jp/bio/e/support/method/antibody-isotype.html> (visited on 12/06/2018).
- [56] B. Byrne *et al.*, “Antibody-Based Sensors: Principles, Problems and Potential for Detection of Pathogens and Associated Toxins”, *Sensors*, vol. 9, no. 6, pp. 4407–4445, Jun. 2009, ISSN: 1424-8220. DOI: 10.3390/s90604407.
- [57] M. Medina-Sánchez *et al.*, “An inkjet-printed field-effect transistor for label-free biosensing”, *Adv. Funct. Mater.*, vol. 24, no. 40, pp. 6291–6302, 2014, ISSN: 16163028. DOI: 10.1002/adfm.201401180.

- [58] W. Zhou *et al.*, “Aptamer-based biosensors for biomedical diagnostics”, *Analyst*, vol. 139, no. 11, p. 2627, May 2014, ISSN: 0003-2654. DOI: 10.1039/c4an00132j.
- [59] M. Chen *et al.*, “An ultrasensitive electrochemical DNA biosensor based on a copper oxide nanowires/single-walled carbon nanotubes nanocomposite”, *Appl. Surf. Sci.*, vol. 364, pp. 703–709, Feb. 2016, ISSN: 01694332. DOI: 10.1016/j.apsusc.2015.12.203.
- [60] M. Asghary *et al.*, “A novel self-powered and sensitive label-free DNA biosensor in microbial fuel cell”, *Biosens. Bioelectron.*, vol. 82, pp. 173–176, Aug. 2016, ISSN: 09565663. DOI: 10.1016/j.bios.2016.04.023.
- [61] A. Miodek *et al.*, “Electrochemical functionalization of polypyrrole through amine oxidation of poly(amidoamine) dendrimers: Application to DNA biosensor”, *Talanta*, vol. 154, pp. 446–454, 2016, ISSN: 00399140. DOI: 10.1016/j.talanta.2016.03.076.
- [62] A. Sassolas *et al.*, “DNA Biosensors and Microarrays”, 2008. DOI: 10.1021/cr0684467.
- [63] Q. Luan *et al.*, “Hairpin DNA probe based surface plasmon resonance biosensor used for the activity assay of E. coli DNA ligase”, *Analyst*, vol. 135, no. 2, pp. 414–418, Jan. 2010. DOI: 10.1039/B920228E.
- [64] Y. Jin *et al.*, “Hairpin DNA probe based electrochemical biosensor using methylene blue as hybridization indicator”, *Biosens. Bioelectron.*, vol. 22, no. 6, pp. 1126–1130, Jan. 2007, ISSN: 0956-5663. DOI: 10.1016/J.BIOS.2006.04.011.
- [65] A. Giannetti *et al.*, “Oligonucleotide molecular beacons for intracellular diagnosis and therapy”, *SPIE Newsroom*, Feb. 2017, ISSN: 18182259. DOI: 10.1117/2.1201611.006665.
- [66] L. Zhou *et al.*, “Biosensing technologies for Mycobacterium tuberculosis detection: status and new developments.”, *Clin. Dev. Immunol.*, vol. 2011, p. 193963, 2011, ISSN: 1740-2530. DOI: 10.1155/2011/193963.
- [67] N. Lawrenson, “Design of an Electrochemically Reactive HIV DNA Biosensor by use of Hairpin DNA Probes on Carbon Nanofibers”, Master of Engineering (Electronic), Stellenbosch University, 2017.
- [68] S. Cotrone *et al.*, “Microcantilevers and organic transistors: Two promising classes of label-free biosensing devices which can be integrated in electronic circuits”, *Anal. Bioanal. Chem.*, vol. 402, no. 5, pp. 1799–1811, 2012, ISSN: 16182642. DOI: 10.1007/s00216-011-5610-2.
- [69] M. Tian *et al.*, “RNA Detection Based on Graphene Field-Effect Transistor Biosensor”, *Adv. Condens. Matter Phys.*, vol. 2018, no. 17 (NOVEMBER, 1974), pp. 1–6, Jun. 2018, ISSN: 1687-8108. DOI: 10.1155/2018/8146765.
- [70] Y.-J. Zheng *et al.*, “Enzyme-based E-RNA sensor array with a hairpin probe: Specific detection of gene mutation”, *Sensors Actuators B Chem.*, vol. 181, pp. 227–233, May 2013, ISSN: 09254005. DOI: 10.1016/j.snb.2013.01.051.
- [71] S. Song *et al.*, “Aptamer-based biosensors”, *TrAC Trends Anal. Chem.*, vol. 27, no. 2, pp. 108–117, Feb. 2008, ISSN: 01659936. DOI: 10.1016/j.trac.2007.12.004.

- [72] Y. Yuan *et al.*, “Aptamer based voltammetric biosensor for endotoxin using functionalized graphene and molybdenum disulfide composite as a new nanocarrier”, *J. Name*, vol. 141, pp. 1–3, ISSN: 0003-2654. DOI: 10.1039/C8AN02139B.
- [73] Z.-M. Ying *et al.*, “Light-up RNA aptamer enabled label-free protein detection via a proximity induced transcription assay”, *Chem. Commun.*, vol. 54, no. 64, pp. 8877–8880, Aug. 2018, ISSN: 1359-7345. DOI: 10.1039/C8CC04498H.
- [74] Y. Wu *et al.*, “Ultrasensitive aptamer biosensor for arsenic(iii) detection in aqueous solution based on surfactant-induced aggregation of gold nanoparticles”, *Analyst*, vol. 137, no. 18, p. 4171, Aug. 2012, ISSN: 0003-2654. DOI: 10.1039/c2an35711a.
- [75] S. M. Borisov and O. S. Wolfbeis, “Optical Biosensors”, *Chem. Rev.*, vol. 108, no. 2, pp. 423–461, Feb. 2008, ISSN: 0009-2665. DOI: 10.1021/cr068105t.
- [76] A. Aray *et al.*, “SPR-based plastic optical fibre biosensor for the detection of C-reactive protein in serum”, *J. Biophotonics*, vol. 9, no. 10, pp. 1077–1084, 2016, ISSN: 18640648. DOI: 10.1002/jbio.201500315.
- [77] P. Skládal, “Piezoelectric biosensors”, *TrAC Trends Anal. Chem.*, vol. 79, pp. 127–133, May 2016, ISSN: 01659936. DOI: 10.1016/j.trac.2015.12.009.
- [78] D. P. Neveling *et al.*, “A nanoforce ZnO nanowire-array biosensor for the detection and quantification of immunoglobulins”, *Sensors Actuators, B Chem.*, vol. 203, pp. 102–110, Nov. 2014, ISSN: 09254005. DOI: 10.1016/j.snb.2014.06.076.
- [79] C. Koçum *et al.*, “Design of temperature controlled quartz crystal microbalance system”, *Instrum. Sci. Technol.*, vol. 38, no. 1, pp. 39–51, Dec. 2009, ISSN: 1073-9149. DOI: 10.1080/10739140903427137.
- [80] E. Haberal *et al.*, “QCM biosensor for testing the inflammatory response to blood-contacting biomaterials”, *Artif. Cells, Nanomedicine, Biotechnol.*, vol. 41, no. 3, pp. 222–226, Jun. 2013, ISSN: 2169-1401. DOI: 10.3109/10731199.2012.716068.
- [81] C. M. Domínguez *et al.*, “Label-Free DNA-Based Detection of Mycobacterium tuberculosis and Rifampicin Resistance through Hydration Induced Stress in Microcantilevers”, *Anal. Chem.*, vol. 87, no. 3, pp. 1494–1498, Feb. 2015, ISSN: 0003-2700. DOI: 10.1021/ac504523f.
- [82] D. Grieshaber *et al.*, “Electrochemical Biosensors - Sensor Principles and Architectures”, *Sensors*, vol. 8, no. 3, pp. 1400–1458, Mar. 2008, ISSN: 1424-8220. DOI: 10.3390/s80314000.
- [83] D. R. Thévenot *et al.*, “Electrochemical biosensors: recommended definitions and classification”, *International Union of Pure and Applied Chemistry: Physical Chemistry Division, Commission I.7 (Biophysical Chemistry); Analytical Chemistry Division, Commission V.5 (Electroanalytical)*, *Biosens. Bioelectron.*, vol. 16, no. 1-2, pp. 121–131, Jan. 2001, ISSN: 09565663. DOI: 10.1016/S0956-5663(01)00115-4.
- [84] B. Piro *et al.*, “Fabrication and Use of Organic Electrochemical Transistors for Sensing of Metabolites in Aqueous Media”, *Appl. Sci.*, vol. 8, no. 6, p. 928, Jun. 2018, ISSN: 2076-3417. DOI: 10.3390/app8060928.
- [85] L. Setti *et al.*, “An amperometric glucose biosensor prototype fabricated by thermal inkjet printing”, *Biosens. Bioelectron.*, vol. 20, no. 10, pp. 2019–2026, Apr. 2005, ISSN: 09565663. DOI: 10.1016/j.bios.2004.09.022.

- [86] B. Silwana *et al.*, “Amperometric determination of cadmium, lead, and mercury metal ions using a novel polymer immobilised horseradish peroxidase biosensor system”, *J. Environ. Sci. Heal. Part A*, vol. 49, no. 13, pp. 1501–1511, Nov. 2014, ISSN: 1093-4529. DOI: 10.1080/10934529.2014.937169.
- [87] T. V. Shishkanova *et al.*, “Ion-selective electrodes: Polyaniline modification and anion recognition”, *Anal. Chim. Acta*, vol. 553, no. 1-2, pp. 160–168, 2005, ISSN: 00032670. DOI: 10.1016/j.aca.2005.08.018.
- [88] T. Luo *et al.*, “Selectivity of ion exchange membranes: A review”, *J. Memb. Sci.*, vol. 555, no. December 2017, pp. 429–454, Jun. 2018, ISSN: 03767388. DOI: 10.1016/j.memsci.2018.03.051.
- [89] G. A. Crespo, “Recent Advances in Ion-selective membrane electrodes for in situ environmental water analysis”, *Electrochim. Acta*, vol. 245, pp. 1023–1034, 2017, ISSN: 00134686. DOI: 10.1016/j.electacta.2017.05.159.
- [90] G. H. C. Mayberry, “Design and fabrication of a paper based bio-sensor”, Stellenbosch University, Stellenbosch, 2016, pp. 1–79.
- [91] C. Viviers, “The Design and Fabrication of an Autophagic Flux Biosensor”, Master of Engineering (Electronic), Stellenbosch University, 2017.
- [92] C.-S. Lee *et al.*, “Ion-Sensitive Field-Effect Transistor for Biological Sensing”, *Sensors*, vol. 9, no. 12, pp. 7111–7131, Sep. 2009, ISSN: 1424-8220. DOI: 10.3390/s90907111.
- [93] A. Covington and P. Whalley, “Simultaneous evaluation of electroactive membranes on a four-function isfet by a constant dilution method”, *Anal. Chim. Acta*, vol. 184, pp. 281–286, 1986, ISSN: 00032670. DOI: 10.1016/S0003-2670(00)86492-2.
- [94] A. Soldatkin *et al.*, “Glucose sensitive conductometric biosensor with additional Nafion membrane: reduction of influence of buffer capacity on the sensor response and extension of its dynamic range”, *Anal. Chim. Acta*, vol. 288, no. 3, pp. 197–203, Apr. 1994, ISSN: 00032670. DOI: 10.1016/0003-2670(93)E0627-J.
- [95] F. Maddalena *et al.*, “Organic field-effect transistor-based biosensors functionalized with protein receptors”, *J. Appl. Phys.*, vol. 108, no. 12, pp. 2–6, 2010, ISSN: 00218979. DOI: 10.1063/1.3518681.
- [96] H. Sun *et al.*, “n-Type organic electrochemical transistors: materials and challenges”, *J. Mater. Chem. C*, vol. 6, no. 44, pp. 11 778–11 784, 2018, ISSN: 2050-7526. DOI: 10.1039/C8TC03185A.
- [97] J. T. E. Quinn *et al.*, “Recent progress in the development of n-type organic semiconductors for organic field effect transistors”, *J. Mater. Chem. C*, vol. 5, no. 34, pp. 8654–8681, 2017, ISSN: 2050-7526. DOI: 10.1039/C7TC01680H.
- [98] K. Melzer *et al.*, “Characterization and simulation of electrolyte-gated organic field-effect transistors”, *Faraday Discuss.*, vol. 174, pp. 399–411, Jun. 2014, ISSN: 1359-6640. DOI: 10.1039/C4FD00095A.
- [99] V. Rani and K. S. V. Santhanam, “Polycarbazole-based electrochemical transistor”, *J. Solid State Electrochem.*, vol. 2, no. 2, pp. 99–101, Mar. 1998, ISSN: 1432-8488. DOI: 10.1007/s100080050072.

- [100] V. Saxena *et al.*, “Copper(II) Ion - Selective Microelectrochemical Transistor”, *Appl. Biochem. Biotechnol.*, vol. 96, no. 1-3, pp. 063–070, 2001, ISSN: 0273-2289. DOI: 10.1385/ABAB:96:1-3:063.
- [101] T. Zhang *et al.*, “Naphthalene diimide-based random terpolymer for efficient all-polymer solar cells with high open circuit voltage”, *Dye. Pigment.*, vol. 146, pp. 169–177, Nov. 2017, ISSN: 01437208. DOI: 10.1016/j.dyepig.2017.07.007.
- [102] L. Torsi *et al.*, “Side-Chain Role in Chemically Sensing Conducting Polymer Field-Effect Transistors”, *J. Phys. Chem. B*, vol. 107, no. 31, pp. 7589–7594, Aug. 2003, ISSN: 1520-6106. DOI: 10.1021/jp0344951.
- [103] T. Kim *et al.*, “Flexible, highly efficient all-polymer solar cells”, *Nat. Commun.*, vol. 6, no. 1, p. 8547, Dec. 2015, ISSN: 2041-1723. DOI: 10.1038/ncomms9547. arXiv: 0906.5419.
- [104] M. J. Panzer and C. D. Frisbie, “Polymer Electrolyte Gate Dielectric Reveals Finite Windows of High Conductivity in Organic Thin Film Transistors at High Charge Carrier Densities”, *J. Am. Chem. Soc.*, vol. 127, no. 19, pp. 6960–6961, 2005. DOI: 10.1021/ja051579+.
- [105] G. C. Faria *et al.*, “On the transient response of organic electrochemical transistors”, *Org. Electron.*, vol. 45, pp. 215–221, Jun. 2017, ISSN: 15661199. DOI: 10.1016/j.orgel.2017.03.021.
- [106] A. Giovannitti *et al.*, “The Role of the Side Chain on the Performance of N-type Conjugated Polymers in Aqueous Electrolytes”, 2018. DOI: 10.1021/acs.chemmater.8b00321.
- [107] G. C. Schmidt *et al.*, “Fully printed flexible audio system on the basis of low-voltage polymeric organic field effect transistors with three layer dielectric”, *J. Polym. Sci. Part B Polym. Phys.*, vol. 53, no. 20, pp. 1409–1415, 2015, ISSN: 10990488. DOI: 10.1002/polb.23778.
- [108] M.-B. Madec *et al.*, “Effect of poly(triarylamine) molar mass distribution on organic field effect transistor behaviour”, *Org. Electron.*, vol. 11, no. 4, pp. 686–691, Apr. 2010, ISSN: 15661199. DOI: 10.1016/j.orgel.2009.12.015.
- [109] H. U. Khan *et al.*, “Effect of passivation on the sensitivity and stability of pentacene transistor sensors in aqueous media”, *Biosens. Bioelectron.*, vol. 26, no. 10, pp. 4217–4221, 2011, ISSN: 09565663. DOI: 10.1016/j.bios.2011.03.031.
- [110] X. Strakosas, “Integration of proteins with organic electrochemical transistors for sensing applications”, PhD thesis, Ecole Nationale Supérieure des Mines de Saint-Etienne, 2015.
- [111] S. Y. Cho *et al.*, “High-performance organic thin film transistors based on inkjet-printed polymer/TIPS pentacene blends”, *Org. Electron.*, vol. 13, no. 8, pp. 1329–1339, Aug. 2012, ISSN: 15661199. DOI: 10.1016/j.orgel.2012.04.007.
- [112] J. T. Friedlein *et al.*, “Device physics of organic electrochemical transistors”, *Org. Electron.*, vol. 63, pp. 398–414, Dec. 2018, ISSN: 15661199. DOI: 10.1016/j.orgel.2018.09.010.
- [113] C. M. Proctor *et al.*, “Understanding volumetric capacitance in conducting polymers”, *J. Polym. Sci. Part B Polym. Phys.*, vol. 54, no. 15, pp. 1433–1436, Aug. 2016, ISSN: 08876266. DOI: 10.1002/polb.24038.

- [114] C. Liao and F. Yan, “Organic Semiconductors in Organic Thin-Film Transistor-Based Chemical and Biological Sensors”, *Polym. Rev.*, vol. 53, no. 3, pp. 352–406, 2013, ISSN: 1558-3724. DOI: 10.1080/15583724.2013.808665.
- [115] J. Wang *et al.*, “Solubilization of Carbon Nanotubes by Nafion toward the Preparation of Amperometric Biosensors”, *J. AM. CHEM. SOC*, vol. 125, pp. 2408–2409, 2003. DOI: 10.1021/ja028951v.
- [116] C. Liao *et al.*, “Highly selective and sensitive glucose sensors based on organic electrochemical transistors with graphene-modified gate electrodes”, *J. Mater. Chem. B*, vol. 1, no. 31, p. 3820, 2013, ISSN: 2050-750X. DOI: 10.1039/c3tb20451k.
- [117] M. E. Welch *et al.*, “A glucose sensor via stable immobilization of the GOx enzyme on an organic transistor using a polymer brush”, *J. Polym. Sci. Part A Polym. Chem.*, vol. 53, no. 2, pp. 372–377, Jan. 2015, ISSN: 0887624X. DOI: 10.1002/pola.27392.
- [118] L. Kergoat *et al.*, “Detection of Glutamate and Acetylcholine with Organic Electrochemical Transistors Based on Conducting Polymer/Platinum Nanoparticle Composites”, *Adv. Mater.*, vol. 26, no. 32, pp. 5658–5664, Aug. 2014, ISSN: 09359648. DOI: 10.1002/adma.201401608.
- [119] L. J. Currano *et al.*, “Wearable Sensor System for Detection of Lactate in Sweat”, *Sci. Rep.*, vol. 8, no. 1, p. 15 890, Dec. 2018, ISSN: 2045-2322. DOI: 10.1038/s41598-018-33565-x.
- [120] C. Karuwan *et al.*, “Inkjet-printed graphene-poly(3,4-ethylenedioxythiophene):poly(styrene-sulfonate) modified on screen printed carbon electrode for electrochemical sensing of salbutamol”, *Sensors Actuators B Chem.*, vol. 161, no. 1, pp. 549–555, Jan. 2012, ISSN: 09254005. DOI: 10.1016/j.snb.2011.10.074.
- [121] S. A. Tria *et al.*, “Validation of the organic electrochemical transistor for in vitro toxicology”, *Biochim. Biophys. Acta - Gen. Subj.*, vol. 1830, no. 9, pp. 4381–4390, 2013, ISSN: 03044165. DOI: 10.1016/j.bbagen.2012.12.003.
- [122] X. Strakosas *et al.*, “Biofunctionalization of polydioxothiophene derivatives for biomedical applications”, *J. Mater. Chem. B*, vol. 4, no. 29, pp. 4952–4968, 2016, ISSN: 2050-750X. DOI: 10.1039/C6TB00852F.
- [123] K. Tybrandt *et al.*, “Organic electrochemical transistors for signal amplification in fast scan cyclic voltammetry”, *Sensors Actuators, B Chem.*, vol. 195, pp. 651–656, Mar. 2014, ISSN: 09254005. DOI: 10.1016/j.snb.2014.01.097.
- [124] I. Gualandi *et al.*, “Textile Organic Electrochemical Transistors as a Platform for Wearable Biosensors”, *Sci. Rep.*, vol. 6, no. 1, p. 33 637, Dec. 2016, ISSN: 2045-2322. DOI: 10.1038/srep33637.
- [125] I. Gualandi *et al.*, “Selective detection of dopamine with an all PEDOT:PSS Organic Electrochemical Transistor.”, *Sci. Rep.*, vol. 6, no. October, p. 35 419, 2016, ISSN: 2045-2322. DOI: 10.1038/srep35419.
- [126] N. Wang *et al.*, “AC Measurements Using Organic Electrochemical Transistors for Accurate Sensing”, *ACS Appl. Mater. Interfaces*, acsami.7b07668, Aug. 2017, ISSN: 1944-8244. DOI: 10.1021/acsami.7b07668.
- [127] R.-X. He *et al.*, “Detection of bacteria with organic electrochemical transistors”, *J. Mater. Chem.*, vol. 22, no. 41, p. 22 072, 2012, ISSN: 0959-9428. DOI: 10.1039/c2jm33667g.

- [128] D.-J. Kim *et al.*, “Organic electrochemical transistor based immunosensor for prostate specific antigen (PSA) detection using gold nanoparticles for signal amplification.”, *Biosens. Bioelectron.*, vol. 25, no. 11, pp. 2477–2482, Jul. 2010, ISSN: 1873-4235. DOI: 10.1016/j.bios.2010.04.013.
- [129] R. Faddoul *et al.*, “Inkjet printing of organic electrochemical immunosensors”, in *IEEE SENSORS 2014 Proc.*, vol. 2014-Decem, IEEE, Nov. 2014, pp. 1088–1091, ISBN: 978-1-4799-0162-3. DOI: 10.1109/ICSENS.2014.6985194.
- [130] P. Lin *et al.*, “Organic Electrochemical Transistors Integrated in Flexible Microfluidic Systems and Used for Label-Free DNA Sensing”, *Adv. Mater.*, vol. 23, no. 35, pp. 4035–4040, Sep. 2011, ISSN: 09359648. DOI: 10.1002/adma.201102017.
- [131] T.-M. Huang *et al.*, “Chemical cross-linking of conducting poly(3,4-ethylenedioxythiophene):poly(3,4-ethylenedioxythiophene) (PEDOT:PSS) using poly(ethylene oxide) (PEO)”, *Polymer (Guildf.)*, vol. 54, no. 23, pp. 6455–6462, Nov. 2013, ISSN: 00323861. DOI: 10.1016/j.polymer.2013.09.046.
- [132] L. Groenendaal *et al.*, “Poly(3,4-ethylenedioxythiophene) and Its Derivatives: Past, Present, and Future”, *Adv. Mater.*, vol. 12, no. 7, pp. 481–494, Apr. 2000, ISSN: 0935-9648. DOI: 10.1002/(SICI)1521-4095(200004)12:7<481::AID-ADMA481>3.0.CO;2-C.
- [133] D. Ohayon *et al.*, “Laser Patterning of Self-Assembled Monolayers on PEDOT:PSS Films for Controlled Cell Adhesion”, *Adv. Mater. Interfaces*, vol. 4, no. 16, p. 1700191, Aug. 2017, ISSN: 21967350. DOI: 10.1002/admi.201700191.
- [134] O. E. Dictionary. (2017). Definition of inkjet printer in English by Oxford Dictionaries, [Online]. Available: https://en.oxforddictionaries.com/definition/inkjet%7B%5C_%7Dprinter (visited on 11/14/2017).
- [135] T. Xu *et al.*, “Inkjet printing of viable mammalian cells”, *Biomaterials*, vol. 26, no. 1, pp. 93–99, Jan. 2005. DOI: 10.1016/j.biomaterials.2004.04.011.
- [136] A. Bernard *et al.*, “Printing Patterns of Proteins”, *Langmuir*, vol. 14, no. 9, pp. 2225–2229, Apr. 1998, ISSN: 0743-7463. DOI: 10.1021/la9800371.
- [137] D. J. Hayes *et al.*, “Micro-Jet Printing Of Polymers And Solder For Electronics Manufacturing”, *J. Electron. Manuf.*, vol. 08, no. 03n04, pp. 209–216, Sep. 1998, ISSN: 0960-3131. DOI: 10.1142/S0960313198000197.
- [138] X. Zhao *et al.*, “Ink-jet printing of ceramic pillar arrays”, *J. Mater. Sci.*, vol. 37, no. 10, pp. 1987–1992, 2002, ISSN: 00222461. DOI: 10.1023/A:1015247131016.
- [139] H. M. Nur *et al.*, “Ink-jet printing of gold conductive tracks”, *J. Mater. Sci. Mater. Electron.*, vol. 13, no. 4, pp. 213–219, 2002, ISSN: 09574522. DOI: 10.1023/A:1014827900606.
- [140] W. Wong *et al.*, “Jet-printed fabrication of a-Si:H thin-film transistors and arrays”, *J. Non. Cryst. Solids*, vol. 299-302, pp. 1335–1339, Apr. 2002, ISSN: 00223093. DOI: 10.1016/S0022-3093(01)01155-3.
- [141] T. Kawase *et al.*, “Inkjet printing of polymer thin film transistors”, *Thin Solid Films*, vol. 438-439, no. 03, pp. 279–287, 2003. DOI: 10.1016/S0040-6090(03)00801-0.
- [142] Y. Yoshioka and G. E. Jabbour, “Desktop inkjet printer as a tool to print conducting polymers”, *Synth. Met.*, vol. 156, no. 11-13, pp. 779–783, Jun. 2006, ISSN: 03796779. DOI: 10.1016/j.synthmet.2006.03.013.

- [143] K. Burg and T. Boland, “Minimally invasive tissue engineering composites and cell printing - Injectable composites combined with tissue-printing technology for improved bioengineered devices”, *IEEE Eng. Med. Biol. Mag.*, vol. 22, no. 5, pp. 84–91, Sep. 2003. DOI: 10.1109/MEMB.2003.1256277.
- [144] L. Pardo *et al.*, “Characterization of Patterned Self-Assembled Monolayers and Protein Arrays Generated by the Ink-Jet Method †”, *Langmuir*, vol. 19, no. 5, pp. 1462–1466, Mar. 2003. DOI: 10.1021/1a026171u.
- [145] V. Mironov *et al.*, “Organ printing: computer-aided jet-based 3D tissue engineering”, *Trends Biotechnol.*, vol. 21, no. 4, pp. 157–161, Apr. 2003. DOI: 10.1016/S0167-7799(03)00033-7.
- [146] X. Cui *et al.*, “Cell damage evaluation of thermal inkjet printed Chinese hamster ovary cells”, *Biotechnol. Bioeng.*, vol. 106, no. 6, pp. 963–969, Apr. 2010, ISSN: 00063592. DOI: 10.1002/bit.22762.
- [147] M. F. Mabrook *et al.*, “Inkjet-printed polypyrrole thin films for vapour sensing”, *Sensors Actuators, B Chem.*, vol. 115, no. 1, pp. 547–551, Oct. 2006. DOI: 10.1016/j.snb.2005.10.019.
- [148] T. Boland *et al.*, “Drop-on-demand printing of cells and materials for designer tissue constructs”, *Mater. Sci. Eng. C*, vol. 27, no. 3, pp. 372–376, Apr. 2007. DOI: 10.1016/j.msec.2006.05.047.
- [149] S. H. Eom *et al.*, “Polymer solar cells based on inkjet-printed PEDOT:PSS layer”, *Org. Electron.*, vol. 10, no. 3, pp. 536–542, May 2009. DOI: 10.1016/j.orgel.2009.01.015.
- [150] M. E. Pepper *et al.*, “Design and implementation of a two-dimensional inkjet bio-printer”, in *Proc. 31st Annu. Int. Conf. IEEE Eng. Med. Biol. Soc. Eng. Futur. Biomed. EMBC 2009*, Minneapolis, Minnesota, Sep. 2009, pp. 6001–6005. DOI: 10.1109/IEMBS.2009.5332513.
- [151] C. Srichan *et al.*, “Inkjet printing PEDOT:PSS using desktop inkjet printer”, in *2009 6th Int. Conf. Electr. Eng. Comput. Telecommun. Inf. Technol.*, vol. 01, Chonburi, Thailand: IEEE, May 2009, pp. 465–468. DOI: 10.1109/ECTICON.2009.5137049.
- [152] P. D’haeseleer. (2013). DIY BioPrinter, [Online]. Available: <http://www.instructables.com/id/DIY-BioPrinter/?ALLSTEPS> (visited on 02/27/2017).
- [153] K. Yoshihiro *et al.*, “Instant inkjet circuits: Lab-based Inkjet Printing to Support Rapid Prototyping of UbiComp Devices”, in *Proc. 2013 ACM Int. Jt. Conf. Pervasive Ubiquitous Comput. - UbiComp '13, Zurich, Switz.*, Zurich, Switzerland, 2013, pp. 363–372, ISBN: 9781450317702. DOI: 10.1145/2493432.2493486. arXiv: 1111.4970.
- [154] Y. Matsuda *et al.*, “Electric Conductive Pattern Element Fabricated Using Commercial Inkjet Printer for Paper-Based Analytical Devices”, *Anal. Chem.*, vol. 87, no. 11, pp. 5762–5765, Jun. 2015, ISSN: 0003-2700. DOI: 10.1021/acs.analchem.5b01568.
- [155] T. Ahuja *et al.*, “An amperometric uric acid biosensor based on Bis[sulfosuccinimidyl] suberate crosslinker/3-aminopropyltriethoxysilane surface modified ITO glass electrode”, *Thin Solid Films*, vol. 519, no. 3, pp. 1128–1134, Nov. 2010, ISSN: 00406090. DOI: 10.1016/j.tsf.2010.08.056.

- [156] T. D. Tsai *et al.*, “Manipulating the hysteresis in poly(vinyl alcohol)-dielectric organic field-effect transistors toward memory elements”, *Adv. Funct. Mater.*, vol. 23, no. 34, pp. 4206–4214, 2013, ISSN: 1616301X. DOI: 10.1002/adfm.201203694.
- [157] Thermo Fischer Scientific. (2018). Amine-Reactive Crosslinker Chemistry - ZA, [Online]. Available: <https://www.thermofisher.com/za/en/home/life-science/protein-biology/protein-biology-learning-center/protein-biology-resource-library/pierce-protein-methods/amine-reactive-crosslinker-chemistry.html%7B%5C#%7D2> (visited on 12/05/2018).
- [158] B. Young *et al.*, “C-reactive protein: A critical review”, *Pathology*, vol. 23, no. 2, pp. 118–124, 1991, ISSN: 00313025. DOI: 10.3109/00313029109060809.
- [159] M. B. Pepys and G. M. Hirschfield, “C-reactive protein: a critical update”, *J. Clin. Invest.*, vol. 111, no. 12, pp. 1805–1812, Jun. 2003, ISSN: 0021-9738. DOI: 10.1172/JCI200318921. arXiv: NIHMS150003.
- [160] J. D. Retief *et al.*, “Modified desktop inkjet printer as low-cost material deposition device”, in *2018 3rd Bienn. South African Biomed. Eng. Conf.*, Stellenbosch, South Africa: IEEE, Apr. 2018, pp. 1–4, ISBN: 978-1-5386-2516-3. DOI: 10.1109/SAIBMEC.2018.8363183.
- [161] H.-P. Corporation. (-). HP DeskJet Ink Advantage 4535 All-in-One Printer, [Online]. Available: http://www8.hp.com/za/en/products/printers/product-detail.html?oid=7317517%7B%5C&%7Djumpid=reg%7B%5C_%7Dr1002%7B%5C_%7Dzaen%7B%5C_%7Dc-001%7B%5C_%7Dttitle%7B%5C_%7Dr0001 (visited on 03/06/2017).
- [162] Unknown. (-). Copierparts.co.zw, [Online]. Available: <https://copierparts.co.zw/copier/product/hp-652-tri-color-original-ink/> (visited on 11/27/2018).
- [163] P. Sallinga, *Electrical Characterization of Organic Electronic Materials and Devices*. John Wiley and Sons, 2009, p. 303, ISBN: 9780470750094. DOI: 10.1002/9780470750162.
- [164] J. Wang, “Printing and Characterizing Inks for Biosensors”, Master’s Thesis, McMaster University, 2014, p. 87.
- [165] H. Shi *et al.*, “Effective Approaches to Improve the Electrical Conductivity of PEDOT:PSS: A Review”, *Adv. Electron. Mater.*, vol. 1, no. 4, p. 1500017, Apr. 2015, ISSN: 2199160X. DOI: 10.1002/aelm.201500017.
- [166] K. Muro *et al.*, “PEDOT/PSS nanoparticles: synthesis and properties”, *RSC Adv.*, vol. 6, no. 90, pp. 87147–87152, 2016, ISSN: 2046-2069. DOI: 10.1039/C6RA16829A.
- [167] O. P. Dimitriev *et al.*, “PEDOT:PSS films-Effect of organic solvent additives and annealing on the film conductivity”, *Synth. Mater.*, vol. 159, no. 21-22, pp. 2237–2239, 2009, ISSN: 03796779. DOI: 10.1016/j.synthmet.2009.08.022.
- [168] F. USA, “Dimatix Materials Printer DMP-2850”, Tech. Rep.
- [169] F. USA. (?). Dimatix Materials Printer DMP-2850 | Deposition Products | Industrial Inkjet Printheads | Fujifilm USA, [Online]. Available: https://www.fujifilmusa.com/products/industrial%7B%5C_%7Dinkjet%7B%5C_%7Dprintheads/deposition-products/dmp-2800/ (visited on 11/30/2018).

- [170] E. Times. (?). Benchtop ink-jet system costs under \$30K | EE Times, [Online]. Available: https://www.eetimes.com/document.asp?doc_id=1297523 (visited on 12/05/2017).
- [171] J. D. Yuen *et al.*, “Electrolyte-Sensing Transistor Decals Enabled by Ultrathin Microbial Nanocellulose”, *Sci. Rep.*, vol. 7, p. 40 867, Jan. 2017, ISSN: 2045-2322. DOI: 10.1038/srep40867.
- [172] V. Kaphle *et al.*, “Contact Resistance Effects in Highly Doped Organic Electrochemical Transistors”, *Adv. Mater.*, vol. 28, no. 39, pp. 8766–8770, Oct. 2016, ISSN: 09359648. DOI: 10.1002/adma.201602125.
- [173] T.-J. Ha, “Low-voltage and hysteresis-free organic thin-film transistors employing solution-processed hybrid bilayer gate dielectrics”, *Cit. Appl. Phys. Lett.*, vol. 105, p. 43 305, 2014. DOI: 10.1063/1.4892005.
- [174] S. Pretl *et al.*, “Low-voltage electrochemical transistor based on ionic liquid-gated PEDOT:PSS with copper electrodes”, in *2016 39th Int. Spring Semin. Electron. Technol.*, vol. 2016-Septe, IEEE, May 2016, pp. 58–61, ISBN: 978-1-5090-1389-0. DOI: 10.1109/ISSE.2016.7563161.
- [175] J. Rivnay *et al.*, “Organic Electrochemical Transistors with Maximum Transconductance at Zero Gate Bias”, *Adv. Mater.*, vol. 25, no. 48, pp. 7010–7014, Dec. 2013, ISSN: 09359648. DOI: 10.1002/adma.201303080.
- [176] J. Baniukevic *et al.*, “Application of oriented and random antibody immobilization methods in immunosensor design”, *Sensors Actuators, B Chem.*, vol. 189, pp. 217–223, 2013, ISSN: 09254005. DOI: 10.1016/j.snb.2013.03.126.
- [177] J. Goddard and J. Hotchkiss, “Polymer surface modification for the attachment of bioactive compounds”, *Prog. Polym. Sci.*, vol. 32, no. 7, pp. 698–725, Jul. 2007, ISSN: 00796700. DOI: 10.1016/j.progpolymsci.2007.04.002.
- [178] C. Liao and F. Yan, “Organic Semiconductors in Organic Thin-Film Transistor-Based Chemical and Biological Sensors”, *Polym. Rev.*, vol. 53, no. 3, pp. 352–406, Jul. 2013, ISSN: 1558-3724. DOI: 10.1080/15583724.2013.808665.
- [179] P. C. Hütter *et al.*, “Influence of geometry variations on the response of organic electrochemical transistors”, *Appl. Phys. Lett.*, vol. 103, no. 4, p. 043 308, Jul. 2013, ISSN: 0003-6951. DOI: 10.1063/1.4816781.
- [180] R. Oppong *et al.*, “Cost-effectiveness of point-of-care C-reactive protein testing to inform antibiotic prescribing decisions”, *Br. J. Gen. Pract.*, vol. 63, no. 612, pp. 465–471, 2013, ISSN: 09601643. DOI: 10.3399/bjgp13X669185.
- [181] Www.payscale.com. (2018). Factory Worker Salary (South Africa) | PayScale, [Online]. Available: https://www.payscale.com/research/ZA/Job=Factory%7B%5C_%7DWorker/Salary (visited on 12/03/2018).
- [182] Tradingeconomics.com. (2017). South Africa Wages Low Skilled | 2018 | Data | Chart | Calendar | Forecast, [Online]. Available: <https://tradingeconomics.com/south-africa/wages-low-skilled> (visited on 12/03/2018).
- [183] B. D. Hao Xiong and D. Fleetwood Ronald Schrimpf Robert Weller Tim Holman Sokrates Pantelides ii, “Low frequency noise and charge trapping in mosfets”, PhD thesis, Graduate School of Vanderbilt University, Dec. 2004.

- [184] S. Ahmed *et al.*, “Paper-based chemical and biological sensors: Engineering aspects”, *Biosens. Bioelectron.*, vol. 77, pp. 249–263, 2016, ISSN: 18734235. DOI: 10.1016/j.bios.2015.09.038.